Alma Mater Studiorum – Università di Bologna

DOTTORATO DI RICERCA IN

Ingegneria Biomedica, Elettrica e dei Sistemi

Ciclo XXX

Settore Concorsuale: 09/G1

Settore Scientifico Disciplinare: ING-INF/04

Electromyography Based Human-Robot Interfaces for the Control of Artificial Hands and Wearable Devices

Presentata da: Roberto MEATTINI

Coordinatore Dottorato:

Chiar.mo Prof. Daniele VIGO

Supervisore:

Chiar.mo Prof. Claudio MELCHIORRI

Esame finale anno 2018

Declaration of Authorship

I, Roberto MEATTINI, declare that this thesis titled, "Electromyography Based Human-Robot Interfaces for the Control of Artificial Hands and Wearable Devices" and the work presented in it are my own. I confirm that:

- This work was done wholly or mainly while in candidature for a research degree at this University.
- Where any part of this thesis has previously been submitted for a degree or any other qualification at this University or any other institution, this has been clearly stated.
- Where I have consulted the published work of others, this is always clearly attributed.
- Where I have quoted from the work of others, the source is always given. With the exception of such quotations, this thesis is entirely my own work.
- I have acknowledged all main sources of help.
- Where the thesis is based on work done by myself jointly with others, I have made clear exactly what was done by others and what I have contributed myself.

Signed:

Date:

"Non senza fatica" ["Not without effort"]

Inscription on the lintel of a doorway in *Annibal Caro 44* street, *Ascoli Piceno*, *Italy,*
casually and indelibly noticed in the summer of 2013

ALMA MATER STUDIORIUM UNIVERSITY OF BOLOGNA

Abstract

School of Engineering and Architecture
Department of Electrical, Electronic and Information Engineering (DEI)
“Gulglielmo Marconi"

PhD in Biomedical, Electrical and Systems Engineering

Electromyography Based Human-Robot Interfaces for the Control of Artificial Hands and Wearable Devices

by Roberto MEATTINI

The design of robotic systems is currently facing human-inspired solutions as a road to replicate the human ability and flexibility in performing motor tasks. Especially for control and teleoperation purposes, the *human-in-the-loop* approach is a key element within the framework know as Human-Robot Interface. This thesis reports the research activity carried out for the design of Human-Robot Interfaces based on the detection of human motion intentions from surface electromyography. The main goal was to investigate intuitive and natural control solutions for the teleoperation of both robotic hands during grasping tasks and wearable devices during elbow assistive applications.

The design solutions are based on the human motor control principles and surface electromyography interpretation, which are reviewed with emphasis on the concept of synergies. The electromyography based control strategies for the robotic hand grasping and the wearable device assistance are also reviewed.

The contribution of this research for the control of artificial hands rely on the integration of different levels of the motor control synergistic organization, and on the combination of proportional control and machine learning approaches under the guideline of user-centred intuitiveness in the Human-Robot Interface design specifications.

From the side of the wearable devices, the control of a novel upper limb assistive device based on the Twisted String Actuation concept is faced. The contribution regards the assistance of the elbow during load lifting tasks, exploring a simplification in the use of the surface electromyography within the design of the Human-Robot Interface. The aim is to work around complex subject-dependent algorithm calibrations required by joint torque estimation methods.

Summary

The thesis is organized in six chapters.

The first two chapters concern general and background notions, such as the interfacing between humans and robots, and the organization and operation of the human motor control system. Particular attention is given to the muscular activity. Chapters three to five cover the electromyography-based human-robot interfaces for the control of artificial hands and wearable assistive devices. First, a review of the state of the art is reported, and then the design and evaluation of the human-robot interfaces, that represent the contribution of the research work reported in this thesis, are illustrated. Finally, the sixth chapter outlines the conclusions.

Chapter 1 is to be intended as introductory, where the concept of human-robot interface is illustrated and contextualized, both from a cognitive and physical point of view.

Chapter 2 describes the basic concepts of human motor control. In particular, such concepts are illustrated starting from the central nervous system principles and ending with the consideration of the electromyographic signal, including its technical aspects.

A review of interfaces based on electromyographic signals for the control of robotic hands and wearable devices is reported in Chapter 3. In particular, the state of the art is illustrated, also outlining problems and future visions.

Chapter 4 presents the design of an interface for robotic hands control based on forearm muscle's electromyographic signals. Experimental results are also presented with respect to the success of grasping tasks with two different robotic devices.

Chapter 5 deals with the development of a control strategy for automatic adjustment of the support provided by wearable assistive devices, by means of the implementation of a human-robot loop based on electromyographic signals, exploring a simplification approach.

Finally, Chapter 6 describes the conclusions and outlines possible future improvements to the human-robot interfaces presented in this thesis.

Acknowledgements

If I have come this far, this is thanks to the support, work, professionalism, love, passion of many people, certainly more than those that can possibly be mentioned.

First, I want to thank my tutor Prof. Claudio Melchiorri for giving me the possibility to follow my research interests, but not only. During crucial steps, he gave me the opportunity to travel to participate in international scientific events, dedicated me time, pushed me to aim high, shared his experience and, finally, advised me on the research topic of my PhD. My sincere thanks also go to Gianluca for believing in me, for supporting, helping and suggesting to work with wearable devices. Special thanks go to Umberto for supporting me, and showing me how to deal with difficult situations and that "thinking outside the box" pays off. Thanks to the other colleagues of the LAR and of the LAB8: Daniele, Federico, Mohssen, Lorenzo, Caccia, Davide, Luigi, Alberto, Riccardo, Christian, Ahmad.

Thanks to my family and especially to my parents, who taught me the values of education and sacrifice, which, together with their unconditional and constant support, have allowed me to achieve extraordinary goals.

Finally, a great hug goes to friends and all the people who have shared any kind of moment with me.

Thank you.

Roberto

Contents

Declaration of Authorship iii

Abstract vii

Summary ix

Acknowledgements xi

1 Human and Robots: Interaction and Interface in Control 1
- 1.1 Historical Framework of Human-Robot Interaction . . . 1
- 1.2 Human-Robot Interfaces . . . 3
  - 1.2.1 Cognitive Human-Robot Interface . . . 4
  - 1.2.2 Physical Human-Robot Interface . . . 5
- 1.3 Human-Robot Interfaces in Control . . . 6
- 1.4 The Human-Robot Loop View . . . 7

2 Human Motor Control and Electromyography 9
- 2.1 Control of the Movement . . . 9
  - 2.1.1 Transmission of the information . . . 9
  - 2.1.2 Neural Control of Muscles . . . 9
  - 2.1.3 CNS Functional Control . . . 10
  - 2.1.4 Joint Biomechanics and Neurophysiology . . . 11
    - Joint Mechanics . . . 11
- 2.2 Muscle Mechanics . . . 14
  - 2.2.1 Force-Length Characteristics . . . 16
  - 2.2.2 Force-Velocity Characteristics . . . 16
  - 2.2.3 Muscle Modelling Principles . . . 17
- 2.3 Electromyography . . . 18
  - 2.3.1 sEMG Recording of Muscle Action Potentials . . . 20
  - 2.3.2 sEMG Recording Specifications . . . 20
  - 2.3.3 Biomechanical Interpretation of sEMG . . . 22

3 sEMG-Based Interfaces for Artificial Hands and Wearable Devices 25
- 3.1 Myoelectric Controls for Artificial Hands . . . 26
  - 3.1.1 Machine Learning and Proportional Control Approaches . . . 29
  - 3.1.2 Synergy-Centered View . . . 32
- 3.2 Myoelectric Controls for Wearable Assistive Devices . . . 32

3.2.1 sEMG-based applications with recent WADs . . . 34
3.2.2 A prospective simplification in WAD's myocontrol . . . 36

4 A sEMG-Based HRI for Robotic Hand Grasping Tasks 39
4.1 Acquisition System and Robotic Hands Setup . . . 40
4.1.1 Robotic Hands Description . . . 40
Architecture of the Hand Controller . . . 41
The UB Hand IV . . . 42
The Industrial Gripper . . . 43
4.1.2 sEMG Signal Acquisition Hardware and Electrodes Placement 44
sEMG Signal Pre-Processing . . . 46
4.2 sEMG-Based HRI Using Machine Learning and Synergies . . . 46
4.2.1 Selection of the Grasp Hand Shape . . . 47
SVM Training Dataset Acquisition Protocol . . . 47
Grasp Hand Shape Transition Logic . . . 49
4.2.2 Myoelectric Grasp Proportional Control . . . 49
Computation of Muscular Synergies for the Grasp Control . . . 50
Calibration Procedure for the Muscular Synergy Matrix . . . 51
The Online Myoelectric Grasp Proportional Control . . . 52
4.3 Experimental Test of the HRI and Results . . . 52
4.3.1 Training session Phase . . . 53
4.3.2 Familiarization Phase . . . 54
4.3.3 Grasping Task Phases . . . 55
Grasping Tasks Controlling the UB Hand IV . . . 56
Grasping Tasks Controlling the Industrial Gripper . . . 58
4.3.4 Conclusion and Future Work . . . 60

5 A sEMG-Based Interface for Elbow Assistive Devices 61
5.1 Assistive Application Setup . . . 62
5.1.1 Twisted String Actuation Module . . . 62
5.1.2 sEMG Signal Acquisition Hardware and Electrodes Placement 63
5.2 sEMG-Driven Assistive Application in Isometric Conditions . . . 64
5.2.1 Model of the Muscle for Isometric Contractions . . . 64
Identification . . . 66
5.2.2 Experimental Evaluation of an Assistive Application . . . 69
sEMG-Driven Control Loop . . . 70
5.2.3 Conclusion . . . 72
5.3 sEMG-Driven Assistive Application for Load Lifting Tasks . . . 72
5.3.1 The Load Lifting Tasks Protocol . . . 72
5.3.2 Myoelectric Control Strategy . . . 74
5.3.3 Experimental Session and Results . . . 76
Selection of the Threshold Values . . . 77
Online Automatic Adjustment Procedure . . . 78

5.3.4 Conclusion and Future Work 80

6 Conclusions **83**

6.1 Future Work 85

Bibliography **87**

List of Figures

1.1 cHRI concept 4
1.2 Human-Robot Loop 7

2.1 Pennation of the muscle fibers 11
2.2 Time course of a muscle twitch 15
2.3 Force-length characteristics 16
2.4 Force-velocity characteristics 17
2.5 Spring and damper elements for muscle modelling 18
2.6 Muscle model with contractile and passive elements 18
2.7 Dipole model of the propagation of a MUAP 19
2.8 Voltage waveform measured by two surface electrodes 19
2.9 sEMG biological amplifier for recording electrode potentials 21

3.1 Main subsystems of a prosthetic robotic hand 27
3.2 Functionally partitioned model for a robotic hand myocontroller . . . 28
3.3 Three dimensional representation of the myocontrol for artificial hands 29
3.4 Structure of a pattern recognition-based myoelectric system 30
3.5 Conceptual view of the structure of an "end-effector" assistive device and a wearable assistive device 34
3.6 mPower arm brace, Hand Mentor and Robot Suit HAL-5 commercial wearable assistive devices 35
3.7 Generic scheme for the architecture of a sEMG-driven control for wearable robots 36

4.1 Robotic hands controller architecture 41
4.2 The UB Hand IV and the gripper 43
4.3 Grasp types of UB Hand IV and gripper 44
4.4 The *Cerebro* sEMG signals acquisition node 45
4.5 sEMG electrodes placement 46
4.6 Functional scheme of the sEMG-based HRI system. 47
4.7 Hand gestures to be classified 48
4.8 Graphical interface for the SVM training dataset acquisition 48
4.9 FSM for the hand shape transition logic. 49
4.10 The user's overall opening/colsing motion and the robotic hand motion relative to the first postural synergy 50
4.11 Synergy-centered block diagram of the sEMG-based HRI 53

4.12 sEMG signals acquired during the training session 54
4.13 Mean value of the muscular synergy weights 54
4.14 Offline neural drives 55
4.15 Graphical simulator of the gripper 55
4.16 Tracking tasks for the subject S1 56
4.17 Grasping tasks with the UB Hand IV and with the gripper 57
4.18 Control signals for the grasp of the objects Big Box, Paper Cup and Rigid Ball 59

5.1 TSA module conceptual structure 63
5.2 View of the TSA module 63
5.3 Muscle mechanical model with lumped parameters 65
5.4 Block diagram that permits to simulate the sEMG-driven muscle behavior 66
5.5 Configuration and setup of the experimental acquisition session for the identification of the muscle model 67
5.6 Representation of the forces acting on the forearm during a load compensation 68
5.7 Biceps load force and estimated biceps tendon force 69
5.8 The TSA module worn by the subject 71
5.9 Muscle model in-loop control architecture 71
5.10 The estimated biceps tendon force F_t and the value of the muscle load during the experimental validation 73
5.11 Future conceptual design of the TSA module-based WAD for elbow assistance 74
5.12 Setup configuration used for the lifting tasks 75
5.13 sEMG-based control loop for the TSA module automatic assistance . . 76
5.14 sEMG signal behaviour during the lifting task without the assistive support 77
5.15 Resulting behaviour for the subject S2 during the lifting task with the assistive support 78
5.16 The online adjustment procedure and the lifting tasks 80

List of Abbreviations

HR	**H**uman-**R**obot
HRI	**H**uman-**R**obot **I**nterface
cHRI	**C**ognitive **H**uman-**R**obot **I**nterface
pHRI	**P**hysical **H**uman-**R**obot **I**nterface
CNS	**C**entral **N**ervous **S**ystem
DoF	**D**egree of **F**reedom
EMG	**E**lectro**M**yo**G**raphy, **E**lectro**M**yo**G**ram
MUAP	**M**otor **U**nit **A**ction **P**otential
sEMG	**s**urface **E**lectro**M**yo**G**raphy
MVC	**M**aximum **V**oluntary **C**ontraction
RMS	**R**oot **M**ean **S**quare
WAD	**W**earable **A**ssistive **D**evice
ML	**M**achine **L**earning
MAV	**M**ean **A**bsolute **V**alue
s/p	**S**imultaneous and **P**roportional
ADL	**A**ctivity of **D**aily **L**iving
TSA	**T**wisted **S**tring **A**ctuation
PAM	**P**neumatic **A**rtificial **M**uscles
PCB	**P**rinted **C**ircuit **B**oard
AFE	**A**nalog **F**ront **E**nd
Ad/Ab	**Ad**duction / **Ab**duction
NMF	**N**on-negative **M**atrix **F**actorization
FSM	**F**inite **S**tate **M**achine
SVM	**S**upport **V**ector **M**achine
ABS	**A**crylonitrile **B**utadiene **S**tyrene
LED	**L**ight **E**mitting **D**iode
PD	**P**hoto**D**etector
CE	**C**ontractile **E**lement
DTS	**D**ouble **T**hreshold **S**trategy

Dedicated to my parents, to my family

Chapter 1

Human and Robots: Interaction and Interface in Control

1.1 Historical Framework of Human-Robot Interaction

The history of interaction between the human and the robots unavoidably starts with the history of robotics. Since the beginning, the evolution of robot development has been guided by the interaction with the human actor. As a consequence, also research in the field of Human-Robot (HR) interaction is not new, even if it is recently receiving a great and growing attention in the academic community, in scientific laboratories, in companies and by media.

Although the technological development of robots have seen the light in the mid 20th century, it is worth to note that the concept of robot-like behaviour (i.e. the operation of a non-human system with artificial skills) and its implications for humans have been around for centuries in mythology, philosophy and fiction. One need only think that the word "robot" has been coined by Karel Čapek in 1920 in his play *Rossum's Universal Robots* (Čapek, 1925), originated from the Czech word *robota* ("hard work, forced labour"). However, that was certainly not the earliest example of robot-like concept. Various types of purely mechanical humanoid robots were developed in ancient Egypt, Greece and China, referred to as *automata*. Golden maids that behave like real humans can be found in the Iliad (Homer, circa 800 BC). During the Renaissance, around 1495, Leonardo da Vinci sketched a mechanical man (Rosheim, 2006). The idea of *golem* as artificial creature endowed with life has been around for centuries (Wiener, 1964) (in modern Hebrew *golem* means also robot). More recently, during the last decades collective robot imagination has had a large presence in science fiction literature, as in the most notably Isaac Asimov's novels. As a matter of fact, the very well-known Asimov's *Laws of Robotics* (Asimov, 1942) for the first time define the robots as artificial systems that stand at some laws implemented by engineers and outline the first designer guidelines for HR interaction.

The modern field of study of the HR interaction regards the understanding, design and evaluation of robots from the point of view of their usage by or with humans (Goodrich and Schultz, 2007). In such a defined context, scholars deal with hybrid systems composed by both human and technological factors. The first main

aspect that has to be considered in such kind of interactive systems is the *communication* between human and robot, that characterizes the interaction itself. In this regard, it possible to highlight a first separation of the HR interaction in two wide general categories: *remote interaction*, in which humans and robots are separated spatially and/or temporally (e.g. teleoperation of an underwater robot), and *proximate interaction*, where humans and robots are in close contact (e.g. exoskeleton robots).

Initially, the first HR interaction applications were developed for the teleoperation of hazardous material (Adams and Skubic, 2005). In this kind of operation context, through a unilateral communication generated by the usage of a hand controller, the robot was intended as a sort of extension of the human body: e.g. a long arm that could safely handle radioactive materials (Sheridan, 1992). Another environment in which the HR interaction has seen a notable development over years is that of industrial applications. Initially the human operator was assumed to provide all the necessary intelligence in order to perform specific activities, whereas manipulators were merely following the input actions directed by their operators using teach pendants. Then, in the 1960s, some autonomy was incorporated in robots. The operator could control a few discrete high-level commands, relieving the demand of human point-to-point supervision since the robot was able to automatically manage predefined aspects of its own operation (Sheridan, 1986). Subsequently, this control concept evolved in some application in the paradigm of shared control, in which the robot controlled preassigned degrees of freedom while the operator directed the rest of the motion. As an example, we can find modern application of this kind of HR interaction in the driving of means of transport (e.g. cruise control of cars, autopilot of airplanes). Later, the development of new sensors provided the possibility to enrich the communication channel between human and robot, as in the case of force sensors for giving back to the user haptic sensing of the contact with objects and environment (Kontarinis and Howe, 1995). This HR interaction paradigm has then led – together with advances in computer graphic and emerging simulated environment for robot programming (Lloyd et al., 1999) – to more advanced interaction techniques for industrial systems as *programming by demonstration* (Skubic and Volz, 2000).

Over the mentioned past decades, the HR interaction for control purposes has been fully based on the classical *Master-Slave* teleoperation paradigm, that is the human operator using an interface device (*Master*) to control a remote robot (*Slave*). Although the communication was also assisted by force feedback about interaction forces between slave robot and environment, tasks characterized by uncertainly which are normally performed by humans, cannot be easily conducted under classical Master-Slave teleoperation (e.g. drilling, reaming, chipping). This can be due to limits related to the quality of the sensory information and/or the stability and transparency of the teloperation system (Hannaford, 1989). The presence of these kind of limitations has led to search for new directions in the development of HR interaction systems, with the aim of reaching robots' interaction performances close

to those achieved by humans. In the current scenario, one main road toward this perspective is the increasing of the interaction entity between human operator and robot, that means no longer only a mere exchange of information in a Master-Slave paradigm, but rather a closer interaction involving physical and cognitive modalities. In particular, this has made possible for HR interaction to be influenced by many different new fields. Indeed, research advances have been made over years in sensing techniques, increased computational capabilities, new control paradigms, new method of artificial intelligence and virtual reality, and HR interaction has gathered and accommodated this new possibilities. Such influences have given to the field of HR interaction an inherently multidisciplinary dimension. It is in this context that the HR interaction field leads also to the development of medical (Taylor et al., 2000) and wearable (prosthetic, rehabilitation and assistance) (Pons, 2008) robots.

The ongoing growing and expansion of the HR interaction field has made it a stand-alone discipline, which deals with the problem of understanding and shaping the interactions between humans and robots, evaluating the related capabilities and designing the technologies and training to produce desirable interaction performances. As already mentioned, the interdisciplinarity is wide and requires contributions from engineering, medical, cognitive science and even linguistic and psychology fields. The design of modern HR interaction systems takes into account specifications related to the level of robot autonomy, the nature of information exchanged between human and robot, the adaptation, learning and training of both people and robots and, last but not least, the shape of the task, guided by the objective of make the HR interaction beneficial in terms of a defined goal (Goodrich and Schultz, 2007).

In such a context, the *interface* used in HR interaction systems has seen the development of new modalities that open the door to a more interactive communication and, at the same time, has gained a leading role for the improvement of the robot control, which are now more then ever capable of performing an incredible variety of tasks and are going in the direction of increasingly being used in everyday life. Indeed, despite robots came to light more than 50 years ago, the way humans control them is still an important issue, and HR interface study and development can bring to new solutions for a more natural and intuitive control techniques.

1.2 Human-Robot Interfaces

Whichever HR interaction is supported by a *Human-Robot Interface* (HRI), which is the link that allows the modulation of the infomation and/or power flow between human and robot. The typologies of HR interaction for control purposes can be divided in two branches : a *physical* HR interaction entails the exchange of a flux of mechanical power between the human and robot actors, whereas a *cognitive* HR interaction involves the cognition process that makes the human capable of controlling a robot while remaining aware of its functional possibilities (Pons, 2008). Similarly, a

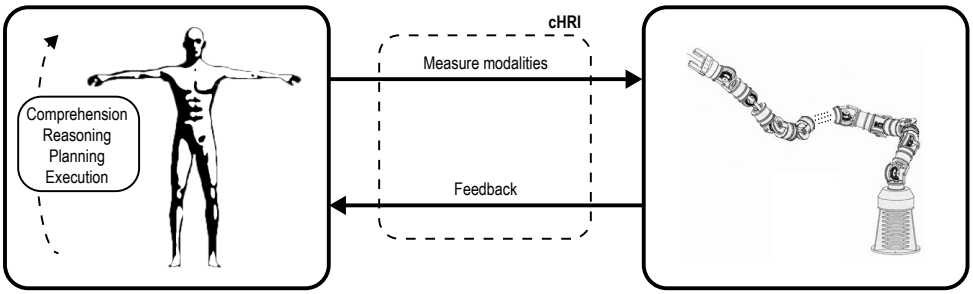

FIGURE 1.1: Cognitive Human-Robot Interface (cHRI) concept.

cognitive HRI (cHRI) is explicitly developed to support the cognitive HR interaction and is normally based on the information adcquired by means of a set of bioelectrical and/or biomechanical measures, whereas a *physical HRI* (pHRI) is based on a set of actuators and/or rigid links to support the physical HR interaction. A cognitive interaction can be triggered by a robot action, as well as a robot behaviour can be modified based on a proper measurement of a cognitive process.

1.2.1 Cognitive Human-Robot Interface

The execution of an action in order to reach a goal is necessarily preceded by a preidentified problem, and it is a consequence of a series of activities including comprehension, reasoning and planning (and, finally, execution) that define a *cognitive process*. Such process can be quantified to a certain extent and dimension through one or more modalities. The derived information is acquired and transmitted through the HR interaction channel by means of the hardware and software components that compose the cHRI. These concepts are depicted in Fig. 1.1.

One of the most interesting and challenging aspects of research in the field of cHRI is the realization of natural control channels, on which also the reasearch reported in this thesis is focused. In this relation, one recent promising direction is the use of information from the human cognitive processes by means of bioeletromechanical measures directly performed during the execution of the interaction and control task (Ratanaswasd et al., 2005). This kind of approach is know as *nautal interface* (Sharma, Pavlovic, and Huang, 1998). The advantages of natural cHRIs can be found in a series of aspects concerning that: *(i)* control strategies can be improved by taking inspiration from humans' natural control mechanisms that are fully optimized, *(ii)* the use of natural outputs for a cHRI can obviate delays introduced by the measurement of the cognitive processes and the training necessary to teach users mapping commands in nonnatural imposed sequences of actions, and *(iii)* interacting directly with natural cognitive processes can improve acceptability and performances of rehabilitation and prosthetic robots.

The direction and the typology of the information along the HR channel influence the design of cHRIs (Fig. 1.1). In this regard, it is possible to make a classification between unidirectional and bidirectional interfaces. Unidirectional cHRIs are

defined as interfaces where the user has no feedback information about the state of the controlled robot (Pons, 2008), yet in practice at least the natural visual and/or auditive feedback modalities are present; therefore we define unidirectional cHRIs as interfaces with no specifically designed artificial feedback. In bidirectional cHRIs the user receive a feedback based on a command sent over the HR channel and/or the consequent robot status, by means of the action of components expressly integrated in the interface. In this way, a symbiotic interaction between the subject and the robot is established, which can increase awareness of the human improving the control performances of the robot (Scholtz, 2002).

In modern cHRI one key element is the exploration of different communication modalities to avoid the saturation of cognitive channels, leading to an interaction at multiple levels. Recently, *multimodal* approaches (e.g. (Jaquier et al., 2017; Nowak, Eiband, and Castellini, 2017; Di Nuovo et al., 2016)) propose the application of such multilevel communication to gather more realistic and robust information and to obtain a better understanding of cognitive phenomena by means of data fusion techniques.

1.2.2 Physical Human-Robot Interface

The principal feature of a pHRI is the intrinsic physical interaction in which human and robot are couple by a controlled exchange of forces between both actors. In this applications, the behaviour of the two agents needs to be modulated in order to reach a level of coordination that leads to a target reciprocal adaptation. The result has to be twofold: to achieve an goal interaction behaviour and to avoid unexpected action that can result in human injuries. It follows that the human being is a fully integrated part of the design of pHRIs, not only at a cognitive level (see Subsec. 1.2.1) but also in the practical physical sphere of forces exchange, making the govern of this kind of system one of the most exciting and challenging aspects in HR interaction research. The present thesis work also deals with this problem.

One of first aspect that it is worth to mention for the design of pHRIs is the physiological factor of the interaction. Indeed, pHRIs imply a touch contact, and therefore the composition of the human sensory receptor system should be known. The sensors directly implied in touch perception are called mechanoreceptors and are mostly located in the human skin (Despopoulos and Silbernagl, 2003). Pressure and tactile sensors are basically sensitive to the skin deformation, working as displacement sensors. Sensation of pain and temperature is due to nerve endings that are located closer to the skin surface. The internal sense of force, position and movement is provided by special mechanoreceptor called proprioceptors, that are present in muscles, joints and tendons. The awareness of movements, pressure, touch, vibration, strain are at the base of the human haptic perception which play a fundamental role in pHRIs.

Realization of suitable pHRIs is one of the most challenging problem in HR interaction. In the design process, mechanical structures, sensors, actuators and control

architectures has to be considered together to obtain a desired result. General guidelines in pHRI development should take into account several aspects: *(i)* the safety of the human operator in terms of generated force that have to not damage joints and limbs, *(ii)* pHRIs should ensure comfort providing forces compatible with the human skeletal structure (e.g. actuator workspaces that prevent misalignment strains on joint axes), *(iii)* soft tissues should be used to ensure proper intensity and mode of transmission of the forces to the human musculoskeletal system and *(iv)* a proper control strategy has to be implemented in the design of the pHRI to permit the adpatation of the HR system in closed-loop, achieving a common goal stability.

1.3 Human-Robot Interfaces in Control

There are different applications where HRIs are used for control purposes. In such context, HRIs aim on provide to the human subject instruments and functionalities through which establish a fruitful communication channels to send commands to the robot. A possible classification can take into account the applications that influence the design of the HRI, which can be grouped in performance augmentation, telerobotics, assistive compensation and rehabilitation.

In performance augmentation, the goal of the control strategy implemented in the HRI is to make the robot track the movements executed by the human subject, while at the same time empowers them so that the effort to move a limb or transport a load is given by the robot's actuators and not by the human's muscles. Mainly pHRIs are involved in the control strategy realization.

In telerobotis applications, the user has to control a remote robot to accomplish a desired task, by means of a bilateral information through a teleoperation channel that has to guarantee maximum possible transparency. The relative HRIs deal with the acquisition of kinetic, kinematic or biological information, where the interaction is normally mostly cognitive.

When humans need to control a robot to get assistance for the performance of certain tasks, it means that the robot has to understand commands in order to provide an assistive compensation. In this kind of applications, differently from performance augmentation, a cHRI is also necessary since the robot as to know when to provide mechanical power: the control strategy is not based only on physical interaction, yet a cognitive process is involved through which the user can send commands to select the timing and/or the type of assistance.

In the field of rehabilitation, the control approach is to use a training program in which the robot become a repetitive trainer to allow the user exercise target articulation on desired axis. In other applications, the the user wants to control an electromechanical wearable robotic limb with the aim of replace a lost limb function, with the goal of achieving it in a way as closer as possible similar to the natural one. Cognitive and physical interactions have to be considered for the related HRI.

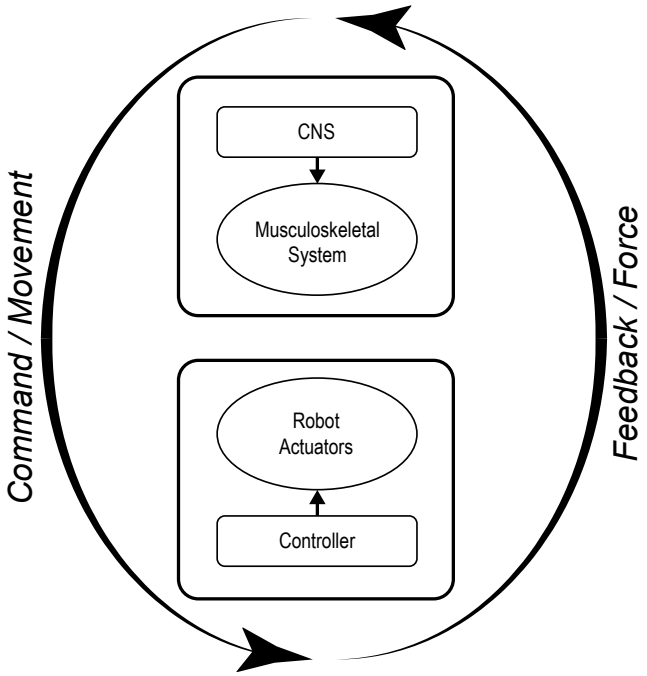

FIGURE 1.2: The human-robot loop scheme.

1.4 The Human-Robot Loop View

As already outlined in the previous sections, in a HRI both human and robot work together to achieve a common goal. We are in presence of a combination of two control systems: the human motor control and the robot controller, which are interacting during the interfacing through their sensory and motor channels. In particular, the body-related physical state and environment are perceived by human receptors, while, at the same time, the Central Nervous System (CNS) records and interprets sensory information in order to deliver motor actions as the result of the elaboration of a cognitive process. On the other hand, similarly, the robot detects machine and environment state, interpreting sensors and commanding actuators through the action of the robot control system. In this scenario, how the human understands the robot in such a coupled scheme is a central point, because it concerns the development of advanced control strategies for a more natural interaction from the user point of view. Indeed, we are in the situation of a human-robot loop scheme – depicted in Fig. 1.2 – in which the capacity of the two systems for mutual adaptation is a key aspect that cannot help but be preceded by a reciprocal understanding.

Within this view, recent studies have highlighted the comprehension of how human motor control modifies mechanical properties during the execution of limb functional tasks as a promising road toward a software and hardware design of robots for a more natural HR interaction (Ajoudani, 2016). In this way, efforts to elucidate underlying human neuromotor strategies can be transferred into robot control modalities enhancing the understanding and adaptation within the human-robot loop paradigm (see Fig. 1.2).

A prominent aspect that has been addressed, is that of the exploitation of viscoelastic properties of the neuromuscular system during motor control tasks. Indeed, the modulation of the impedance of the neuromuscular system is used by the CNS to simplify the high complexity of controlling multi-joint and multi-muscle limbs (Hogan, 1984), thanks to the exploitation of the restitution forces against external actions and of the viscoelasticity as a peripheral control gain.

In the context of the research interests of the present thesis work, it is worth to highlight that the modulation of the viscoelasticity in humans is performed by regulating the level of muscle co-contraction. In particular, it has been demonstrated that surface electromyographic signals can be used for the measurement of muscle co-contraction, because they are highly correlated with muscle tensions and joint stiffness (Osu and Gomi, 1999). Together with a general overview, this is one of the aspects that will be deepened in the next chapter.

Chapter 2

Human Motor Control and Electromyography

2.1 Control of the Movement

In humans the control of the movement lies in the nervous system, and originates in the transmission of bioelectrical signals through the body. If we think to robotic systems, information is generally processed in a digital form by the controller. Then, the outputs of the controller – in a similar way – are generally digital values that are converted to analog inputs to the actuators. The transmission of the information is normally along parallel lines in which the values are encoded, connecting the various components of the robot. In humans, the nervous system transmits along a serial line, in which the value is encoded by means of electrical impulses, and in particular in terms of their frequency. This impulses are know as *action potentials*.

2.1.1 Transmission of the information

The transmission of the information is due to specialized cells called *neurons*, which also generate the action potentials (Kandel et al., 2000). For a voluntary activation of muscles, the signal transmission path originates in specific regions of the brain and goes through the brainstem to the spinal cord, finally reaching the target muscles. The CNS is composed by neurons present in the brain, the brainstem and the spinal cord, and can be seen as a hierarchical controller. In this view, the output of neurons in the brainstem and spinal cord are modulated by the neurons in the brain, whereas neurons in the brainstem principally modulate the output of spinal cord neurons (Burdet, Franklin, and Milner, 2013).

2.1.2 Neural Control of Muscles

To understand the way a muscle is controlled at low level, first it is necessary to consider that a muscles consist of bundles of individual fibers. A single neuron located in the spinal cord, called *α-motoneuron*, controls tens of muscle fibers. Note that the fibers are relatively randomly distributed throughout the muscle. A very important basic functional component of the motor control system is the *motor unit* (Heckman

and Enoka, 2012), composed by the α-motoneuron and its group of controlled muscle fibers. The *nerve fibers* are individual axons leaving the spinal cord, whereas bundles of nerve fibers are calles simply *nerves*. Various locations of the body can be reached by groups of nerve fibers, in order to control specific muscles. It is important to highlight that a single muscle fiber is controlled by a single α-motoneuron.

Sensory receptors are also sending signals to motoneurons, from different location of the body. Some important receptors have the role of transforming mechanical events into action potentials, and are located principally in the skin. The *peripheral nervous system*, is the part of the nervous system located outside of the spinal cord that is composed by sensory receptors and motoneurons.

The output of an α-motoneuron is determined by an integration of several inputs that come from various neurons, including peripheral sensory neurons. The nature of some of them can be excitatory, or inhibitory for others. The overall results of the integration of such multitude of inputs represents the motor unit control signal. In particular, the inverse of the interval between successive action potentials (known as *train* of action potentials) determines the modulation of the amount of motor unit force. In this way, a greater force produced by the muscle fibers of the motor unit is due to a higher firing rate. Any change of in the muscle fiber force command must correspond to a change in the firing rate.

2.1.3 CNS Functional Control

The structure of the CNS includes the brain, the brainstem and the spinal cord. The spinal cord accommodates the so-called *lower* motoneurons, which are the neurons that send control signals directly to the muscles. However, it is important to notice that the CNS is composed by billions of neurons and also many of them are involved in the control of the movement.

Motoneurons in the spinal cord receive inputs from local circuit neurons that are called *interneurons* and also from neurons in the brainstem and brain which are normally referred to as *upper* motoneurons. Signals from brain and brainstem are also sent to interneurons. Lower motoneurons and brainstem upper neurons are both receiving the control signals from the upper motoneurons in the brain, thanks to a very complex network connections that involves a great number of brain areas belonging to regions with specialized functions different from the motor control.

In recent years, it has been suggested a simplification view in the way the CNS control groups of muscles. According to this view, the motor control is simplified by coordination of groups of muscles by engaging spinal interneurons (Bizzi et al., 2008). The relative activation of muscles of the same group can be modulated by a network of spinal interneurons that regulates the synaptic input to the different fibers. The emerging relative activation pattern, if sufficiently constant, is referred to as a *muscular synergy*. By selecting the relative timing and weights of each synergy, the idea is that the higher-level control can more simply achieve a wide number and type of movements for different kind of tasks.

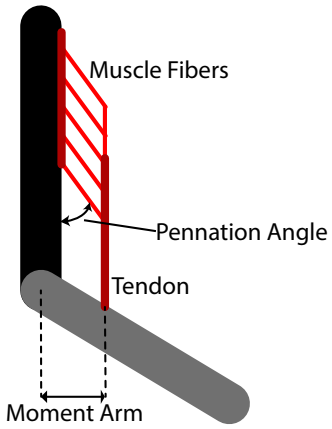

FIGURE 2.1: Pennation of the muscle fibers and attachment of the muscle to a skeletal segment.

2.1.4 Joint Biomechanics and Neurophysiology

In order to report basic notions of neuromechanics it is necessary to go in some details of the mechanics of the muscles attached to the body segments and of the control of the joints by the CNS. In particular the focus will be related to the single joint, in the sense of a single degree of freedom (DoF) of movement of an articulation, that means a rotation of a body segment.

Joint Mechanics

The transformation of muscle force to joint torque – and therefore of muscle motion to joint motion – is determined by the perpendicular distance from the line of action of the muscle to the instantaneous axis of rotation of the joint, which takes the name of *moment arm* (see Fig. 2.1) (Burdet, Franklin, and Milner, 2013). For a given muscle force, a greater joint torque is obtained with a longer muscle moment arm, at a cost of less joint motion for a given amount of muscle length variation. This can be seen in the following equations.

$$\begin{aligned} \tau &= \rho\mu \\ \rho &= \frac{d\lambda}{dq} \Rightarrow dq = \frac{d\lambda}{\rho} \end{aligned} \tag{2.1}$$

where τ is the joint torque, μ is the muscle force, q is the joint angle, λ is the muscle length and ρ is the muscle moment arm.

Changes in the length of the muscle moment arm can be due to differnt factors. Often, there is a variation due to a modification in the direction of the line of action of the muscle when a joint angle changes. This is the case when he angle between tendon and bone varies during rotations or when muscle fibers are displaced as the result of a contraction.

When a joint is considered, the muscles acting on it can be classified as *agonistic* or *antagonistic*. Antagonistic muscles produce torques that cause opposite rotations of the joint, whereas agonistic muscles produce torques that cause rotations of a joint in the same direction. The net torque τ resulting from the counteracting forces generated by antagonistic muscles is equal to the difference of the torques created by each muscle.

$$\tau = \tau_+ - \tau_- = \rho_+\mu_+ - \rho_-\mu_- \tag{2.2}$$

where τ_+ is the joint torque due to the force μ_+, which is generated by the muscles that makes the joint rotates in the same direction (with a moment arm ρ_+), and τ_- is the joint torque generated by the force μ_- due to muscles that would make the joint rotate in opposite directions (with a moment arm ρ_-).

It is possible to define joint stiffness and damping, considering that they are rotational quantities. Indeed, joint torque is proportional to the muscle moment arm, whereas joint stiffness and viscosity are proportional to the square of the moment arm. This can be described with the following equations.

$$\begin{aligned} K &= \frac{d\tau}{dq} = \rho\frac{d\mu}{dq} = \rho\frac{d\mu}{d\lambda/\rho} = \rho^2\frac{d\mu}{d\lambda} = \rho^2 K_\mu \\ D &= \frac{d\tau}{d\dot{q}} = \rho\frac{d\mu}{d\dot{q}} = \rho\frac{d\mu}{d\dot{\lambda}/\rho} = \rho^2\frac{d\mu}{d\dot{\lambda}} = \rho^2 D_\mu \end{aligned} \tag{2.3}$$

where K is the joint stiffness, τ is the joint torque, q is the joint angle, μ is the muscle force, ρ is the moment arm, λ is the muscle length, K_μ is the muscle stiffness, D is the joint viscosity, $\dot{q}$ is the joint angular velocity, $\dot{\lambda}$ the rate of change of muscle length and D_μ is the muscle viscosity.

During a joint angle displacement, generated forces are increased for stretched muscles and decreased for shortened ones. For this reason, it possible to consider the joint stiffness and viscosity of the joint as a summation of all the contributes from all muscles:

$$\begin{aligned} K &= \frac{d\tau}{dq} = \frac{d(\tau_+ - \tau_-)}{dq} = \rho_+\frac{d\mu_+}{dq} - \rho_-\frac{d\mu_-}{dq} = \rho_+\frac{d\mu_+}{d\lambda_+/\rho_+} - \rho_-\frac{d\mu_-}{d\lambda_-/\rho_v} \\ &= \rho_+^2\frac{d\mu_+}{d\lambda_+} - \rho_-^2\frac{d\mu_-}{-d\lambda_-} = \rho_+^2 K_{\mu+} + \rho_-^2 K_{\mu-} \\ D &= \frac{d\tau}{d\dot{q}} = \frac{d(\tau_+ - \tau_-)}{d\dot{q}} = \rho_+\frac{d\mu_+}{d\dot{q}} - \rho_-\frac{d\mu_-}{d\dot{q}} = \rho_+\frac{d\mu_+}{d\dot{\lambda}_+/\rho_+} - \rho_-\frac{d\mu_-}{d\dot{\lambda}_-/\rho_v} \\ &= \rho_+^2\frac{d\mu_+}{d\dot{\lambda}_+} - \rho_-^2\frac{d\mu_-}{-d\dot{\lambda}_-} = \rho_+^2 D_{\mu+} + \rho_-^2 D_{\mu-}. \end{aligned} \tag{2.4}$$

It results that the total joint stiffness and viscosity are functions of muscle force, given that the muscle stiffness and viscosity are functions of muscle force too. In the following equations, the expression of the joint stiffness and viscosity are written in

the light of a linear approximation in the relation between stiffness or viscosity and muscle force.

$$K = \rho_+^2 K_{\mu+} + \rho_-^2 K_{\mu-} = \rho_+^2 (k_+ + c_K \mu_+) + \rho_-^2 (k_- + c_K \mu_-)$$
$$D = \rho_+^2 D_{\mu+} + \rho_-^2 D_{\mu-} = \rho_+^2 (\delta_+ + c_D \mu_+) + \rho_-^2 (\delta_- + c_D \mu_-) \tag{2.5}$$

where (k_+, k_-) and (δ_+, δ_-) are the contributions to muscle stiffness and viscosity by passive forces and c_K and c_D are coefficients relating active muscle force to muscle stiffness and damping, respectively.

The limbs and the environment can be seen in the view of their mechanical interaction, which is an important concept in relation to the execution and contol of motor tasks (Milner, 2009). A formal definition of mechanical impedance can be given considering an imposed motion and therefore the relative forces that a mechanical system generates in response. Considering the mechanical nature of the muscles, we can say that the moment arms and the muscle viscoelasticity will determine the mechanical impedance of a joint, as it clear from eq. 2.5.

Looking at eq. 2.2, the number of possible solutions is not unique with respect to μ_+ and μ_-. In particular, when the number of muscles acting across the joint increases, the number of solutions increases as well. Therefore, for a given net joint torque, the generation of a possible joint impedance can be done according with a relatively large range of possibility: in other terms, the joint torque and the joint impedance – over a certain range – can be controlled independently by the nervous system. This provides flexibility in the selection of a dynamic behavior of the joint, allowed by the modulation of the co-contraction of antagonistic muscles.

In this relation, generally muscle contractions generate movements that are initiated from rest, and the related motion about a joint is controlled in a reciprocal manner by antagonistic group of muscles. Accelerations are produced by muscles *agonists* of the movement, whereas decelerations are given by muscles *antagonists* of the movement. An interesting aspect is that, considering movements in which high velocity must be achieved over a brief interval, large bursts of agonists muscle activation is used to achieve high accelerations. In this way, high firing rates in relation to the recruiting of many motor units can provide very rapid activations. However, since muscle force does not instantaneously relax, the intended final position would tend to be overshooted in the case of movements that are rapid and small. As a consequence, it happens that antagonists muscles must be activated shortly after agonists muscles in order to create a torque impulse in the opposite direction, with the aim of limiting the extent of rapid and small amplitude movements. Therefore, in this case, the mechanical impedance of the joint can be seen as a consequence of the overlapping of agonists and antagonists muscle activations. Furthermore, another point of view is also related to the fact that the stability around the final position will be increased thanks to the muscle co-contraction.

The motion of a limb segment can be modelled as a linear second-order system, described by the equation

$$\tau(t) = I\ddot{q}(t) + D(\dot{q}_u(t) - \dot{q}(t)) + K(q_u(t) - q(t)) \tag{2.6}$$

where I is the limb inertia, $q_u(t)$ is the desired trajectory and D and K are joint viscosity and stiffness, respectively. Note that, for example, negative impedance is also possible in case of interaction that assists imposed motions. This comes from the fact that D and K are not constant but vary with the amount of muscle activation and, furthermore, torque and impedance are adapted to the dynamics of such activity.

2.2 Muscle Mechanics

The muscles can be considered one of the most interesting and challenging area of study in biomechanics. Research in this field continues to deal with concepts related to neural control, metabolism and biomechanical characteristics.

As already introduced in subsec. 2.1.2, the motor unit is the smallest subunit that can be controlled in a muscles. This comes from the fact that muscle fibers are innervated by a single motor axon.

Going through some details of basic structure of a muscle, the part that generates the tension is known as *contractile element*, that is the elemental region that shortens and lengthens as positive or negative work is done. Here, myosin filaments interact with narrower actin filaments, by means of special structure known as *cross-bridges* where the tension is created and proper shortening or lengthening takes place. With the term *sarcomere length* it is indicated the basic length of the myofibril. A single contractile element is composed by many sarcomere elements in series, in an overall muscle structure that is such that many filaments are positioned in a parallel way. In particular, the *fascia* is a fibrous structure of connective tissue that contains the active contractile elements. Connection to the tendons and separation of the muscle fibers into layers and groups si also due to the same connective tissue.

In a muscle, the tension can be increased in two ways: by an increase in the stimulation rate for a motor unit or by the recruitment of an additional motor unit. Note that each nerve ending separately controls a motor unit – which relative quantity in a muscle is finite – and the mechanical response as a result of an action potential drive (subsec. 2.1.2) is a twitch of tension (Winter, 2009). The motor units during a muslce contraction are recruited in a sequential way. A reverse process happens when the muscle tension has to be reduced. In particular, given an order from that the motor units were recruited for increasing tensions, they drop out in the reverse order when tension decreases. Note that the firing rates increase nonlinearly when force increases, thought it always grows in a monotonic way.

Let's now take into account an individual twitch, that is the the smallest increment of tension. All motor units present the same characteristic shape, though they

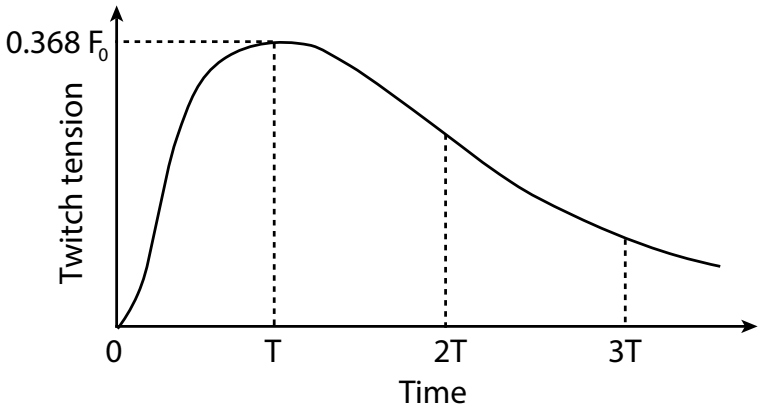

FIGURE 2.2: Time course of a muscle twitch.

are characterized by individual differences in each newly recruitment process. In particular, a critically damped second-order system can describe the time-course curve of a motor unit quite closely, if the response to the impulse is considered (Milner-Brown, Stein, and Yemm, 1973). Indeed, the consideration of the electrical stimulus of a motor unit is lecit since it has a short duration. The much longer duration twitch is the mechanical response to this impulse. In the following equation, the second-order critically damped impulse response is expressed.

$$F(t) = F_0 \frac{t}{T} e^{-t/T} \tag{2.7}$$

where, referring also to Fig. 2.2, T is the twitch time (that is, the time for the tension to reach the maximum) and F_0 is a specific motor unit-dependent constant. In Tab. 2.1 it is possible to observe some typical mean values of T (Buchthal and Schmalbruch, 1970).

It has been found that in case of cooled muscles, the value of T increases, caused by slower metabolic rates and increased muscle viscosity. In general, it is important to consider that muscle and person characteristics, as well as experimental/external conditions that considerably influence the contraction time.

TABLE 2.1: Typical mean values of T.

Tricepsbrachii	44.5ms (16–68 ms)
Biceps brachii	52.0 ms (16–85 ms)
Tibialis anterior	58.0 ms (38–80 ms)
Soleus	74.0 ms (52–100 ms)
Medial gastrocnemius	79.0 ms (40–110 ms)

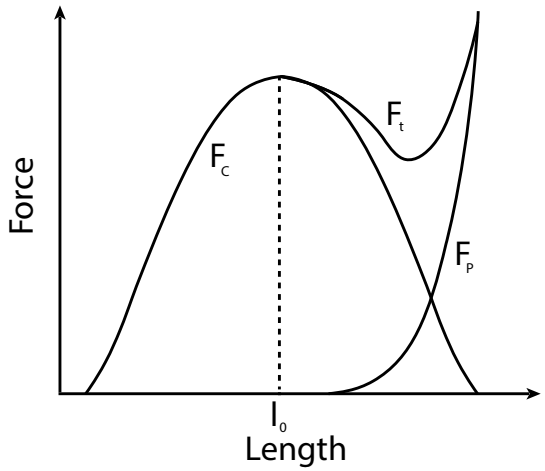

FIGURE 2.3: Force-length characteristics of a skeletal muscle.

2.2.1 Force-Length Characteristics

The passive connective tissue and contractile element (the active element) are the components of a muscle, as already illustrated. Therefore, in order to have a resulting muscle force-length characteristics, a combination of both active and passive elements characteristics is necessary.

The force-length curve is influenced by the connective tissue, which surrounds the contractile element. In particular, it is similar to an elastic band, known with the name of *parallel elastic component*. The state of the parallel elastic component is slack when the muscle is at resting length (or less), that means there is no tension on it. Tension begins to build up as the muscle lengthens, making the parallel element no longer loose. The parallel element is quite nonlinear, differently from most springs that present a linear force-length relationship. In Fig. 2.3 it is possible to observe the overall force-length characteristic F_t, that is given by the summation of the force-length curve of the parallel elastic element F_p and of the overall contractile component F_c (at maximum contraction).

The *series elastic element* includes the tendon and all connective tissues in series with the contractile component. In the case of isometric contractions, the increasing of the tension causes a slightly lengthen of such element. Differently, during dynamic situations it influences the time course of the muscle tension, in conjunction with viscous components.

2.2.2 Force-Velocity Characteristics

The changing in muscle length is fundamental for the accomplishment of movements. Any given motion is regularly generated by alternative muscle shortening and lengthening. Therefore, to know how muscle tension is affected by muscle velocity has particular importance.

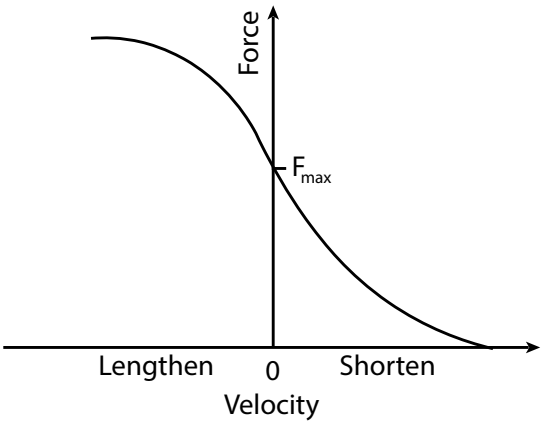

FIGURE 2.4: Force-velocity characteristics of a skeletal muscle.

Fig. 2.4 shows the force-velocity characteristics (depicted for maximum contraction), considering that the tension in a muscle decreases as it shortens under load. Such characteristics is related to a certain muscle length. For this reason, a three-dimensional plot is necessary to represent the contribution of the length as a variable as the velocity. In such graph, the resultant characteristics is actually a surface.

The causes of the decrease of tension when shortening velocity increases are multiple. First, the loss in tension in the contractile element appears to be the main reason. Second, the fluid viscosity is generating friction that needs to be overcome by an internal force, resulting in a reduction in the tendon force. For these reasons the force-velocity curve is typically complicated to describe.

2.2.3 Muscle Modelling Principles

In order to go over the principles behind the modelling of muscles for the prediction of the tension, a crucial point is that one related to the representation of the different components (Winter, 1976; Winter, 2009). Generally, force-displacement and force-velocity relationships of linear and nonlinear springs and dampers (see Fig. 2.5) are used to describe the behaviour of the passive components. Many configurations are possible for the total passive elements model. Possible structures can be with the damper in parallel with the parallel elastic component, or alternatively the latter can be in parallel with the series of the damper and the series elastic component. Note that, in case of linear components, different configuration are equivalents with the same dynamic characteristics.

Furthermore, a force generator is also necessary in the total model in order to represent the active contractile component (Winter, 2009). The term *active state* is normally used to refer to the time course of the tension from the contractile component. The active state is quite often assumed to be an exponential response to a stimulus, as illustrate in Fig. 2.6 where it is present the combination of the passive components and the contractile component along with the time course of the active state F_c and the relative tendon force F_t.

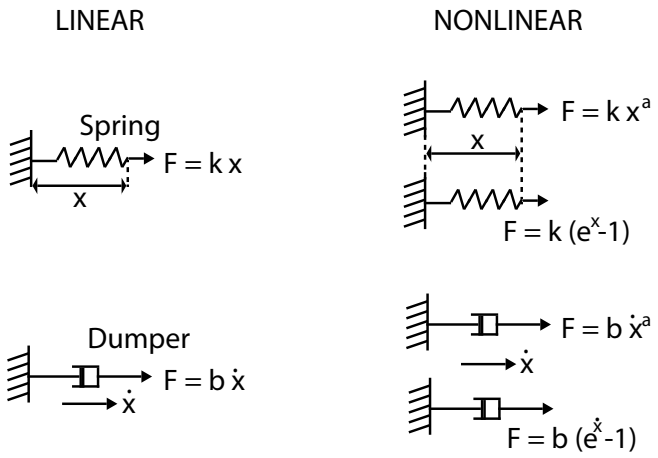

FIGURE 2.5: Spring and damper elements to represent passive characteristics of muscle.

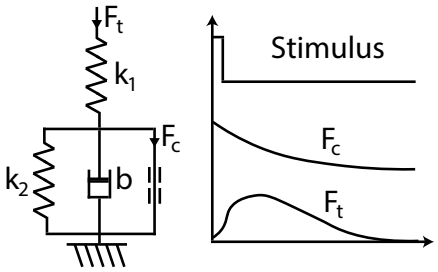

FIGURE 2.6: Muscle model with contractile and passive elements.

Finally, in order to take into account the motoneuron drive of a muscle, a realistic model must have a valid input for its representation. A good and widely used compromise is to record the electromyographic signal from the muscle, so that it is available a summation of the activity of a certain number of recruited motor units coming from the measurement the outputs superposition of a motoneuron pool.

2.3 Electromyography

The *electromyogram* is the electrical signal measured from the contraction of a muscle, whereas the *electromyography* is a term indicating the studies and the techniques related to the electromyogram. Both electromyogram and electromyography can be indicated with the acronym EMG in this thesis work. Although at any given time there are normally many variables that influence the electromiogram, the voluntary increase of the muscle tension generates an increase of the magnitude of the EMG signal that is clearly appreciable.

In such regard, it is important to take into account that as axons transmit action potentials, in a very similar way also the muscle tissue will conduct electrical potentials. This electrical activity comes from the muscle fibers as a result of the recruitment of motor units (see subsec. 2.1.2), and takes the name of motor unit action

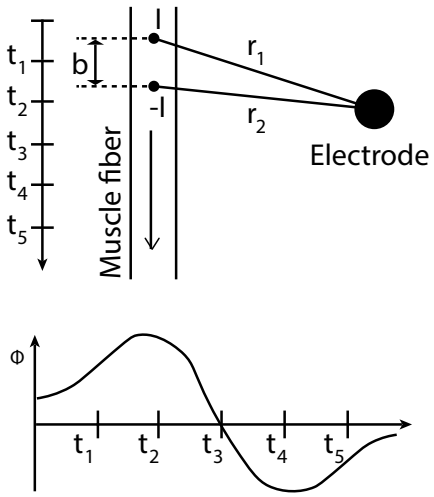

FIGURE 2.7: Dipole model of the propagation of a MUAP wave recorded by a surface electrode.

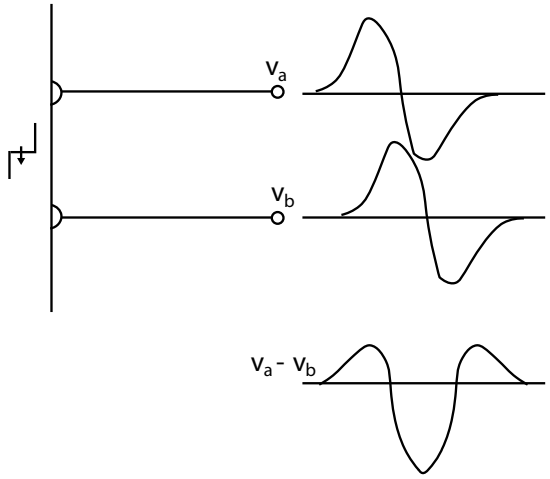

FIGURE 2.8: Voltage waveform measured by two surface electrodes.

potential (MUAP). In practice, along the direction of the muscle fibers, the result is the propagation of a depolarization wave, which, together with the subsequent repolarization wave, composes what is recorded by EMG electrodes.

There are two groups of EMG electrode types: intramuscular and surface. Surface electrodes (sEMG, surface electromyopgrahy) – on which there is more interest in relation of the present thesis work – consist of disks with about 1 cm in diameter made of silver or silver chloride. In general, the recordings of this kind of electrodes are more reproducible, but detect only the average activity limited to the more superficial muscles (Kadaba et al., 1985). On the other hand, fine movements or deep muscles related recordings can be assessed using indwelling electrodes, which are composed by a fine hypodermic needle with an insulated conductor located inside.

2.3.1 sEMG Recording of Muscle Action Potentials

To see how the propagation of motor unit action potential waves is recorded by surface skin electrodes, it is useful two consider the dipole scheme depicted in Fig, 2.7. In such a model, two points are considered: I, where the depolarization is represented by means of a source of current, and $-I$, where the repolarization is represented. Along the fiber, the current is assumed to be concentrated only in these two points, separated by a distance b. A point electrode is located at a distance r from the current source. In this configuration, the potential Φ can be expressed by (Fuglevand et al., 1992)

$$\Phi = \frac{I}{4\pi\sigma}\frac{1}{r} \tag{2.8}$$

where σ is the conductivity of the medium. At the point electrode, the net potential is recorded from both source and sink currents. It can be expressed as

$$\Phi_{Electrode} = \frac{I}{4\pi\sigma}\frac{1}{r_1} - \frac{I}{4\pi\sigma}\frac{1}{r_2} = \frac{I}{4\pi\sigma}\left(\frac{1}{r_1} - \frac{1}{r_1}\right) \tag{2.9}$$

where r_1 and r_2 are the distances to the source and sink currents. Note that r_1 and r_2 vary with time as the wave propagates along the muscle fiber, influencing the time history of the recorded action potential. The single electrode is therefore recording a biphasic wave (see Fig. 2.7). Such wave is affected by a number of recording and biological factors (Winter, 2009), as the depth of the fiber, the distance b and the velocity of propagation. In particular, also the electrode surface area plays a role, which in real application presents a finite surface with a potential that is the average of all point-source potentials.

The voltage waveform that is recorded with most sEMG setups is the difference in potential between two electrodes located over the muscle site. The results is a triphasic potential waveform, that comes from the subtraction of two biphasic potential waveforms that are shifted slightly in time, as depicted in Fig. 2.8.

2.3.2 sEMG Recording Specifications

sEMG is basically a biological amplifier and certain specifications are required for its electrodes in order to avoid problems and get a clean myoelectric signal. Usually power lines or machinery are generators of noise, but it can be also ascribed to the amplifier. False components of the signals generated by the electrodes themselves or by the cabling system are normally indicated as *artifacts*. In particular, *movement artifacts* are a standard type of noise resulting from touching the electrodes and moving the cables, generating low-frequency baseline jumps. In general, there are some considerations to take into account about a sEMG amplifier for signal recording.

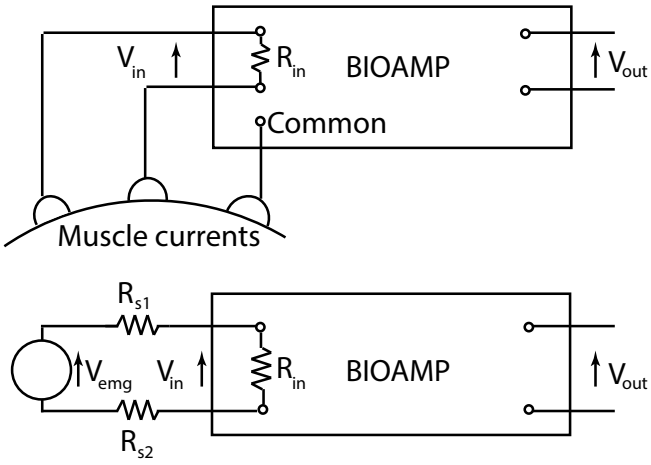

FIGURE 2.9: sEMG biological amplifier for recording electrode potentials.

The bioamplifier normally has to work in a range of gains selectable from 100 to 10,000, considering that sEMG can reach peaks of 5 mV in amplitude during Maximum Voluntary Contractions (MVCs) (Winter, 2009), defining the gain of the amplifier as the ratio of the output voltage to the input voltage. Furthermore, the appearance of the amplitude of the signal at the electrodes should be reported faithfully in the output.

In order to not attenuate the EMG signal as it is connected to the input terminals of the amplifier, the relative input impedance must be sufficiently high. The impedance of each surface electrode is finite and depends on many factors such as the temperature of the electrode conductive past, the cleaning and thickness of the skin and the electrode's area. This situation is schematically represented in Fig. 2.9 with two active inputs and one common terminal. In particular, a voltage drop at the input terminals V_{in} is caused by the current flow through the electrode resistances used to represent the electrode-skin interface, resulting in a voltage that is less than the desired V_{EMG}. In this relation, a general specification would be to have an input impedances of 1 MΩ or higher, and to prepare the skin to reduce the impedance to 1000 Ω or less (Winter, 2009).

It is important to consider that electromagnetic radiations are easily picked by the human body, that is a good conductor and therefore acts as an antenna. It is possible that sEMG quality is critically degraded by such interferences, that appear as added noise to the signal when the muscle contracts. Most of this interference can be eliminated with a differential amplifier instead of a single-ended configuration. Indeed, all locations of the body pick up the same noise, and therefore this unwanted signal is common to both active terminals. This is know as a *common-mode signal*, and considering the net signal at the first terminal with the expression $V_{noise} + EMG_1$ and at the second terminal as $V_{noise} + EMG_2$, its is clear the (ideal) output of an amplifier with gain A is

$$V_o = A(V_{noise} + EMG_1 - V_{noise} - EMG_1) = A(EMG_1 - EMG_2) \tag{2.10}$$

where V_o is the amplified difference between the signals on the first and second electrodes composing the sEMG channel. Of course, unfortunately, a perfect cancellation never occurs in real applications.

Another important phenomenon to take into account is the so called *cross-talk* in multiple channels sEMG recording. Often, it can happen that two or more electrodes have an overlapping zone of pick-up where they detect MUAPs from motor units related to the same muscle. Indeed, for the larger motor units the detectable pick-up distance is around 1.5 cm, whereas for small units around 0.5 cm (Fuglevand et al., 1992). Therefore, sites for electrode placements should be chosen based on anatomy knowledge in order to minimize the cross-talk.

2.3.3 Biomechanical Interpretation of sEMG

Measures of muscle functions can be obtained from the extraction of useful relationships between a processed sEMG signal and biomechanical variables. One of the most important and addressed by researchers is the muscle tension, that can be predicted from sEMG in order to measure the level of muscle activation.

The processing of sEMG signals by the calculation of the root mean square (RMS) value feature has been widely used to obtain tension-related relationships, and in general both linear and nonlinear relationships between EMG amplitude and tension have been discovered. Another processing method used quite often is to estimate the number of the action potentials from sEMG over a given period of time, which increases with muscle tension in an almost linear fashion.

When dynamic contraction conditions are considered, the relationship between tension and RMS sEMG values still holds and the latter can be used to predict muscle tension in case the length is not changing too rapidly.

In general, it is worth to note that the sEMG signal anticipate the muscle force in time. Such delay derives from the resulting summation of twitch forces that corresponds to the related MUAPs, each one reaching its peak with a 40–100 ms lag. Thus, such lag is then reflected with sEMG.

Finally, it is important to know that sEMG signals can change considerably during muscle fatigue, which occurs when the muscle tissue cannot supply the metabolism at the contractile element. Assuming that a muscle activation remains constant, the fatigue manifests mechanically by decreasing tension (Vredenbregt and Rau, 1973). In addition, also the shape of the motor action potentials can be altered during fatigue, and the sEMG spectrum shifts to reflect these changes. In particular, the result is a decrease in the sEMG frequencies attributed to fatigue-related causes, as the lower conduction velocity of the action potentials and the tendency for the motor

units to fire synchronously (which also increases the amplitude of the EMG). Therefore, changes in the frequency content and amplitude of the sEMG are the major myoelectric indicators of fatigue (Winter, 2009).

Chapter 3

sEMG-Based Interfaces for Artificial Hands and Wearable Devices

In recent decades, most studies and works are considering the integration of biological signals in the control systems of robotic devices, reporting for particular interests and developments primarily in the area of assistive devices (Oskoei and Hu, 2007). At the same time, as robotics research goes in the direction of compliant manipulation and human-like control strategies, biological signal-based interfaces are of great interest also for applications in HRIs for teleoperation purposes (Wolpaw et al., 2002; Artemiadis and Kyriakopoulos, 2006; Artemiadis and Kyriakopoulos, 2011; Hocaoglu and Patoglu, 2012). In this context, one of the most concrete possibility that has been explored for the realization of HRIs is the use of EMG signals, because they record the activation potentials from the user's muscles (see Chap. 2). In such types of HRIs, it is possible to find both non-invasive and invasive applications. In the latter, the signal is acquired directly from the area of the muscle where it is generated, and therefore invasive applications contain high quality information. On the other hand, non-invasive applications do not need surgery procedures, and are normally preferred because they result as more acceptable interfaces for users and researchers, even if much efforts are required in signal processing, due to a lower quality of the information. After all, sEMG gives the possibility to understand which muscles are voluntarily activated, resulting in an easy and inexpensive method for the detection of human intentions.

In typical applications, the control of robotic devices is possible processing in real-time a given number of sEMG signals acquired from differential electrodes pairs. This kind of control should give to the user the possibility of commanding a robotic device by using his/her muscle activity in a natural way, and it is referred to as *myoelectric control* (Santello et al., 2016) (or *myocontrol*).

In this chapter, in accordance with the research work of the present thesis, the focus will be put on the sEMG-based HRIs for the control of robotic hands and Wearable Assistive Devices (WADs). Indeed, despite nowadays artificial hands and wearable robots are particularly advanced and increasingly diffused, the way they

are controlled via sEMG HRIs is still an open issue. This is particularly reflexed on the difficulties in using such kind of interfaces from the users point of view. In this context, a first distinction for sEMG-based controls can be made: we talk about *natural control* when the user controls the robotic device in a transparent way, that is controlling the robotic hand or the WAD with the same sEMG patterns that are used to control his/her own limbs, otherwise we will talk about *non-natural control* when the user has to learn new muscle activation patterns in order to regulate the behaviour of the teleoperated devices.

3.1 Myoelectric Controls for Artificial Hands

In order to find one of the earliest uses of the sEMG signals in the control of robotic hands, we have to go back in 1950's (Battye, Nightingale, and Whillis, 1955) where an electrode pair was used to command the closing motion of a powered hook gripper. This is a very basic approach that is conceptually still in use because of its simplicity. However, a new branch of approaching the problem by advanced algorithms for the sEMG signal decoding was initiated in the 1960's, when (Finley and Wirta, 1967) used a linear pattern-matching algorithm to understand which grasp a user wanted to execute among a predefined set (Gijsberts et al., 2014). However, it is possible to state that nowadays there exists still no myocontroller able to extract the required information from sEMG signals needed to make a fully satisfactory natural control of artificial hands (Hahne et al., 2014).

This aspect is clearly observable, for example, in the issues associated with the acceptance of myoelectric forearm prostheses by the users (Biddiss and Chau, 2007). The problem can be seen as a consequence of the difficulties in extracting information from the sEMG signals, but also of general design choices: non-intuitive control, lack of useful feedback and insufficient functionality of the robotic hand can be critical in such sense (Peerdeman et al., 2011). In order to increase the intuitiveness of the control, one possible way is to design the sEMG-based HRI such that the signal flow between user and artificial hand emulates that of the control of the human hand itself. To do this the HR system should be designed according with the integration of three subsystems: *(i)* the EMG sensing, for the acquisition and interpretation of the muscular activity, (*ii*) the control system, that has to translate the information of the EMG sensing in control inputs for the robotic hand and (*iii*) the feedback, to provide to the user sensory awareness. The combination of this subsystems can be observed in Fig. 3.1 for a prosthetic hand application (Peerdeman et al., 2011).

Furthermore, since the current development in the design of robotic hands is providing devices increasingly flexible and humanoid, the number of possible controllable functions is growing, and therefore can be useful to identify the "macro-functions" that a user should have at his/her disposal: the control of the correct

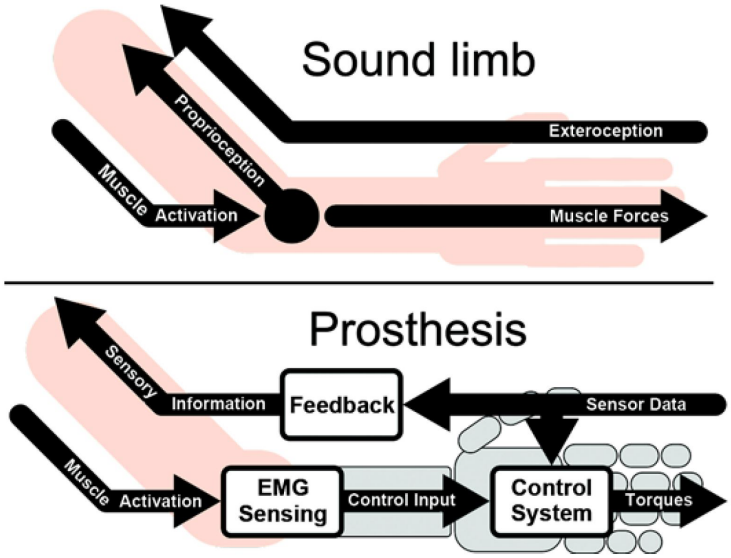

FIGURE 3.1: Main subsystems of a prosthetic robotic hand controlled with EMG signals (Peerdeman et al., 2011).

grasp type, the forces involved in such grasp and a meaningful corresponding feedback. According to this view, in this thesis work, the focus will be put on the myoelectric controllers for grasping tasks.

Another functionally partitioned model of a myocontroller is reported by the pioneering review study of (Fougner et al., 2012), again inspired by the upper limb prosthetics field. In particular, this model regards the sEMG-driven control problem of a teleoperated device, and is divided in eight layers (see Fig. 3.2): (*i*) the input signal capture, in which the sEMG signal is acquired, (*ii*) the signal conditioning, for the filtering of the raw data, (*iii*) the feature extraction, for the extraction of useful and meaningful information from the filtered sEMG, (*iv*) the control channel decoding, where the signal feature are transformed in controllable signals, (*v*) the motor function determination, for the mapping of the control signals to the available motor functions of the robotic hand, (*vi*) the actuator function selection, in which the motor functions are translated into setpoints for the (*vii*) low-level motor control, that provides directly the input for artificial hand motors, the latter being part of the (*viii*) actuation/sensing level, together with the feedback sensors.

(Fougner et al., 2012) also splits the myoelectric control problem in three orthogonal axes (see Fig. 3.3), that is worth to mention because of the very clear classification of myoelectric control methods given by the space spanned by such three axes and for a valuable terminology specification for the standardization of myocontrol vocabulary. In particular, a brief focus on the Activation Profile and Intent Interpretation axes (Fig. 3.3) is reported. Along the vertical Activation Profile axis, different approaches are defined: the *on/off control* in which the user can only activate or deactivate a function without further degrees of control provided; the *multi-level control* that gives the possibility of controlling multiple actuator functions of the artificial

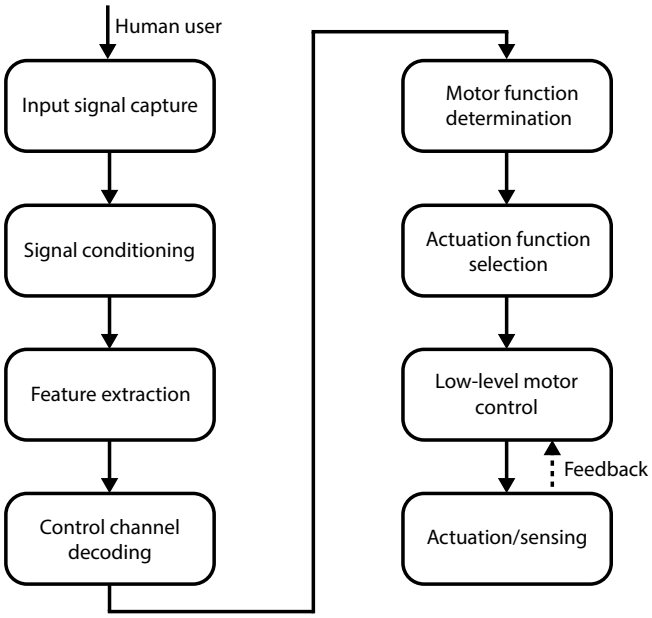

FIGURE 3.2: Functionally partitioned model for a robotic hand myocontroller (readapted from (Fougner et al., 2012), licensed under Creative Commons BY-NC-SA license).

hands in a discrete fashion; and the *proportional control*, defined as the continuous control of the robotic hand's functionalities. On the other hand, the Intent Interpretation axis report for various method for the understanding of the user's intention, in particular: the *state machine*, in which the user can switch between different states controlling the inputs; the *classification*, where pattern recognition is used to give to the user the possibility of select between different motor function (without the possiblity to control them simultaneously); the *simultaneous control*, in which the user can activate different functions at the same time.

Among the different solutions of implementing a myocontrol, a common important aspect in the HRI for the control of robotic hands is the feedback directed to the user, which is mostly related to force and position information. In the case of amputee subjects, the most natural way to close the loop between the sensing of the robotic device and the feedback would be the direct stimulation of afferent nerves, which has been actually investigated (Di Pino, Guglielmelli, and Rossini, 2009). For more general applications, and to avoid the invasive methods, it is possible to use the information measured by sensors to transmit to the user stimuli applied on the skin, reproducing the amplitude of the measures detected by the sensors' perception apparatus (Fan et al., 2008).

In general, it is possible to say that force is the most important type of information for feedback, because it is not possible to determine it through standar visual feedback, and at the same time it is essential when handling fragile objects or interacting with other humans. An example of other types of feedbacks different from

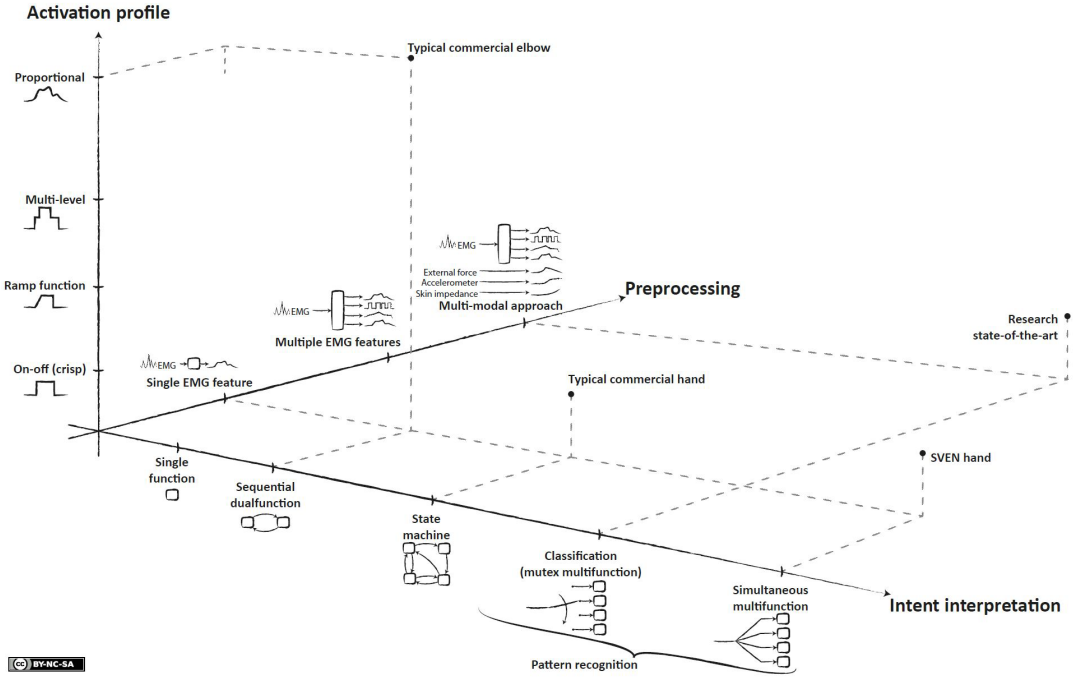

FIGURE 3.3: Three dimensional representation of the myocontrol for artificial hands (the picture is taken from (Fougner et al., 2012), licensed under Creative Commons BY-NC-SA license).

force and position is the indication of the control system status. Finally, it is fundamental to consider that studies have proved that the feedback is considered useful by the users only if it is intuitive, simple and comfortable (Peerdeman et al., 2011).

Coming back to the mother theme, the grasp control using sEMG-based interfaces is mainly implemented through two methods: a discrete selection of grasp types by means of classification or the proportional control of the robotic hand fingers joints. Anyway, it is important to rember that nowadays a reliable control via sEMG is an open problem in the research community. The changing in the myoelectric signal over time is at the base of deteriorated performances that afflicts also the most advanced machine learning techniques used in myocontrol. In this view, recently an approach based on the concept of *incremental learning* has been proposed to allow adaptation of the myocontroller to signal changes (Gijsberts et al., 2014). More details on specific myocontroller approaches are provided in the following subsections.

3.1.1 Machine Learning and Proportional Control Approaches

Over the last 20 years, the focus of the literature has been on increasing the number of robotic hand functions that can be controlled, and several Machine Learning (ML) methods have been proposed with the purpose of providing more dexterity to the related sEMG-based HRIs. Classification schemes have generally been studied for use with prostheses and the control of kinematic outputs, and a vast variety of

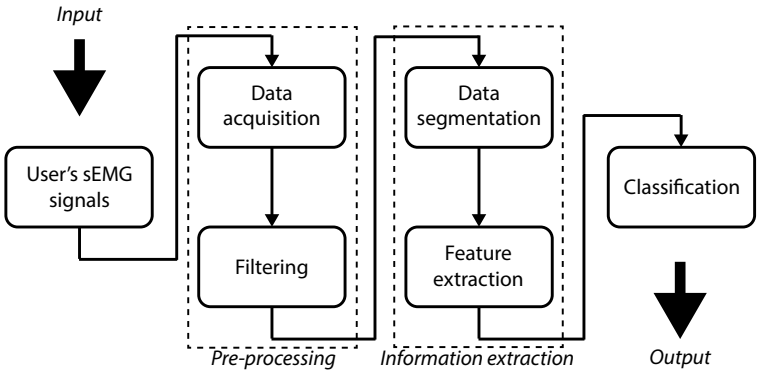

FIGURE 3.4: Structure of a pattern recognition-based myoelectric system.

applications in myoelectric control have implemented schemes using classification techniques (Oskoei and Hu, 2007). Indeed, significant efforts have been spent by the research community in these sense for the control of many DoFs, reporting for a very high accuracy particularly in relation to recent works (Erik Scheme, 2011). With discrete outputs, classification approaches generally provides sequential control, in which only one function can be active at a time. However, it is worth to mention that recent studies have also proposed to extend such concept to multi-class trainings of the classifiers, allowing the activation of more than one function at a time (Young et al., 2013).

In general, the number of controllable functions can be increased by using pattern recognition-based ML approaches. To do this, it is necessary to extract useful features from the sEMG signals. The most frequently used feature are related to the amplitude of the myoelectric signal: mainly Mean Absolute Value (MAV) and Root-Mean-Square (RMS). Typical applications distinguish different contraction patterns, up to nine if accuracies grater than 90% are considered (Hargrove et al., 2007; Oskoei and Hu, 2008). In Fig. 3.4 it is possible to observe the typical structure of a pattern recognition-based myocontrol system.

ML has been used in sEMG-based HRI related to grasping tasks for the hand postures classification, e.g. in (Ferguson and Dunlop, 2002; Bitzer and Van Der Smagt, 2006) and by (Castellini and Smagt, 2009) that highlighted how hand pose-related sEMG patterns are related to force configurations.

However, ML-based approaches present a certain level of criticality, even if they are able to perform accuracies of classification up to 98%. The major criticality is represented by a *reliability issue* (Santello et al., 2016). This is mainly caused by two reasons: *(i)* the surface signals are influenced by a number of factors such as sweat, sensor positioning and muscle fatigue and *(ii)* the presence of a lack of natural control limits the usability of the system. Indeed, ML-based myocontrols are not able to assure that a certain pattern will be stably recognized, because of relying on a discrete classification that suffer from the ambiguity when the signal crosses the boundary between two decision zones of the input space (Jiang et al., 2012).

For the reasons just mentioned, researchers are also exploring sEMG-based mapping techniques different from classification, in which the controller does not let the user decide among a finite and discrete number of robotic hand functions, but instead allows a continuous regulation of the teleoperated device functionalities, in a paradigm known as *simultaneous and proportional control* (s/p) (Hahne et al., 2014). (Fougner et al., 2012) clarifies the terminology, defining that we are in presence of proportional control when the user can control at least one mechanical quantity of the robotic hand within a finite, useful and essentially continuous interval, by varying the control inputs within a corresponding continuous interval. This kind of approach for myoelectric interfaces can also go in the direction of overcoming the lack of natural control of classification-based methods. Indeed, the human neuromotor system exhibits proportional control abilities, in the sense that we can vary joint torques, speeds, positions and contact forces continuously at will. This allows for a simultaneous and proportional control of the mechanical quantities. Such concept has been introduced in sEMG-based interfaces by a series of studies (Jiang, Englehart, and Parker, 2009; Nielsen et al., 2009; Muceli and Farina, 2012) in the field of prosthetic applications. In particular, in order to find the mapping between the sEMG-based input signals features and the motor function, various linear and nonlinear regression models have been used, obtaining accurate s/p controls of multiple motions of the artificial hand. Among most popular regression models there are linear regression, multilayer perceptrons, kernel ridge regression (Hahne et al., 2014).

For the exaction of feature from the sEMG signal, most applications of s/p myoelectric control have used the mean square value, RMS value and lowpass filtering. However also other time-domain-based feature as the MAV, zero-crossings, slope sing changes and waveform length can be used (Fougner et al., 2012).

A recent remarkable approach in the field of proportional myoelectric control of mechanical quantities of a teleoperated artificial hand is the time-to-time modulation of the impedance, inspired to the human ability in producing restoring forces with respect to environmental displacement by modulating limb impedance through muscle co-contraction (Gomi and Osu, 1998). Indeed, it is present a correlation between muscle activation and stiffness of the limbs' joints (see Chap. 2) that can be exploited in the usage of sEMG signals for the estimation of both position and stiffness in realt-time for a controlled device. In (Ajoudani et al., 2014), such approach has been implemented in the teleoperation of a robotic hand using two differential sEMG electrode pairs applied on the forearm in a "tele-impedance" control paradigm counterposed to multi-sEMG signal pattern regression (Santello et al., 2016).

Despite the advancements and the more natural sEMG-based interfaces introduced by the s/p control approach, the practical application of these systems is still not running with respect to the research and design efforts spent by the academic community. This is due – again – to the fact that the sEMG presents an inherent non-stationarity difficult to bypass. The signal changes due to the already mentioned causes (muscle fatigue, electrode placement, skin conditions) plus the variation of

the configuration of the muscles when the human limbs assume different poses. According to such unmodeled variations, the performances of the myoelectric control reflect a certain level degradation, and a repetition of the training procedure is required to allow the adaptation of the interface to the new conditions. A possible solution recently proposed uses the concept of an *incremental learning* method in a prosthetic hand teleoperation scenario. In this paradigm, the model for the s/p control obtained by a training procedure can be further refined after the initial calibration phase (Gijsberts et al., 2014), using *model updates* within an overall HRI framework denoted as *interactive learning* (Castellini, 2016b; Nowak, Engel, and Castellini, 2017).

3.1.2 Synergy-Centered View

Recent sEMG-based HRIs for robotic hands can also rely on a large number of electrodes, reaching even up to several tens fo them, with the aim of better capturing the muscular electrical activity for the decoding of user intentions (Muceli, Jiang, and Farina, 2014). The possibility of such larger set of measurements suggests to take also in consideration the concept of muscle synergies (see Chap. 2) detected by means of sEMG signals (Castellini and Smagt, 2013).

Furthermore, it is also possible, in the view of multifuctional – and, particularly, proportional – myocontrols, to consider the mappings between the sEMG signals and the artificial hand motor functionalities as a synergistic interaction of multiple muscles (Ison and Artemiadis, 2014). In this way it possible to obtain description of force and motion pattern with a reduced dimensionality, that can contribute for a better user intents understanding (Berger and d'Avella, 2014). Supporting these observations, several studies have used the concept of muscle synergies as an explicit element of sEMG-based HRIs for the control of artificial hands, e.g. (Ajiboye and Weir, 2009; Choi and Kim, 2011; Jiang, Englehart, and Parker, 2009; Castellini, 2016a).

Although sEMG-based synergies shows a concrete possibility towards a successful exploitation of the muscle synergy concept in the teleoperation of robotic hands, still a lot of effort is necessary before to elect such approach as properly "safe and reliable". Indeed, there are a series of complexities associated with sEMG recording, wide inter- and intra-user variability (Hug, 2011) and general nonlinear properties of sEMG signals that have to be carefully considered by the research community (Ison and Artemiadis, 2014).

3.2 Myoelectric Controls for Wearable Assistive Devices

In this thesis work, with *Wearable Assistive Devices* (WADs) we refer to wearable robotic systems designed to assist humans in performing movements (Pons, 2008). The assistance provided by such robotic devices can be used to several goals. The

principal applications are the compensation for musculoskeletal disorders or the enhancement of neuromuscolar rehabilitation (Rocon et al., 2007; Vallery et al., 2009; Tsukahara, Hasegawa, and Sankai, 2009). Indeed, in the case of injuries or loss of muscular strength, performing Activities of Daily Living (ADL) becomes very difficult and rehabilitation is the main treatment to regain use of the limbs and, consequently, independence. On the other hand, WADs enable also human power augmentation such as improvement of endurance and strength performances during physical task execution (Walsh, Endo, and Herr, 2007; Pratt et al., 2004).

However, it is possible to find only few uses of WADs in real world applications (e.g. commercial stage) (Kong and Jeon, 2005; Miller and Rosen, 2010), mainly because further improvements are necessary to make them easier to control and to adapt to different human motor intentions during specific tasks. This would be currently a very important motivation on using robotics for the health services, because it will open the possibility to provide optimized and automated rehabilitation therapies to victims of injuries. Compared to manual therapy, WADs can provide intensive rehabilitation for long periods of time (Huang and Krakauer, 2009) without having to deal with the fatigue level of a human therapist. In this way, WADs can enable more frequent treatments, potentially reducing the costs. In addition, for such kind of devices, it is generally possible to accurately quantitatively measure and evaluate patient's condition related data.

In such regard, early works in the research community were made for the upper limb, based on exoskeleton-like "end-effector robots". In this contex, the term end-effector robot refers to a device capable to hold the hand of the patient – or his/her forearm – and to generate external supports for human motions assistance (Fig. 3.5). In this case, the kinematic structure of the robotic system do not match with that of the human limb. Although this kind of assistive devices presented a low level of complexity and they were easy to manufacture, determining the force to be provided to the user for a large enough rage of limb postures can be difficult (Hogan et al., 1992; Burgar et al., 2000; Loureiro et al., 2003). Anyway, it is important to highlight that the results reported by the employment of such kind of early – and not wearable – assistive devices indicated a certain degree of improvement of motor impairment rehabilitation processes of the upper limb, and an actual support of the motions. This justify the research toward wearable and more sophisticated devices, and on the related HRIs for the control of such robotic systems (Lo and Xie, 2012).

Since WADs are tightly coupled to the human body, the design of effective HRIs is extremely important. Firstly, it should be considered the location of the pHRI (see Chap. 1) and carefully defined the location and the size of the contact area of the human skin, because this aspect can significantly influence the user's pain tolerance, and therefore safety and comfort. Considering the cognitive side of the interface (see Chap. 1) between the user and the WAD, we enter in the field of controlling the device with the objective of dealing with the detection and the interpretation of the human motion intentions. This fundamental aspect in the control of wearable

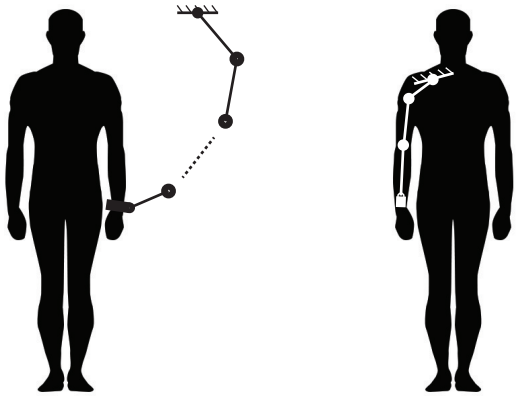

FIGURE 3.5: Conceptual view of the structure of an "end-effector" assistive device (right side) and a wearable assistive device (left side) for the upper limb.

systems has been approached with the use sEMG signals in several studies (Lenzi et al., 2011; Gopura, Kiguchi, and Li, 2009; Gopura and Kiguchi, 2012). In particular, nowadays, there are still a lot of sEMG-based control methods for WADs that are based on binary (on-off) strategies, and therefore the research community is focusing on finding reliable advanced methods to enhance their performances. Other kinds of HRIs for WADs, as visual interfaces (Kiguchi and Liyanage, 2008; Baklouti et al., 2008), vibrotactile (Kapur et al., 2009) or electroactive garments (De Rossi et al., 2009) are not addressed in this thesis work.

3.2.1 sEMG-based applications with recent WADs

Recently, research in the field of robotic assisted motions and therapy has definitely taken the direction of designing wearable devices. In case of exoskeletons, the WAD have a structure which resembles the skeleton of user's limbs, using links and actuated joints with axes that match the limb's joint axes (Fig. 3.5).

Some sEMG-driven devices of such kind can be found commercially. The mPower arm brace (Myomo Inc., Cambridge, MA) is a 1 DoF wearable exoskeleton which uses sEMG from biceps and triceps muscles for HR control interface to assist elbow motions; the Hand Mentor (Kinetic Muscles Inc., Tempe AZ) is an exoskeleton for the rehabilitation of the hand, with a structure composed by 1 DoF that permits to transfer forces to the user controlled by sEMG; the Robot Suit HAL-5 (CYBERDYNE Inc., Japan) is a full body exoskeleton that generate assistive supports based on sEMG (Lo and Xie, 2012). In Fig. 3.6 the mentioned devices are shown. Furthremore, also in literature it possible to find several works implemented systems with exoskeletons controlled by sEMG signals (Gopura and Kiguchi, 2009; Cavallaro et al., 2006; Rahman et al., 2006; Lee et al., 2010).

The development of WADs has reached a high point due to recent developments in technology, in particular in relation to the advances in embedding sensors and electronics, and in the actuation strategies over the past two decades (Gopura et al.,

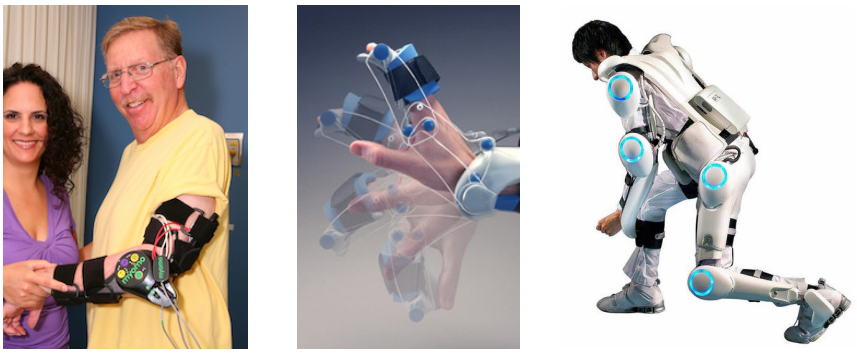

FIGURE 3.6: From left to right: mPower arm brace, Hand Mentor and Robot Suit HAL-5 commercial wearable assistive devices.

2013). In particular novel actuation strategies have introduced WADs in which the actuators can be used to directly transmit forces on the human body without the necessity of external exoskeletal structures (i.e. rigid links), as in the case of Twisted String Actuation (TSA) (Palli et al., 2013) and Pneumatic Artificial Muscles (PAMs) (Kobayashi and Nozaki, 2007). There are some common features between the TSA and PAMs actuation strategies: as the human muscles, they are both flexible motors that generate a force in only one direction through a "contraction", and therefore to obtain a bidirectional movement of a DoF normally an antagonistic configuration is needed (i.e. a pair of motors actuating in opposite directions). In this thesis work, there is particular interest on the TSA strategy, since a TSA-based WAD has been used for the implementation and the experimental evaluation of a myoelectric control to assist the elbow joint, as reported in Chap. 5. These kind of recent robotic system are raising interest since they particularly go in the direction of matching lightness and compactness requirements demanded by WADs. In this way the potential wearability and portability of the assistive devices increases critically, opening scenarios in which the demanding for intuitive, simple and adaptive sEMG-based HRI for an effective control is more and more strong and the research community is actually seeking to go in such direction.

Fig. 3.7 depicts the general scheme for the architecture of a sEMG-based control interface for WADs, according to which different myocontrollers can be implemented, and a multitude of solutions can be found in literature.

Several algorithmical approaches have been proposed in literature for the design of sEMG-based HRIs for the control of WADs, estimating joint torques from muscular activations using methods that range from proportional control (e.g. in (Lenzi et al., 2011)), fuzzy-neuro-control (e.g. in (Gopura and Kiguchi, 2012)), black-box neural networks (Song and Tong, 2005), phenomenological-based approaches with Hill models (Cavallaro et al., 2006; Cavallaro et al., 2006), till to general teleoperation controls for robotic arms based on force–position estimations from sEMG (Artemiadis and Kyriakopoulos, 2009).

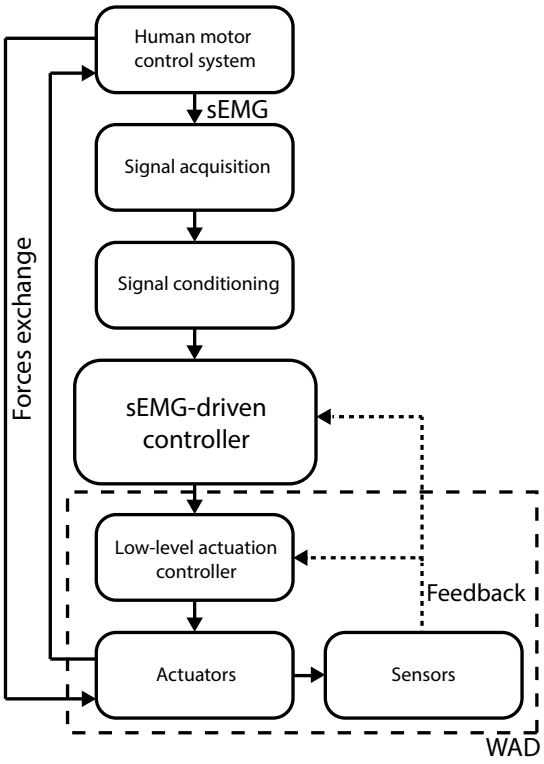

FIGURE 3.7: Generic scheme for the architecture of a sEMG-driven control for wearable assistive devices (WADs).

3.2.2 A prospective simplification in WAD's myocontrol

The principal use of the sEMG signals for the design of HRIs for WADs consists in the estimation of the joint torques that are necessary for the user to perform a voluntary movement and then, on such basis, provide a support force applied to the user's limb by the robotic assistive device. The specific shape of such force is different with respect to the goal in assistance that one wants to give to the user, in accordance with the human intentions detected by means of the myoelectric measurements themselves (Lenzi et al., 2012). Although encouraging results reported by the research community (see Subsec. 3.2.1), this kind of approach presents some important drawbacks. Primarily, it exists a problem in estimating with reliable accuracy (and in real-time) the necessary torque to give a correct help to the user while performing a specific motion. Indeed, the relation between sEMG signals and human joint torques is, in general, very complex. It involves several nonlinearities under both static and dynamic conditions, and strongly depends on the subject anatomy and the placement of electrodes on the skin (see Chap. 2). The sEMG-based torque estimation methods strongly lie on articulated subject- and task-dependent training session for the algorithms calibrations, which cannot be disregarded if a reliable myocontroller model for providing assistance is wanted. This requires a certain period

of time, great efforts for the users in focusing on the calibration tasks and the presence of an experimenter (or expert/professional) for the supervision of the procedure and the usage of specific technical equipments. This situation generally causes frustration in the users of sEMG-driven WADs, basically resulting in systems not really usable outside research laboratories.

Anyway, the use of sEMG for the control of WADs still presents clear advantages. The information about muscle activation measurable trough sEMG begins 40-100 ms before the actual muscle contraction (see Chap. 2). This delay comes to the aid of the WAD for the computation of real-time assistive torques and for the bandwidth specifications of the its actuation system. Moreover, since sEMG is able to provide force information about muscles without the necessity of modelling or formally take into account interactions of the user with the external environment, the use of myocontrol-based methods gives the possibility to avoid dynamic models of the limbs and relative parameters estimations.

In order to still exploit such advantages provided by the sEMG signals to meet the necessity for using WADs in daily life environments, one way that can be explored is a simplification in the myoelectric HRI. In this view, even if there are works that have given attention to increase the accuracy of myocontrollers based on the estimation of joint torques from sEMG signals – e.g. reducing complexity level and the time duration of the calibration procedures (Fleischer and Hommel, 2007) – it is possible to consider that a precise estimation of the joint torques could be possibly unnecessary when sEMG signals are used.

The idea is to search for solutions that provide motion assistance at a cost of some compromises in the quality of the information extracted from the sEMG signal. This road toward simplicity has recently been explored by some research laboratories. In (Lenzi et al., 2012) the authors use an exoskeleton to provide assistive torques proportional to the muscle's sEMG envelop, without however providing the possibility to quantify an assistance objective to be reached.

In general, the simplified solutions in the design of the myoelectric HRI should be able to combine ease of use and effectiveness in assisting the movement by the WADs. In addition, even if the user's reactions to the external forces provided by the wearable robot is not modelled, they should be taken into account, in particular, exploiting them to achieve effectiveness in the assistance, taking advantages – within the HR loop (see Fig. 3.7) – by the adaptation of the user's motor behaviour to external forces (Gopura, Kiguchi, and Bandara, 2011). These concepts are exploited in the research work of this thesis, as reported in Chap. 5.

Finally, the road toward a simplification in the sEMG-driven control will be totally fulfilled only if accompanied by a proper adaptation/adjustment strategy, that has to be in charge of accounting for the variability between different users as well as for the sEMG-related electrode placements and muscular fatigue. The not so many studies that have dealt with strategies of adaptation for sEMG-based interfaces for

wearable robotic systems concerns to the parameters of the human joint torque estimation models, and therefore they don't really directly deal with a simplification of the control paradigm, e.g. (Öberg, 1995; Kiguchi et al., 2008; Kiguchi et al., 2008). An effective, automatic and online calibration of WAD's HRI to different users is what one should aim to, in order to enable these systems to see a real simplification and therefore to be used in practice.

Chapter 4

A sEMG-Based HRI for Robotic Hand Grasping Tasks

This chapter presents a sEMG-based HRI for human-like control of robotic hands for grasping tasks. The work starts from the observation that the teleoperation of robotic grasping devices, especially in industrial, rescue and aerospace applications, is mostly based on non-intuitive approaches, such as remote controllers. Indeed, in the research community, the development of intuitive control strategies in general represents an intriguing challenge in the design of HRI systems for robotic hands. On the other hand, recent sEMG-based HRIs have shown the possibility of implementing control solutions able to transfer the ability to manage multi-finger grasps and finely modulate grasp impedance from the human to the robotic hand.

However, despite the inherent potentiality of sEMG-based interfaces, current myoelectric HRIs for grasping tasks only partially fulfil user-centered requirements for a stable control, as already introduced in Chap. 3. In order to enhance the user's acceptance, an increasing of the level of intuitiveness and naturalness in the control strategies is needed. Indeed, several applications in teleoperation and higher level telesupervision of robotic grasping devices could benefit from human-inspired control interfaces, as astronaut commanding of construction robots in space missions, operators of disaster search and rescue robots, direct operations of bomb disposal experts and dexterous hand prosthesis (Wolf et al., 2013; Artemiadis and Kyriakopoulos, 2011).

To this end, in the work presented in this chapter, the overall hand musculoskeletal structure is taken into consideration for the HRI design process. The human hand is a very complex and versatile sensorimotor system characterized by 21 DoFs controlled by 29 muscles (Jones and Lederman, 2006), able to perform an incredible number of different poses and grasps. In addition, recent views have highlighted how the overall organization underlying the motor control of the human hand can be seen in a synergistic fashion, reflecting a spatial and temporal coordination at different levels: postural, muscular and neural (Santello et al., 2016). This is in agreement with the concept of muscular synergies, according to which multiple muscles can be activated as a unit by a single neural drive (see Chap. 2). In this connection, it

is significant that linear decomposition algorithms such as Non-negative Matrix Factorization (NMF) or Independent Component Analysis (ICA) have been used to extract muscular synergistic weights, which represent the modulation of supraspinal activation signals (d'Avella et al., 2006). Furthermore, the multitude of kinematic DoFs of the hand can also be dimensionally reduced thanks to the concept of postural synergies (Santello, Flanders, and Soechting, 1998; Santello et al., 2016). Moreover, another fundamental aspect of the human hand control is the modulation of the grasp stiffness in order to accomplish a wide number of different grasping tasks, thanks to the regulation of the joints impedance by means of antagonistic muscles co-activation (see Chap. 2).

These concepts are used in the work presented in this chapter for the design of a sEMG-based HRI, in particular to define the human-like approach of the robotic hand control. In other words, the aim is to implement a more natural and intuitive HRI integrating directly the – by definition – natural and intuitive aspects of the motor control used by the humans themselves: multiplicity of performable grasps, dimensionality reduction by means of muscular and postural synergy concepts, and combination/interface between the different synergistic motor control levels.

The overall system consists of a wearable sensor interface which implements a myoelectric control composed by a hybrid approach, exploiting a ML-based method for the selection of the appropriate grasp hand shape and a factorization-based method to continuously control the closure and stiffness level of the selected grasp configuration. The experimental evaluation of the HRI has been performed through a series of grasping tasks controlling the UB Hand IV (University of Bologna Hand, version IV) anthropomorphic robotic hand, and a three-fingered industrial gripper.

4.1 Acquisition System and Robotic Hands Setup

The details of the implemented myoelectric controller will be provided in the next sections, whereas here an overview on the tools and setup is given. In particular, the teleoperated artificial hands and the sEMG signals acquisition-related hardware and procedures are presented.

4.1.1 Robotic Hands Description

Two robotic devices that have been used with the sEMG-based HRI are described: the UB Hand IV (Melchiorri et al., 2013; Palli et al., 2014), as anthropomorphic device to perform human-like tasks, and a three-fingered gripper mounted on a 6 DoF industrial manipulator to perform teleoperation in a manufacturing simulated application. The artificial hands are characterized by different kinematics, number of joints and number of DoFs. On the other hand, the actuation system of the two devices is composed by tendons driven by Dynamixel servomotors (*Robotis Corp.* 2016) and for this reason a common control architecture has been designed for both of them.

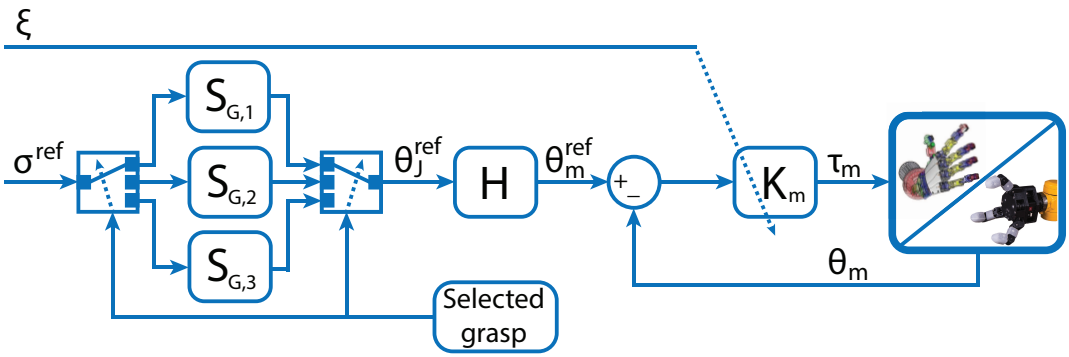

FIGURE 4.1: Controller architecture of the robotic hands.

Architecture of the Hand Controller

Fig. 4.1 schematically shows the control architecture of the two grasping devices. In the following, n_J denotes the total number of joints of all fingers, and n_m denotes the number of tendons actuating the joints, each one driven by a servomotor. The control strategy is implemented in order to vary both joint positions and the grasp stiffness. In order to do this, a three-level hierarchical structure has been realized, structured in the motor, joint and synergy control levels.

Exploiting the compliance characteristics (*Robotis Corp.* 2016) embedded in the Dynamixel servomotors, the lower motor level of the architecture is controlled according to

$$\tau_m(t) = K_m(\theta_m^{ref}(t) - \theta_m(t)) \,, \tag{4.1}$$

where $\tau_m \in \mathbb{R}^{n_m}$ is the motor torques vector, $K_m \in \mathbb{R}^{n_m \times n_m}$ is a diagonal matrix with the desired motor stiffness values, θ_m^{ref} and $\theta_m \in \mathbb{R}^{n_m}$ are the reference and the actual position of the motors, respectively.

Then, to move to the joint control level, a mapping $H \in \mathbb{R}^{n_m \times n_J}$ between the joint and motor spaces is necessary (Melchiorri et al., 2013; Palli et al., 2014). Using this mapping, the reference angle of the motors can be computed once the desired joint configuration θ_J^{ref} is known, that is

$$\theta_m^{ref}(t) = H\, \theta_J^{ref}(t), \tag{4.2}$$

(and 4.1) can be mapped in the joint space using (4.2), resulting

$$\tau_J(t) = K_J(\theta_J^{ref}(t) - \theta_J(t)) \,, \tag{4.3}$$

where the joint stiffness matrix is computed as $K_J = H^T K_m H \in \mathbb{R}^{n_J \times n_J}$.

The higher synergy control level defines the joint reference configuration θ_J^{ref}, by the expression

$$\theta_J^{ref}(t) = S_{G,i}\, \sigma^{ref}(t), \quad i = 1, 2, ..., n_g \,, \tag{4.4}$$

where σ^{ref} is the synergistic hand closure reference given by the myoelectric control

TABLE 4.1: Robotic hand grasps and related human hand gestures.

User's gesture	Gesture label	UB Hand IV grasp	Three fingered gripper grasp	Grasp label
Three Fingers	TF	Tripodal grasp	Tripodal grasp	G1
Ulnar Pinch	UP	Ulnar grasp	Parallel grasp	G2
Fist	F	Power grasp	Cylindrical grasp	G3
Open Hand	OH	-	-	-
Neutral Pose	NP	-	-	-

system (see (4.9)), $S_{G,i} \in \mathbb{R}^{n_J \times 1}$ is referred to as the *grasp synergy matrix* and n_g is the number of grasp shapes that the robotic hand is programmed to perform, based on the application. As will be explained in the next subsections, in the implemented system we have $n_g = 3$, and $S_{G,1}$, $S_{G,2}$ and $S_{G,3}$ represent specific *ad-hoc* joint grasp patterns, that are reported in Tab. 4.1 indicated with the labels G1, G2 and G3.

With regard to the modulation of the grasp stiffness, it can be achieved by acting on the matrix K_m, taking into account that the relation $K_J = H^T K_m H$ holds. In this way, the modulation of the stiffness gains in the diagonal matrix K_m is made according to

$$K_m = K_m(t) = diag\{k_{min} + (k_{max} - k_{min})\xi(t)\}\ , \tag{4.5}$$

where k_{min} and k_{max} are the minimum/maximum settable stiffness values, and $\xi(t)$ is the grasp stiffness level determined by the user using the sEMG-based interface, described later in Sec. 4.2.2 (eq. 4.9).

The control architecture outlined so far gives the possibility to regulate both grasp closure and stiffness, that is a fundamental aspect for the aim of our myoelectric control interface. In the following, specific descriptions of the two different grasping devices are provided paragraphs, also in relation to the just described architecture.

The UB Hand IV

The dexterous anthropomorphic artificial hand UB Hand IV (Melchiorri et al., 2013; Palli et al., 2014) is a fully actuated grasping device, that is observable in Fig. 4.2. It implements a particular actuation system, requiring for each finger of the hand (with 3 actuated DoFs) 5 coupled tendons. Therefore in this hand, with regard to the control architecture of Subsec. 4.1.1, the number of actuated DoFs is $n_j = 15$, by means of $n_m = 25$ tendons driven with Dynamixel RX-24F servomotors (*Robotis Corp.* 2016).

In particular, the weights of the grasp synergy matrices $S_{G,1}$, $S_{G,2}$ and $S_{G,3}$ are determined by modifying the first postural synergy matrix, implemented on the UB Hand as in Ficuciello et al., 2014, such that the hand pose given by (4.4) for the maximal value of $\sigma^{ref}(t)$ matches the hand shape of the respective grasp of interest,

FIGURE 4.2: The UB Hand IV (left) and the gripper (right).

i.e. the Power, Tripodal and Ulnar grasps. In this regard, Fig. 4.3(a) shows the UB Hand joint configurations obtained by varying the value of the synergistic hand closure reference $\sigma^{ref}(t)$.

The Industrial Gripper

In Fig. 4.2 it is possible to observe the gripper used in this work. This robotic hand is composed by a palm and three fingers, each of which has three phalanges. Two of the fingers have 3 joints each: one for the proximal phalanx adduction/abduction movement (Ad/Ab joint) and the other two for the middle and distal phalanges flexion/extension motions. The third finger has only 2 articulations (the Ad/Ab joint is not present). The total number of joints composing the industrial gripper is therefore 8. Considering the notation of the controller architecture equations in Subsec. 4.1.1, there are $n_m = 3$ Dynamixel RX-106T servomotors that actuate $n_J = 3$ DoF. In particular, this is possible thanks to a proper pulley-based tendon network specifically implemented for the actuation system of the gripper. Therefore, the three DoFs of this artificial hand are: the flexion/extension motion of the middle and distal phalanges (independently), and the abduction/adduction motion of the two Ad/Ab joints (coupled).

The Cylindrical, Tripodal and Parallel grasps are the controllable grasp types by means of the myoelectric interface for the gripper. First, in order to have a suitable coordinated flexion of the hand's phalanxes for the cylindrical grasp, the weights of the related grasp synergy matrices $S_{G,i}$ are set empirically, matching the behaviour visible in the top row of Fig. 4.3(b). Then, on this basis, the synergy matrix is modified to have the Ad/Ab joint angles equal to $\pi/6$ rad for the Tripodal grasp and the distal joint angles equal to the opposite of the proximal joint angles value for the Parallel grasp.

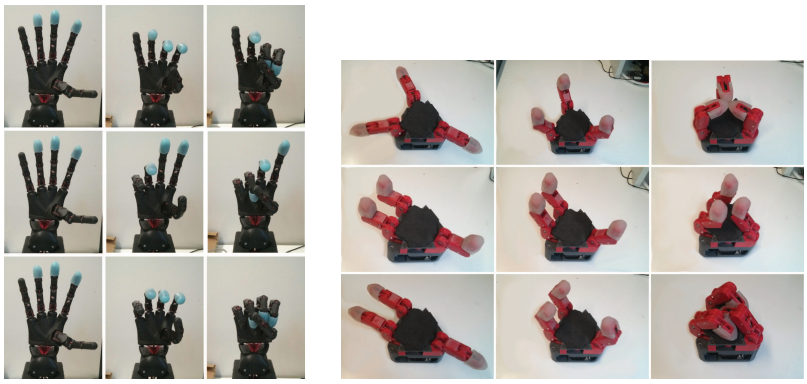

(a) Tripodal (top), Ulnar (middle) and Power (bottom) grasps for the UB Hand IV.

(b) Tripodal (top), Parallel (middle) and Cylindrical (bottom) grasps for the three-fingered gripper.

FIGURE 4.3: Grasp types of UB Hand IV (a) and gripper (b).

4.1.2 sEMG Signal Acquisition Hardware and Electrodes Placement

A particular board (*Cerebro*) has been used for the acquisition of the sEMG signals (Benatti et al., 2015). The Printed Circuit Board (PCB) is designed for wearable multisensory applications and is built in 6 layers technology, allowing the acquisition of analog signals through robust solid ground planes design. The power supply planes separate the analog and the digital part of the board. The high-performance Analog Front End (AFE) (Schonle et al., 2013) acquires the sEMG signals and is connected with an ARM Cortex M4 Microcontroller. In this application, the data are acquired at 1 kHz and streamed to a computer using an onboard Bluetooth interface. The system is battery powered and the power management circuitry allows to switch off unused sensors to enable power consumption optimization. In fact, the board mounts also an IMU interface and a pressure sensor that can be used for further applications. The performance of the acquisition board are summarized in Tab. 4.2, and a picture is reported in Fig.4.4.

Eight sEMG signal channels (i.e. 8 pairs of differential electrodes) are acquired from the user's forearm muscles. Low-cost disposable surface skin electrodes equipped with conductive gel are used. The electrodes are equally distributed around the forearm forming an armband, as shown in Fig. 4.5(a). Since the sEMG armband has to acquire muscular information about both hand gestures and grasp execution, it is placed in proximity of the *Flexor Digitorum Superficialis* and *Extensor Digitorum Communis* muscles bellies, because such muscles are mainly involved in digit flexions and extensions, in accordance with the methods and best practices outlined in (Perotto, 2011), see Fig. 4.5.

TABLE 4.2: sEMG signal acquisition board.

AFE:	
Acquisition channels	8 EMG channels
Acquisition bandwidth	1 kHz
Input range	±300 mV
Power consumption	15 mW
Microcontroller:	
Type	ARM Cortex M4
Operating frequency	168 MHz (210 DMIPS)
Flash	1Mb
RAM	192Kb
Power consumption	86 mW
Wireless link:	
Standard	Bluetooth v2.1
Embedded platform:	
Dimensions	85x50x6 mm
Total power cons.	29.7 mW

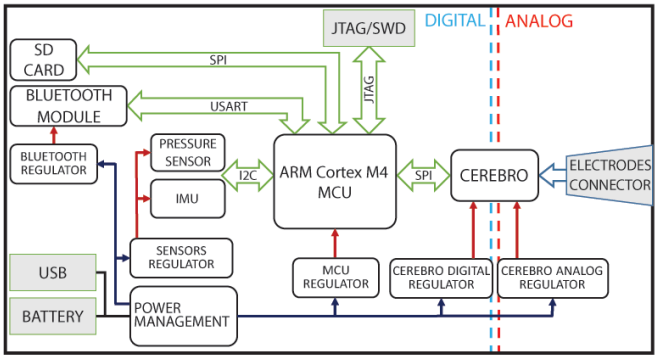

(a)

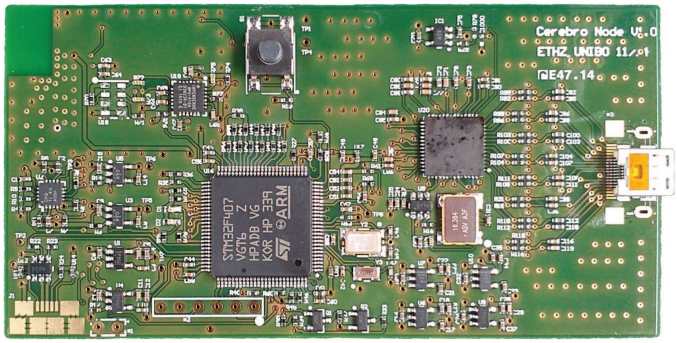

(b)

FIGURE 4.4: The *Cerebro* sEMG signals acquisition node: (a) architecture diagram; (b) real board.

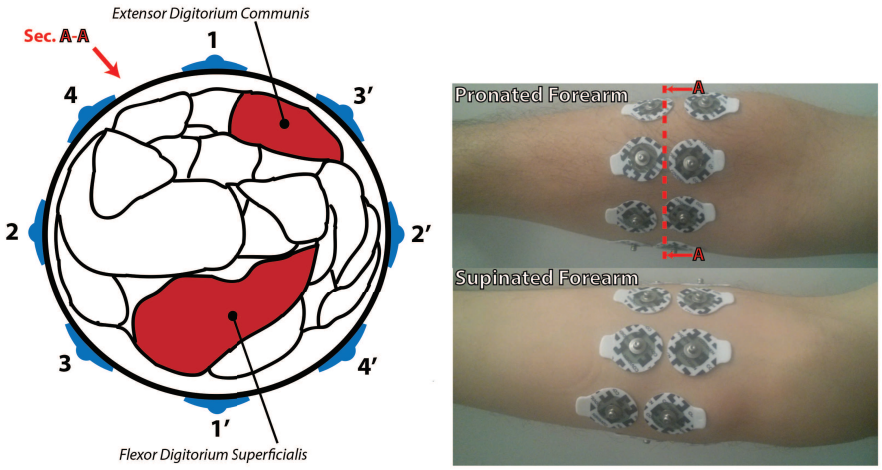

(a) Forearm section.

(b) Pronated and supinated forearm electrodes placement views.

FIGURE 4.5: sEMG electrodes placement.

sEMG Signal Pre-Processing

Each channel of the sEMG data is subject to a processing chain. Once the sEMG signals are acquired by the Cerebro board and transmitted to a nearby computer, the applied processing procedure consists of: *(i)* a 50 Hz notch filter for powerline interference cancellation; *(ii)* a 20 Hz high-pass filter, that results as the best compromise to reduce baseline noise (mainly thermal, chemical and movement artefact noises) and obtain the desired informational content (De Luca et al., 2010); and finally *(iii)* the RMS value of the signal is calculated on a 200 ms window with no overlapping.

4.2 sEMG-Based HRI Using Machine Learning and Synergies

A conceptual and functional-oriented scheme of the sEMG-based HRI resulting from the research work of this thesis is shown in Fig. 4.6. According to the figure, useful information is extracted from the sEMG signals acquired from the user's forearm, and used for two purposes: (i) let the user select the robotic hand shape according to a set of possible grasp types, specifically by means of gesture recognition and a Finite State Machine (FSM) logic; (ii) allow the user to proportionally control the grasp of the teleoperated device, regulating both the relative closure and stiffness level. In this way, the myoelectric signals are online translated in actuation commands for the motors of the robotic hand. Within such translational process, the goal is to provide to the user an interface for an intuitive and natural control. Therefore, the human hand gestures for the pattern recognition are chosen in such a way to be related to the selectable robotic hand shapes, and muscular and postural synergies are implicated and interfaced in the myoelectric grasp proportional design. Two feedback signals

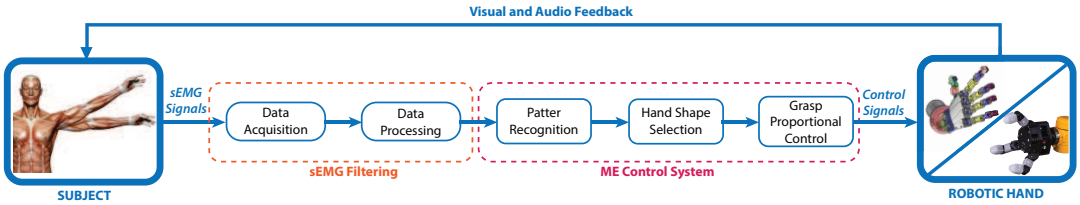

FIGURE 4.6: Functional scheme of the sEMG-based HRI system.

are available for the user: *(i)* the standard visual feedback, due to the observation of the device and the task evolution, and *(ii)* an audio feedback, to allow the user understand which grasp type has been selected and the current level of the stiffness controlled on the robotic device, by means of two different kinds of sound. As already mentioned in the previous sections of this chapter, two different robotic hands have been used: the anthropomorphic UB Hand IV and a three-fingered gripper. In addition, a graphically simulated three-fingered gripper has been used for an initial familiarization phase of the user with the HRI.

4.2.1 Selection of the Grasp Hand Shape

The Support Vector Machine (SVM) (Cortes and Vapnik, 1995) is the classifier used to implement the pattern recognition technique for the selection of the different types of grasps. The SVM is a supervised ML technique according to a model that is trained on the basis of the solution of a convex optimization problem to find the optimal separation hyperplane between two classes of a trainset. The outcome of the training algorithm is then used by the classifier to discriminate between the two classes in new data. The procedure can be applied to n-class problems by means of a *One Versus One* approach. In this work the SVM classifier is implemented using the libSVM opensource library (Chang and Lin, 2011) for Matlab.

SVM Training Dataset Acquisition Protocol

The training session necessary to collect the training dataset in order to build the classifier is composed by 8-dimensional samples of the RMS values of the sEMG channels (see Subsec. 4.1.2). Fig. 4.7 shows the five gestures to be classified, that are Open Hand, Three Fingers pose, Fist, Ulnar Pinch, and Neutral Pose, as also reported in Tab. 4.1. Note that, referring to the table, the Open Hand and Neutral Pose are not associated to any shape because they are used according to a specific grasp transition logic (see Subsec. 4.2.1). The protocol of data acquisition for the classifier training consists in the repetition of each gesture (without considering the Neutral Pose) 6 times. Every gesture has to be executed for 3 seconds followed by 3 seconds where the user has to rest his/her fingers (i.e. Neutral Pose), except between two different gesture repetition groups where the Neutral Pose duration becomes 6 seconds. It is important to note that such kind of structured training protocol is a not trivial operation for a user: the execution of 24 gestures with a precise timing can be

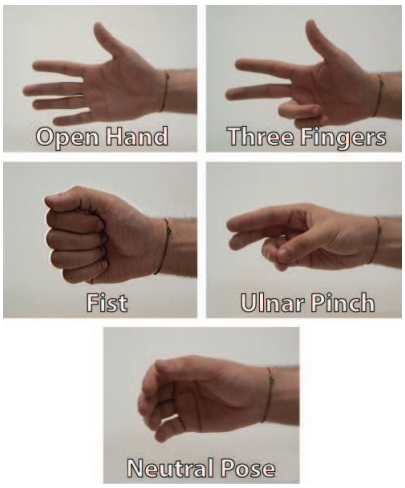

FIGURE 4.7: Hand gestures to be classified.

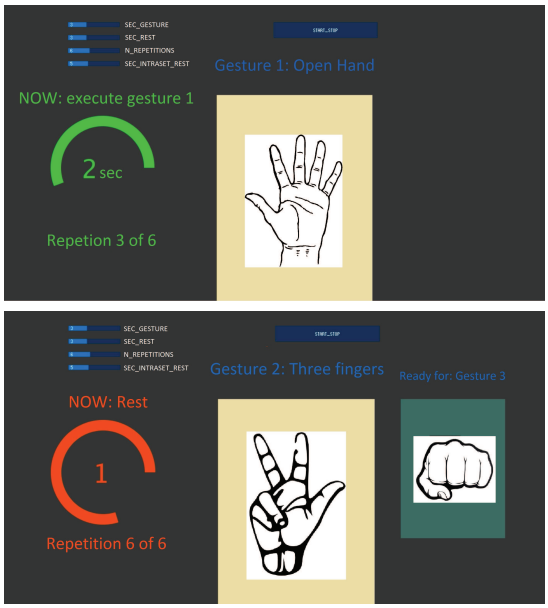

FIGURE 4.8: Graphical interface for the SVM training dataset acquisition protocol.

tedious and difficult, and it may create frustration in case of errors and therefore affect subject's motivation. This can critically compromise the performance when using the sEMG-based HRI. To reduce this effect, a specific graphical interface has be designed and implemented using Processing (*Processing Foundation* 2016), in order to help the user in executing the sequence of gestures. As can be seen in the frames of Fig. 4.8, this graphical interface shows on a screen a timer, with different colours for gesture execution and finger rest moments, and displays which gesture has to be performed, the number of the current repetition, and, finally, advises in advance when a new group of gestures has to be performed.

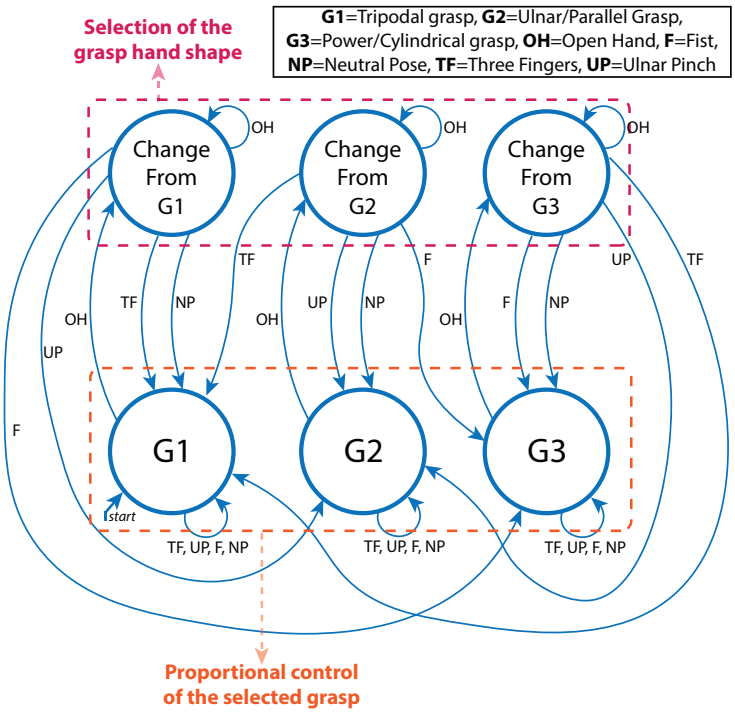

FIGURE 4.9: FSM for the hand shape transition logic.

Grasp Hand Shape Transition Logic

For the online selection of the grasp hand shape, the output of the pattern recognition is used as input to a FSM logic, that has been implemented according to the graph of Fig. 4.9. In detail, the user has to perform the Open Hand as an "exit gesture" in order to access to the grasp shape selection states, in which the system waits for a new shape indication. In the grasp selection states, a new grasp shape is enabled if a new gesture is recognized by the SVM classifier. However, once the Open Hand gesture has been detected, the user can also execute the Neutral Pose to remain in the current grasp configuration. When a grasp control state of the FSM has been accessed, the robotic hand takes the joint configuration corresponding to the relative shape, i.e. G1, G2 or G3 in Fig. 4.9. Let us take an example for the sake of clarity: if the current state is G1, to access the grasp control state G2 the user has to perform Open Hand followed by Three Fingers, whereas, to access G3, has to perform Open Hand followed by Fist. Then, in the end, once a grasp hand shape has been selected, the proportional control is enabled (see the following Subsect. 4.2.2), and it can be used to regulate closure and stiffness of the hand grasp.

4.2.2 Myoelectric Grasp Proportional Control

With the aim of providing a natural grasp proportional control of the robotic hand, the concepts of muscular and postural synergies have been jointly used in the sEMG-based HRI.

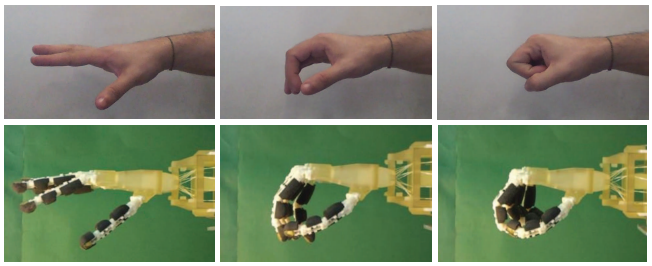

FIGURE 4.10: The user's overall opening/colsing motion of the hand (top) and the robotic hand motion relative to the first postural synergy pattern (bottom).

On the basis of the muscular synergy concept (see Chap. 2, 3), a certain pattern of muscle activations can be seen as a neural drive shared by different muscles, each of which is individually activated with a certain degree of excitation determined by spinal cord circuitries (i.e., the muscular synergy weights). Muscular synergies can be computed from a multichannel sEMG signal, and the NMF algorithm[1] can be successfully applied for this purpose. In the context of the design of the myoelectric proportional control of our HRI, the NMF algorithm is applied to forearm's sEMG signals to determine the muscular synergy matrix related to hand grasping actions. In order to give priority to the stability of the teleoperation of the robotic device, that can degrade when the control of multiple DoFs is considered (see Chap. 3), the muscular synergies are computed in relation of the activation of only one DoF. The considered single DoF regards a synergistic coordination of the hand joints: the opening and closing movements of the user's hand fingers, with the possibility of modulate both closure and stiffness of the robotic hand during grasping tasks. Furthermore, it is important to note that such hand movements involve all the joints of the hand and the wrist, and can be reasonably associated with the hand motions when only the first postural synergy is considered, see Fig. 4.10, in accordance with the postural synergy concept (Santello, Flanders, and Soechting, 1998; Santello et al., 2016).

Therefore, resuming, the grasp hand shape is firstly selected by the SVM classifier as illustrated in the Subsec. 4.2.1, whereas all the grasps are controlled by the same overall opening and closing movement of the user's hand.

Computation of Muscular Synergies for the Grasp Control

For the computation of the muscular synergy weights, the RMS value of a 8-channel sEMG recording (see Sect. 4.1.2) is considered, corresponding to n samples and collected in the matrix $E \in \mathbb{R}^{8\times n}$. On the basis of the sEMG generative model proposed

[1] Given a nonnegative matrix $A \in \mathbb{R}^{m\times n}$ (a matrix whose elements are all non-negative), the product WH is called nonnegative matrix factorization of A if nonnegative matrices $W \in \mathbb{R}^{m\times k}$ and $H \in \mathbb{R}^{k\times n}$, with $k < \min(m,n)$, are found such that the functional $f(W,H) = \frac{1}{2}\|A - WH\|_F^2$ is minimized (Berry et al., 2007).

in (Jiang, Englehart, and Parker, 2009), E can be expressed as

$$E = S_M U, \tag{4.6}$$

where $S_M \in \mathbb{R}^{8\times 2d}$ is the *muscular synergy matrix* and $U \in \mathbb{R}^{2d\times n}$ is the *neural drive matrix*, with d the number of DoFs controlled during the sEMG recording acquisition. In (4.6), E is a known matrix containing the acquired processed sEMG values, whereas U and S_M are unknown and can be assumed nonnegative, since they represent the values of $2d$ neural drives modulated by $2d \cdot 8$ muscular synergy weights, respectively. Therefore, the activation of each DoF can be expressed in terms of two nonnegative control signals of U.

Since, in our case, only the control of one synergistic DoF is considered, i.e. the overall opening and closing motion of the hand fingers, it restults that $d = 1$. As a consequence, the matrix E represents the muscle activity during the regulation of such a single DoF. Such movement, as already mentioned in the Subsec. 4.2.2, can be rasonably considered as the hand motion related to the first postural synergy. Then, in relation to this synergistic DoF, the concept of the antagonistic actuation model (Burdet et al., 2014) is exploited.

According to this view, two groups of forearm flexor and extensor muscles are considered involved in the control the synergistic DoF, representing two antagonistic actions for the regulation of the closure reference and the stiffness level of the hand. In this relation, it is therefore possible to consider two neural drives that activate such antagonistic actions, and the matrices S_M and U in (4.6) can be written for only one DoF (i.e. $d = 1$) as

$$S_M = \begin{bmatrix} s_{M_e} & s_{M_f} \end{bmatrix}, \quad U = \begin{bmatrix} u_e^{\mathrm{T}} \\ u_f^{\mathrm{T}} \end{bmatrix}, \tag{4.7}$$

where s_{M_e}, $s_{M_f} \in \mathbb{R}^{8\times 1}$ are the extension and flexion components of the muscular synergy matrix and u_e, $u_f \in \mathbb{R}^{n\times 1}$ are the extension and flexion components of the neural drive matrix. Therefore, taking into account (4.7), there is only one possible solutions of (4.6) with respect to S_M and U, that can be computed by the NMF algorithm.

Calibration Procedure for the Muscular Synergy Matrix

A short calibration phase is required for the estimation of S_M. The user has to perform a simple specific motion: open and close his/her hand (two times). During the execution of such movements, the sEMG signal is acquired to build the matrix E and then the muscular synergy matrix S_M and the offline neural drives U are computed applying the NMF algorithm.

The Online Myoelectric Grasp Proportional Control

The architecture of the online proportional control is reported in Fig. 4.11, in which it possible to clearer observe how different synergistic level are integrated in the HRI. Referring to the figure, the user opens/closes his/her hand *de-facto* controlling the fingers according to the first postural synergy joint pattern (see Subsec. 4.2.2). It follows that the human motor control system generates proper supraspinal neural drives to activate extensor and flexor groups of antagonistic muscles. These neural drives are not directly measurable, and therefore the muscular synergy matrix S_M is exploited to online estimate such neural drives from sEMG signals of the forearm muscles. Such online neural drives are used to control a virtual first postural synergy DoF, and to modulate the stiffness level of the grasp. The virtual synergistic DoF position reference is then mapped into the robotic hand joint space for the closure of different grasps by means of *ad hoc* grasp synergy mappings, as explained in the Subsec. 4.1.1, that reports the specifically designed robotic hand control architecture.

Once the muscular synergy matrix S_M is estimated, it is possible to online compute the neural drives as

$$U(t) = S_M^{+} E(t), \tag{4.8}$$

where $U(t) = \begin{bmatrix} u_e(t) & u_f(t) \end{bmatrix}^{\mathrm{T}} \in \mathbb{R}^2$ is the vector of the instantaneous values of the neural drives, S_M^{+} is the pseudo-inverse matrix of S_M and $E(t) = \begin{bmatrix} e_1(t) & \cdots & e_8(t) \end{bmatrix}^{\mathrm{T}} \in \mathbb{R}^8$ is the vector of the instantaneous values of the sEMG channels. Two control signals for the robotic hand are derived from the estimated neural drives: the synergistic closure reference of the hand $\sigma^{ref}(t)$, used in (4.4), and the grasp stiffness level $\xi(t)$, in (4.5). These control signals are obtained by linear combination of the neural drive values (in accordance with the antagonistic model concept given in Subsec. 4.2.2):

$$\begin{array}{rcl} \sigma^{ref}(t) & = & \frac{h_1}{2} u_e(t) - \frac{h_2}{2} u_f(t) + h_3 \\ \xi(t) & = & h_4(u_e(t) + u_f(t)) \end{array} \tag{4.9}$$

where h_1, h_2, h_3 and h_4 (note that $h_3 = 1$) are proper constants to normalize the neural drives values related to the flexor/extension actions and to scale σ^{ref} and ξ in the range $[0, 1]$. In this way, the user can freely use his/her natural opening/closing hand movements for the control of the teleoperated grasping device, in order to regulate the joint configurations and the he stiffness level of different grasp types.

4.3 Experimental Test of the HRI and Results

The experimental evaluation of the sEMG-based HRI system has been performed involving four right-handed and healthy male subjects (mean age 31 years, standard deviation: 4.63) in a series of grasping experiments. In the following, the subjects will be indicated as S1, S2, S3 and S4.

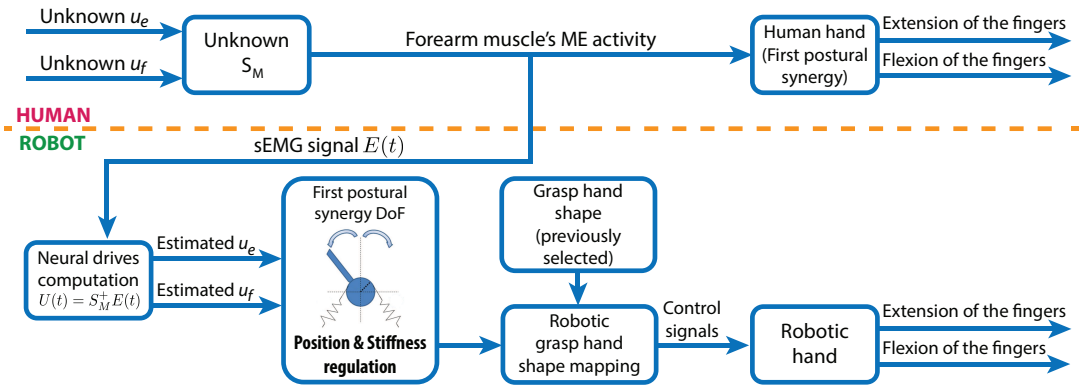

FIGURE 4.11: Synergy-centered block diagram of the sEMG-based HRI architecture.

TABLE 4.3: List of the objects for the grasping tasks.

Object type	Size [mm]	Weight [g]	UB Hand grasp	Gripper grasp
Bottle	$363 \times 96 \times 96$	400	Power	Cylindrical
Soft ball	$73 \times 73 \times 73$	180	Tripodal	Tripodal
Rigid ball	$73 \times 73 \times 73$	230	Tripodal	Tripodal
Small box	$88 \times 54 \times 40$	190	Ulnar	Parallel
Big box	$380 \times 200 \times 60$	500	Ulnar	Parallel
Paper cup	$114 \times 61 \times 61$	40	Power	Cylindrical
Adhesive tape	$84 \times 84 \times 50$	80	Tripodal	Tripodal
Spray can	$155 \times 45 \times 45$	255	Power	Cylindrical
Level	$420 \times 50 \times 20$	240	Ulnar	Parallel

Four phases compose the experimental session: *(i)* training session, *(ii)* familiarization with the system, *(iii)* grasping tasks with the UB Hand IV and *(iv)* grasping tasks with the industrial gripper. The first and second phases include the acquisition of the training datasets for the myocontroller algorithms and the use of the HRI with a robotic hand graphical simulator, whereas in the third and fourth phases the users are asked to grasp a series of 9 objects that differ by shape, weight and rigidity, as listed in Tab. 4.3. However, first of all, the user is asked to autonomously place the electrodes on his forearm (after the explanation of the experimenter), see Subsect. 4.1.2.

4.3.1 Training session Phase

Since the placement of the electrodes is not completely repeatable, and the forearm size and muscular structure vary among the users, the training session is intended to be subject- and session-dependent. After the electrode placement, the user performs

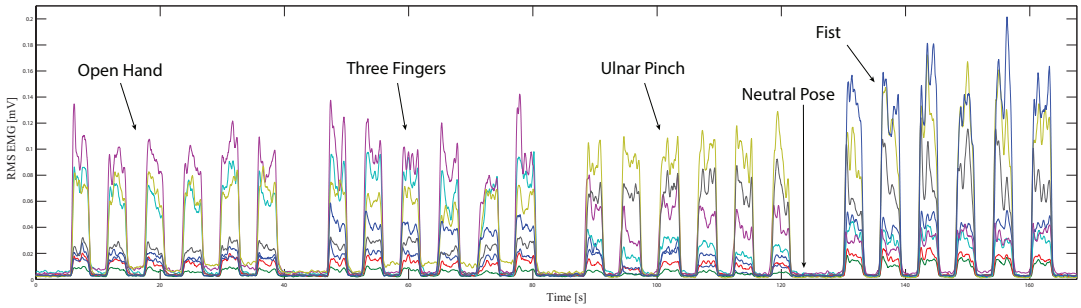

FIGURE 4.12: sEMG signals acquired during the training session of the subject S1.

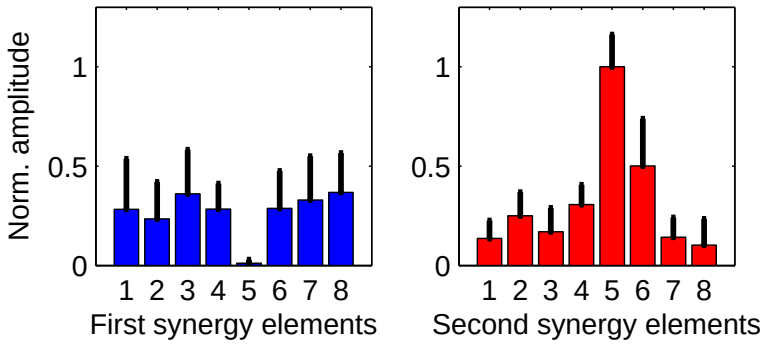

FIGURE 4.13: Mean value of the muscular synergy weights for the four subjects.

the sequence of gestures necessary to build the SVM classifier training dataset, composed by the recording of the sEMG channels. The user follows the indications of the graphical interface illustrated in Fig. 4.8, according to the protocol already explained in Subsect. 4.2.1. Fig. 4.12 shows an example of the sEMG signals acquired during the training session of subject S1, which are followed by segmentation and labelling in order to create the proper trainset for the SVM training algorithm.

Once the SVM classifier has been built, the second part of the training session is dedicated to the NMF-based estimation of the muscular synergy matrix S_M. During this stage, the user executes opening and closing movements of the hand while sEMG signals are acquired, as explained in Sect. 4.2.2; the NMF algorithm in then applied to such calibration recording and the weights of the muscular synergy matrix are obtained. In Fig. 4.13, the synergy coefficients averaged over the four subjects for the two columns of the muscular synergy matrix S_M are reported. The offline neural drives $u_e(t)$ and $u_f(t)$ estimated through the NMF algorithm for subject S3 are shown in Fig. 4.14. Thereafter, once the muscular synergy matrix estimation is completed, the myoelectric control system is ready to be used.

4.3.2 Familiarization Phase

After the training session, the user has the possibility to familiarize with the HRI controlling a graphical simulator of the three-fingered gripper, which can be observed in Fig. 4.15. In this simulator, it is implemented a graphical reference named "ghost

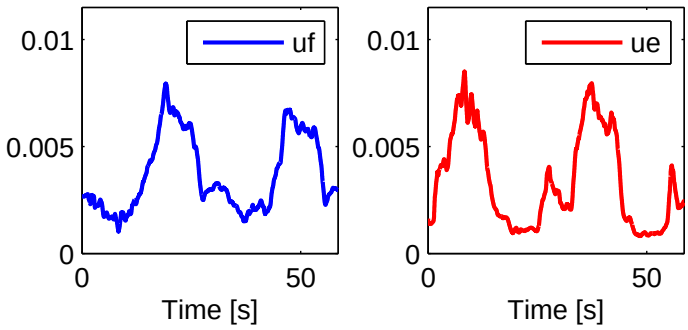

FIGURE 4.14: Offline neural drives u_e, u_f for subject S3.

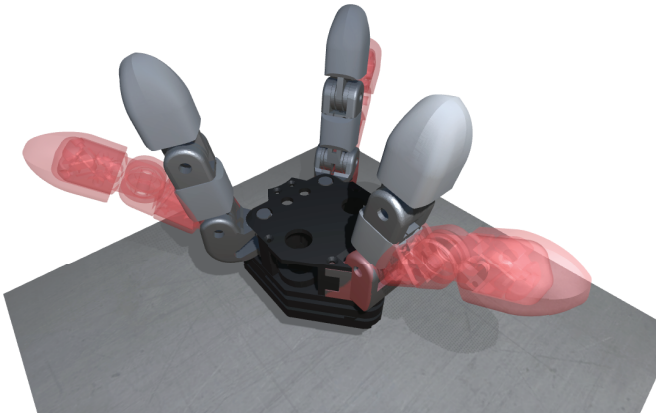

FIGURE 4.15: Graphical simulator of the gripper, with the "ghost gripper" in red.

gripper", in order to implement pre-programmed closure and stiffness profiles, that user is required to track after having freely tested the control interface for 10 minutes. Fig. 4.16 shows the results obtained by the subject S1: in Fig. 4.16(a), it is possible to see that the hand closure control signal modulated by the user (red) follows the desired tracking profiles (blue) of the ghost gripper, whereas, in Fig. 4.16(b), it can be observed how the subject successfully applies three different requested levels of stiffness.

4.3.3 Grasping Task Phases

The experiment that the users have to perform consist in grasping 9 objects with a type grasp that is previously decided on the basis of the object physical form (see Tab. 4.3). In particular, the user has to teleoperate the robotic hand such that the grasp is successfully executed, that is the object is stably held (without squeezing it in case of a soft object) and then released, once it is asked by the experimenter. During the grasping experiments, the subject is seated while looking at the nearby robotic hand, and the experimenter hands out the objects one at a time, reminding to the user the correct object-related grasp hand shape.

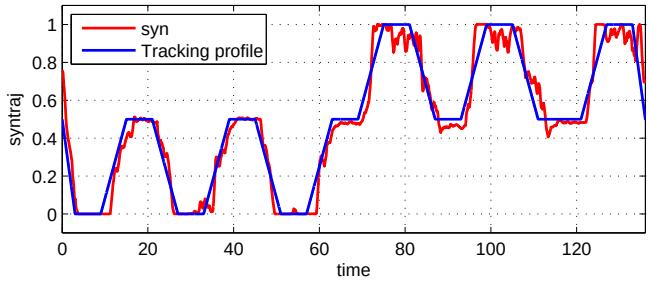

(a) Closure profile tracking.

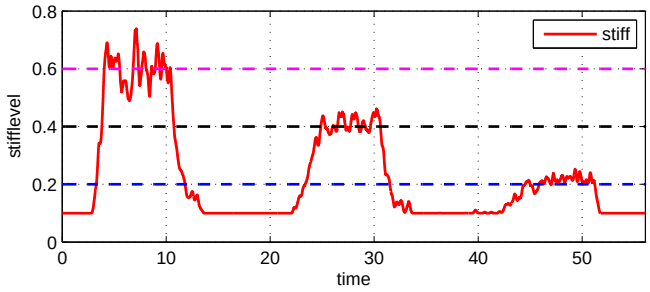

(b) Stiffness level tracking.

FIGURE 4.16: Tracking tasks for the subject S1 with the simulated gripper.

The experimental protocol is composed by 5 repetition of the grasp of the 9 objects, executed in a random order for the UB Hand and for the gripper (avoiding the same grasp type for two consecutive objects), resulting in a total of 360 grasping tasks over all the subjects.

Grasping Tasks Controlling the UB Hand IV

The anthropomorphic robotic hand is used in the first part of the grasping tasks. Fig. 4.17 shows three moments of this session, one for each type of grasp. In this phase, the evaluation is focused on the rate of success respect to two tasks: (i) the selection of the desired grasp hand shape (i.e., the experimental accuracy of the SVM-based pattern recognition), and (ii) the overall grasp tasks (i.e., grab, hold and release the object). The success percentages computed over the five grasping series for each subject are reported in Tab. 4.4. This results show average success greater than 90% for the considered tasks "G1 selection", "G2 selection", "G3 selection" ad "Grasp completion" (with 7 cases of total success for single subjects), and a mean success rate of 96.3% over the 4 healthy subjects.

Such scores reveal a higher accuracy of the classifier, also with respect to the design of the training session protocol. Furthermore the users were not failing the overall grasp task in case of an error in the gesture classification, since it concerns only the grasp *shape* selection, contributing to reduce the reliability issue of the myoelectric controller and the linked subjects frustration.

TABLE 4.4: Success rates computed over the five grasping task series.

Evaluated Task	Success for S1	Success for S2	Success for S3	Success for S4	Average Success
G1 selection	100%	86.7%	93.3%	100%	95%
G2 selection	93.3%	100%	93.3%	80.7%	91.8%
G3 selection	100%	93.3%	100%	93.3%	96.7%
Grasp completion	100%	97.5%	95%	92.5%	96.3%

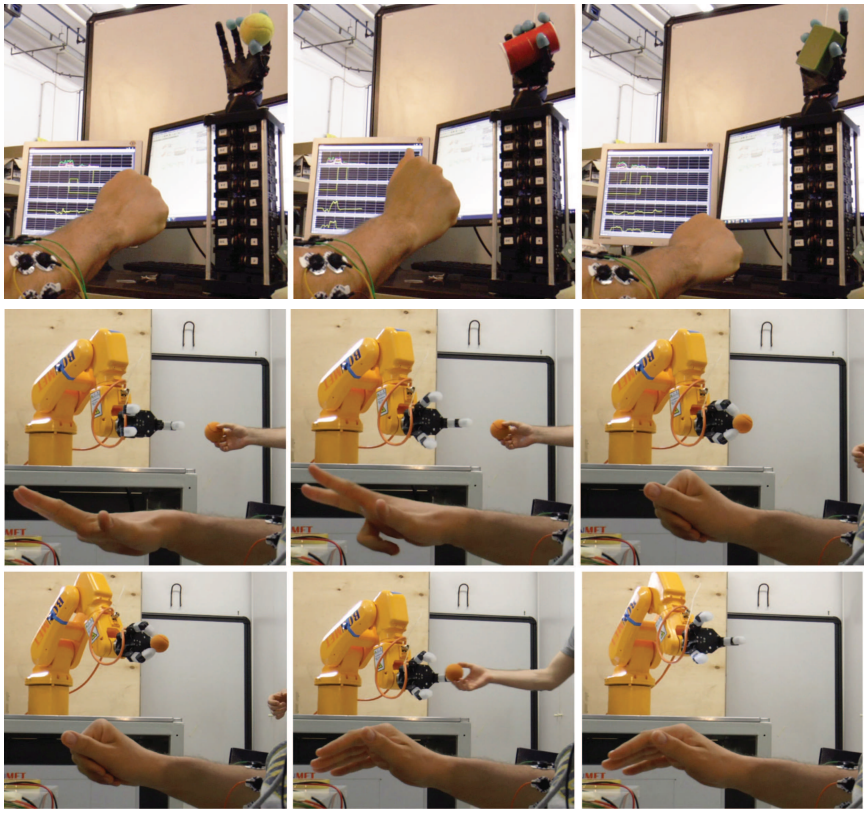

FIGURE 4.17: Frames from the grasping tasks experiments with the UB Hand IV (top row) and with the gripper (middle and bottom-rows).

Grasping Tasks Controlling the Industrial Gripper

The sequences of grasps for this test with the three-fingered gripper are the same used with the UB Hand, but now the robotic hand is mounted as end-effector of a 6 DoFs industrial manipulator, that is programmed in order to automatically execute a sequence of movements. In detail, the following motions are executed: *(i)* move to the workspace area where the object has to be grasped, *(ii)* lift and lower the held object, *(iii)* go to the release area and, finally, *(iv)* go back to the initial position. The subject has to perform the grasp (between the steps *(i)* and *(ii)*), stably hold the object (during the stages *(ii)-(iii)*) and release the object at the end of the task (between the steps *(iii)* and *(iv)*). This sequence can be observed in Fig. 4.17. An interesting aspect in these experiments is that the user has to synchronize to pre-programmed manipulator motions in order to successfully complete the overall grasp task, simulating an industrial-like situation with predetermined automatic sequences.

In this phase, the evaluation is focused on the degrees of control provided to user through the grasp proportional control, that are the regulation of closure and stiffness of the grasp. Fig. 4.18 depicts along time the output of the gestures classifier during the selection of the grasp hand shape, the closure reference σ^{ref} and the stiffness signal ξ, for the grasp of the representative objects Big Box, Paper Cup and Rigid Ball (Fig. 4.18(a), 4.18(b), 4.18(c) respectively). The dashed lines delimit two parts of the graphs: one related to the grasp selection phase, and the other regarding the proportional control phase. For example, on the left part of Fig. 4.18(a) it is possible to observe that the user executes an Open Hand, followed by an Ulnar Pinch to select the ulnar grasp for the robotic hand. Differently, on the right side the subject continuously controls the closure and stiffness of the chosen grasp, according to the object characteristics and to the visual and audio feedbacks (see Sec. 4.2). It is possible to see how the stiffness value is naturally adjusted: a higher level is used to grasp the Big Box (Fig. 4.18(a)), that presents greater dimensions and weight, whereas a lower level is necessary to grasp the lighter, but not flexible, Rigid Ball (Fig. 4.18(b)), and an almost minimum value is provided to not squeeze the very soft Paper Cup (Fig. 4.18(c)). Note also that, in the latter case, the synergistic closure reference is not brought to the maximum limit by the user, in order to act a more delicate grasp action.

Similar behaviors have been performed by all the subjects in a totally independent and natural manner, once the training and familiarization phases were carried out. This means that the users have the capability, thanks to the proposed sEMG-based HRI, to adjust both the joint (synergistic) positions and the level of stiffness during the teleoperation of the grasp, being able to do it naturally inasmach the myoelectric controller reflexes intuitive and neuromuscular-related specification. Finally, the subjects also showed to properly understand – in a passive/indirect manner – the integration of the different synergistic levels of the system for the control purposes, suggesting that a synergy-based design of HRI for teleoperation of grasping tasks is easily comprehensible for the users.

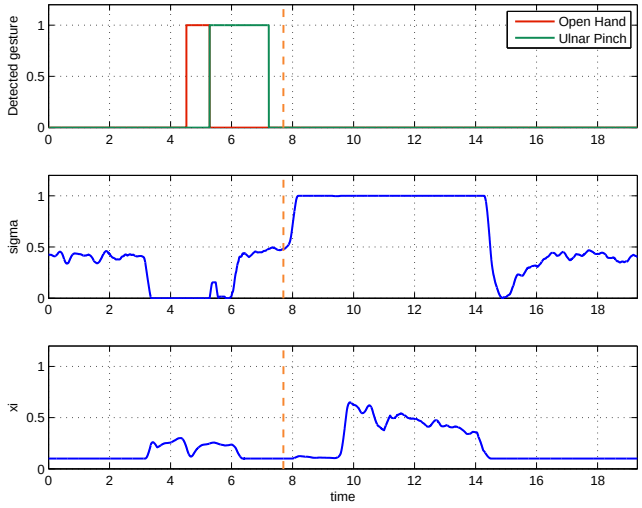

(a) Big Box

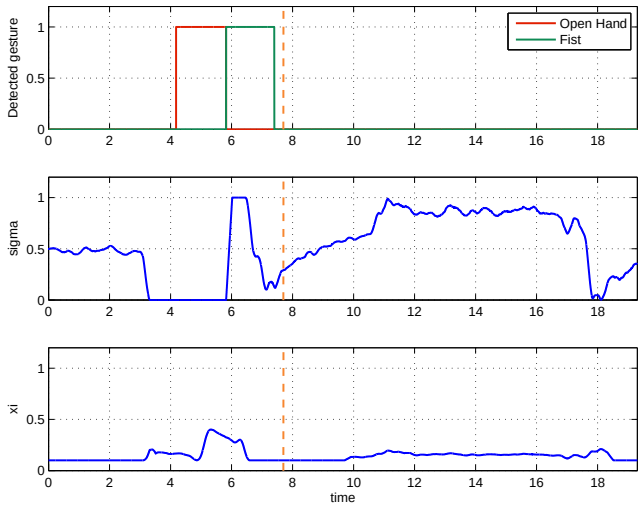

(b) Paper Cup

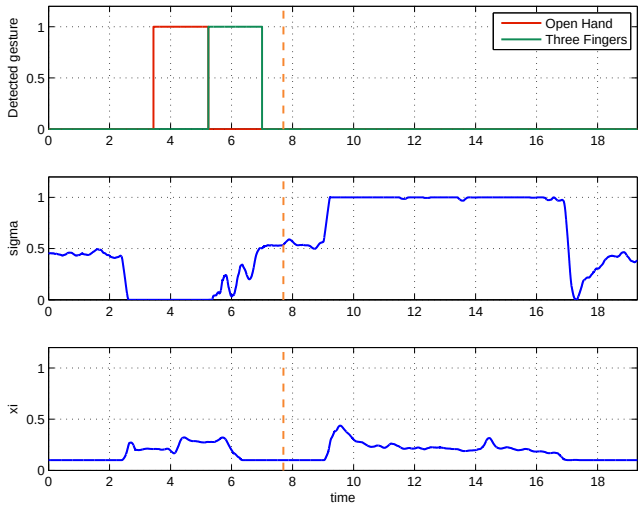

(c) Rigid Ball

FIGURE 4.18: Temporal plot of the control signals for the grasp of the objects Big Box, Paper Cup and Rigid Ball.

4.3.4 Conclusion and Future Work

In this chapter the design of sEMG-based HRI exploiting neuromuscular information to allow the user regulating in a natural fashion the behaviour of robotic hands during grasping tasks has been proposed. In particular, the human-like degrees of control provided to the user of the HRI, combined with the possibility of selecting the grasp shape by means of gestures classifications, have been tested through several grasping experiments. The users controlled a dexterous anthropomorphic robotic hand and an industrial gripper mounted on a manipulator, resulting in a mean overall grasp success ratio of 96.3% among 4 healthy subjects. By virtue of the combination of ML-based pattern recognition and grasp proportional control, the teleoperation of the artificial hands resulted stable, intuitive and natural, allowing a proper modulation of the grasp closure and stiffness in a way as the antagonistic actuation is responsible in the human body.

Future work will be focused on several aspects. The improvement of the HRI system performance from a user-centred point of view will be studied, first of all investigating for a more effective feedback information modality, preferably based on a haptic feedback interface. Further investigation on the extraction of additional information about postural synergies from sEMG signals will be among future interests, for example exploring the measurements of the activations of also intrinsic muscles of the human hand. Finally, it will be explored the possibility of sensor fusion techniques (e.g. exploiting the IMU sensor) to increase the intuitiveness of the control of the artificial hands.

Chapter 5

A sEMG-Based Interface for Elbow Assistive Devices

Recently, the mechanization of physical therapies is showing a substantial development (see Chap. 3). One important contribution to this trend can be found in the repetitive training tasks as a form of rehabilitation for limb injuries, resulting from accidents, cerebral apoplexy, strokes and problems in motion due to advanced ages (Sugar et al., 2007). Indeed repetitive movements can improve muscular strength in subjects with both neurological or orthopedic problems. In addition, this kind of therapy serves also to prevent and support the recovery of secondary complications such as muscle atrophy, especially experienced when subjects are restricted in movements or confined in a bed for a long time (Topp et al., 2002), e.g. during extensive hospitalization. However, therapies for the cited categories are difficult to be provided and evaluated in a quantitatively and objectively form (Sugar et al., 2007), resulting in a discrepancy between potential and real efficiency of the treatments. Therefore, in this context, the application of advanced robotic systems can play a crucial role in the evaluation, enhancement and documentation of the rehabilitation processes, bringing to an optimization of the intervention for the motor activity recovery. In particular, the focus of this chapter will be on control interfaces for Wearable Assistive Devices (WADs) (see Chap. 3), that are robotic systems designed to assist human movements. WADs are principally employed for compensation of musculoskeletal disorders and enhancement of neuromuscolar rehabilitation, but also for human power augmentation such as improvement of endurance and strength performances during physical task executions.

As a central point, it is important to note that, despite the different goals and implementations of WAD systems, the control strategy to be used in order to obtain appropriate behaviours is a common issue and still a challenge for the research community (Chap. 3). This arises mainly from the fact that WAD systems are characterized by a close interaction with the human user, in a *human-in-the-loop* framework where the operator is directly a part of the control system. In this relation, it becomes fundamental to design a proper HRI in order to correctly provide to the user the required assistance, in view of an understanding of human efforts and/or intended movements. In the next sections, the design and implementation of sEMG-based

interface solutions as a contribution to address such requirements is presented.

First – just after the presentation of the hardware setup used within the research work of this chapter – a preliminary study about an assistive application based on sEMG-driven modelling of the muscle during isometric contractions is reported. The proposed model has been exploited to drive a WAD in order to limit the force of the user's biceps muscle to a maximum desired threshold value in isometric condition, against the application of a force profile on the forearm.

Thereafter, a sEMG-based control solution for elbow WADs during load lifting tasks in dynamic conditions is presented. In particular, the proposed control lies on a sEMG-based error-related proportional-integral action. The aim is to avoid myoelectric control strategies based on algorithms for the estimation of the joint torques, therefore working toward a simplification in the use of the HRI, which bypasses complex task- and subject-dependent training sessions for tuning the control algorithms (see Chap. 3).

5.1 Assistive Application Setup

The sEMG-based HRIs presented in this chapter are used for the control of a wearable system for elbow joint assistive applications. Such system includes the sEMG acquisition hardware and the Twisted String Actuation (TSA) module used as WAD to support muscle activity applying a suitable external force on the users' forearm.

5.1.1 Twisted String Actuation Module

In order to experimentally test the sEMG-based control interfaces for elbow WAD proposed in this thesis work, a TSA module (Hosseini et al., 2017) to provide external physical support to the user is used. The TSA module has been specifically designed for wearable assistive and rehabilitation applications, and for this reason its structure is thought to be light-weight and to have lower size and mechanical complexity. Indeed, the TSA concept itself implements a light-weight, low cost and compact linear transmission system (Shoham, 2005).

The details of the TSA modelling can be found in (Palli et al., 2013), whereas here the concept is briefly reported. A couple of strands are attached to a rotative electrical motor and twisted on one end, whereas on the other end the strands are connected to a linear moving element, i.e. the load. The overall string length is reduced by the rotation produced by the electrical motor. Therefore, the rotative motion of the electric motor is converted into a linear motion on the other side of the string. Specifically, with an appropriate choice of the string parameters (in particular the strand radii and lengths) and of the rotative electric motor, it is possible to fulfil the generally stringent requirements for the implementation of a miniaturized and highly-integrated mechatronic device, in which the slender structure of the TSA makes it particularly suitable for wearable devices.

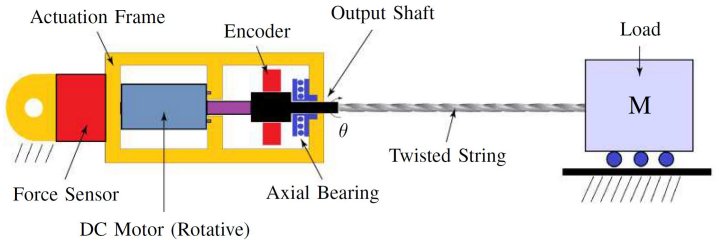

FIGURE 5.1: TSA module conceptual structure.

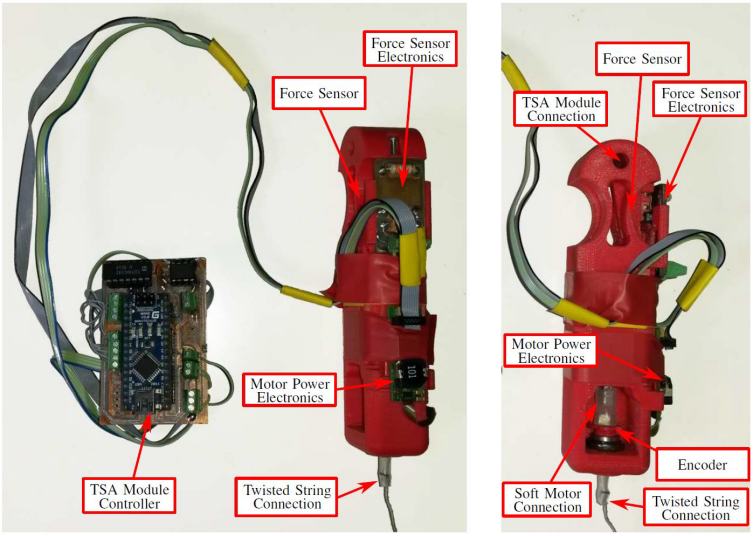

FIGURE 5.2: View of the TSA module: frontal view and control electronics (left); lateral view (right).

The main components of the structure of the TSA module are conceptually depicted in Fig. 5.1. The module body is manufactured in Acrylonitrile Butadiene Styrene (ABS) plastic by 3D printing, and a commercial optoelectronic component called light fork – because of its forked structure – has been adopted for the force sensor implementation. The light fork hosts in its package both the Light Emitting Diode (LED) and the Photodetector (PD) that are required in order to measure the deformation of the compliant frame on which the the force measure is based. The module is driven by a low-cost DC motor, and a combined axial-radial bearing is adopted to support the output shaft at the location of the twisted string connection. Moreover, the actuation module is also equipped with an optical encoder for output shaft position measurements. In Fig. 5.2 it is possible to observe a picture of the TSA module, together with the control electronics.

5.1.2 sEMG Signal Acquisition Hardware and Electrodes Placement

For the sEMG-based HRIs presented in this chapter, a couple of differential sEMG electrodes have been placed in proximity of the *biceps brachii* muscle belly in the upper arm, referring to methods and best practices outlined in (Perotto, 2011). Since

the goal of the assistive tasks considered in this research work is to provide support to the elbow joint during the application of loads on the forearm (see Sec. 5.2, 5.3), only the sEMG activity of the principally involved biceps muscle is acquired, without considering the triceps activation within the enclosure of this study.

The sEMG signal has been acquired by means of low cost disposable surface electrodes, connected to the acquisition board *Cerebro* (see Chap. 4) and applying a filtering procedure composed by *(i)* a 50 Hz notch filter and *(ii)* a 20 Hz high-pass filter for the assistive application of Sec. 5.2, whereas for the application of Sec. 5.3 also *(iii)* the RMS value over a 200 ms running window, using the exactly same acquisition procedures already described in Chap. 4.

5.2 sEMG-Driven Assistive Application in Isometric Conditions

A HRI for the control of the TSA module WAD based on a sEMG-driven isometric contraction muscle model is presented. The goal of the myocontrol is the online regulation of the external support action provided by the wearable device to the user, with the aim of assisting the user's forearm such that the biceps exerts an arbitrary residual tendon force. The isometric configuration is obtained by asking the user to keep the forearm held at a fixed angle, with the WAD compensating for an external load profile applied to the wrist.

This is possible thanks to the integration of the muscle model within a HR control loop including the TSA module low-level controller. Such muscle model takes as input the sEMG activity measured during the isometric contractions and translates it into the muscle force. An experimental evaluation test has been carried out as a preliminary proof of the validity of this assistive application paradigm, especially with regard to its use in the regulation of the WAD action.

5.2.1 Model of the Muscle for Isometric Contractions

In order to reconstruct the force exerted by the muscle, a model of the muscle mechanics during isometric contractions is here presented. Specifically, the model is driven by sEMG-based measurements of the muscle activation, which are provided as an input, exploiting that the myoelectric signal can be used as a valid average MUs activation measure (see Chap. 2). Furthermore, it is important to note that for this reason the absolute value of the sEMG activity can be considered, net of a non-linearity to be taken into account, to represent the muscle contractile element's impulsive force, according to (Winter, 2009).

Referring to the general musle modelling concepts reported in Chap. 2, Fig. 5.3 depicts the lumped parameters scheme of the muscle model presented in this section. The following components are included: *(i)* the muscle tissue mass m; *(ii)* a linear damper characterized by damping coefficient b (for the consideration of the

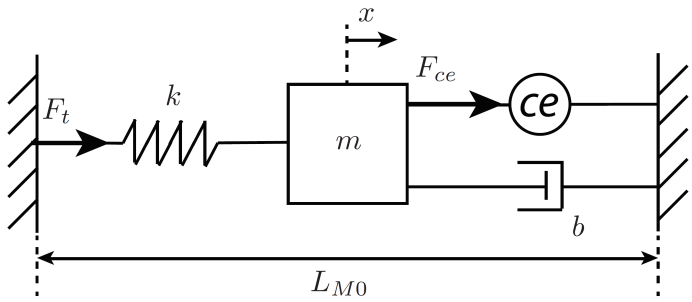

FIGURE 5.3: Muscle mechanical model with lumped parameters during isometric contractions.

muscle internal viscous behavior); *(iii)* a linear spring with stiffness k (for the consideration of the series-elastic behaviour of mainly tendon, cross-bridges and fascia); *(iv)* a force generator (to represent the contractile element (CE) impulsive force). Our model is based on the assumption that only isometric contractions are considered in this study. It follows that it is possible to consider the total length of the muscle constant, which is indicated by L_{M0}. According to what mentioned so far, the muscle behavior can be described by the following equations

$$F_{ce}(t) = m\,\ddot{x}(t) + b\,\dot{x}(t) + F_t(t), \tag{5.1}$$

$$F_t(t) = k\,x(t), \tag{5.2}$$

where $F_{ce}(t)$ is the impulsive force generated by the contractile elements and $F_t(t)$ is the muscle tendon force. In order to predict the muscle force exerted on a body segment given the force generated by the contractile element, the second order differential equation (5.1) must be numerically integrated, and to do this it is possible to exploit the fact that the muscle twitch waveform exhibits a second-order critically damped response (Milner-Brown, Stein, and Yemm, 1973), because it gives knowledge about the muscle parameters m, b and k, that are not directly measurable (see Chap. 2). Indeed, a critically damped response for the considered muscle model is achieved by assuming a twitch time equal to $T = 2m/b$. In this way, considering that $b = \sqrt{mk}$, it is possible to compute the two ratios $b/m = 2/T$ and $k/b = 1/2T$. Adding to these assumptions that the Laplace transform of the differential equation (5.1) is

$$F_{ce}(s) = m\,s^2 x(s) + b\,s\,x(s) + k\,x(s), \tag{5.3}$$

the solution can be computed by means of the scheme reported in Fig. 5.4.

The force F_{ce}, in accordance with what has just been said above, is given by

$$F_{ce}(t) = f(\,|\,Z(t)\,|\,) \tag{5.4}$$

where $Z(t)$ denotes the sEMG signal value and $f(\bullet)$ is a curve-fitted non-linearity empirically determined. In order to obtain the expression of such a nonlinear fitting,

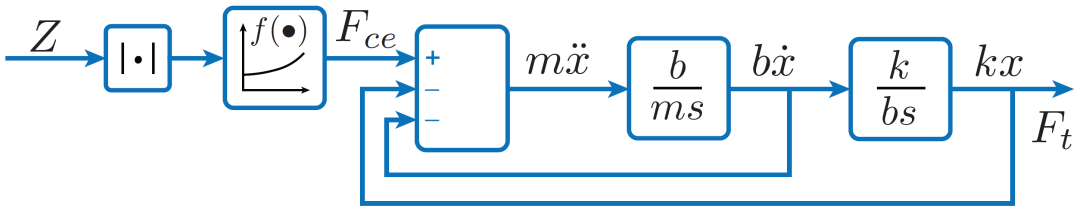

FIGURE 5.4: Block diagram that permits to solve the differential equation (5.1) and to simulate the sEMG-driven muscle behavior.

$f(\bullet)$ is approximated with a second-order polynomial:

$$f(\,|\,Z(t)\,|\,) = a_1\,|\,Z(t)\,|^2 + a_2\,|\,Z(t)\,| + a_3. \tag{5.5}$$

The constant parameters a_1, a_2 and a_3 have been calculated by means of the simplex search algorithm (Lagarias et al., 1998), with cost function

$$e = \frac{1}{N}\sqrt{\sum_{n=1}^{N}(F_{e_n} - F_{t_n})^2}, \tag{5.6}$$

where: $F_{e_n} = F_{e_1}, ..., F_{e_N}$ represent a set of constant force values, that are applied to the muscle tendon due to an external load over proper temporal windows; $F_{t_n} = F_{t_1}, ..., F_{t_N}$ represent a set of mean values of the force F_t estimated by the here presented sEMG-driven muscle model that is necessary to ensure the isometric configuration during the same temporal windows in which the external load is applied; N is the number of value pairs (F_{e_n}, F_{t_n}). Please refer to Fig. 5.4 and to the next subsection for further details.

Identification

In the following, the methods, procedures and an experimental sEMG recording for the identification of the coefficients for the muscle model non-linear fitting (Sec. 5.2.1) are reported. The myoelectric signal has been acquired from the biceps muscle during isometric contractions of a healthy subject involved for the study.

The procedure for the acquisition of the data requires the subject to stand upright in a natural pose, flexing the upper arm such that it is parallel to the trunk and keeping an elbow angle of 90 degrees. This configuration is observable in Fig. 5.5, where it is possible to see that a downward load F_L is applied in proximity of the wrist. In particular, the subject is asked to keep the elbow joint angle constantly at 90 degrees, in order to assume a reasonably acceptable static condition to ensure the biceps isometric contraction only. The load F_L is applied to the user's forearm by means of a cuff connected to a linear motor equipped with a load cell sensor (Fig. 5.5). Note that the linear motor is controlled to act as an ideal force generator, compensating for the slider inertia and friction, for details see (Palli and Melchiorri, 2008). With the illustrated setup, a trapezoidal profile composed by eight increasing

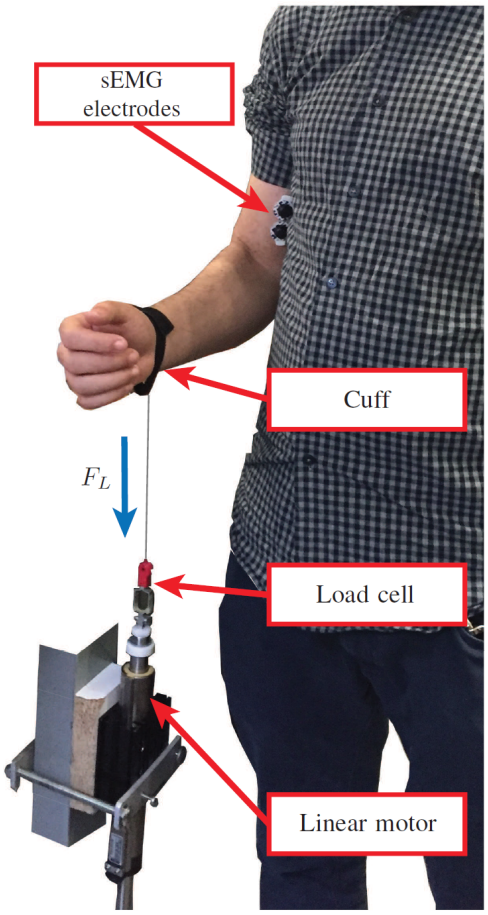

FIGURE 5.5: Configuration and setup of the experimental acquisition session for the identification of the muscle model non-linear fitting.

load values ranging from 0 N to 40 N has been applied to the forearm during the sEMG signal acquisition in order to identify the model fitting parameters.

To this purpose, let us consider the diagram depicted in Fig. 5.6. With respect to the elbow joint, the torque equilibrium can be described by the equations

$$\begin{aligned} \tau_B &= \tau_e, \\ \tau_B &= F_B\, l_B, \\ \tau_e &= F_P\, l_P + (F_M + F_L)\, l_L \end{aligned} \tag{5.7}$$

where τ_e is the torque due to the external forces, τ_B is the torque generated by the biceps to balance the external load, F_P is the gravitational force acting on the arm and the hand (considered concentrated on a single point of distance l_P from the elbow rotation axis), F_M and F_L are the weight of the linear motor and the load applied at a distance l_L from the elbow, and F_B is the force that the biceps exerts in order to balance the external forces, with l_B denoting the muscle moment arm (see Chap. 2).

The force F_B can be computed considering that it is equal to the resultant of the external forces acting on the forearm transposed to the biceps side, named F_e, as

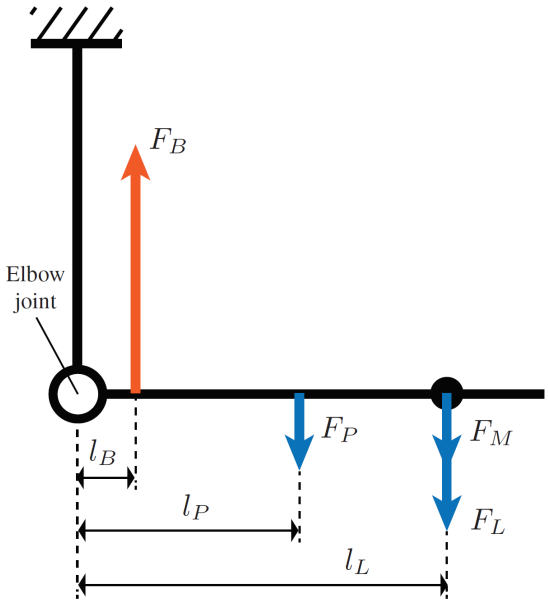

FIGURE 5.6: Representation of the forces acting on the forearm during a load compensation with the elbow joint angle flexed at 90 degrees.

$$\begin{aligned} F_B &= F_e, \\ F_e &= \frac{F_P\, l_P + (F_M + F_L)\, l_L}{l_B}, \end{aligned} \tag{5.8}$$

that can be used for the estimation of the parameters appearing in eq. (5.5). It is worth to highlight that the biceps moment arm l_B used in (5.8) is only an approximative estimation of a reasonable value for the subject involved in the experimental session. However, the introduced error is caused by an approximative measurement that only correspond to a scaling of the estimated muscle force, and therefore do not deprive the muscle model properties and the practical validity of the non-linearity estimation.

The muscle model and musculoskeletal parameters referred to eqs. (5.1) and (5.8) are reported in Tab. 5.1, where a typical mean value has been chosen for the biceps brachii twitch time T (Winter, 2009). For the identification of the model non-linear fitting parameters a_1, a_2 and a_3, the required signals are the linear motor load force F_L and the biceps myoelectric activity. Note that, the sEMG signal is pre-processed to obtain the input signal $Z(t)$ used in the muscle model, with the filtering procedure reported in Subsec. 5.1.2. The linear motor load force F_L is acquired by means of the embedded load cell. Figure 5.7 shows the resulting external force acting on the biceps F_e, calculated through eq. (5.8) and compared with the muscle tendon force F_t, the latter computed by means of the proposed muscle model, where the non-linear fitting has been obtained through the optimization procedure described in the Sec. 5.2.1. Note that the values F_{e_n} and F_{t_n} in the cost function (5.6) are obtained

TABLE 5.1: Musculoskeletal parameters.

Parameter	Value	Parameter	Value
T	$52\,ms$	F_P	$10\,N$
b/m	$38.46\,ms^{-1}$	l_L	$26\,cm$
k/b	$9.61\,ms^{-1}$	l_P	$19.5\,cm$
F_M	$9.8\,N$	l_B	$2.5\,cm$

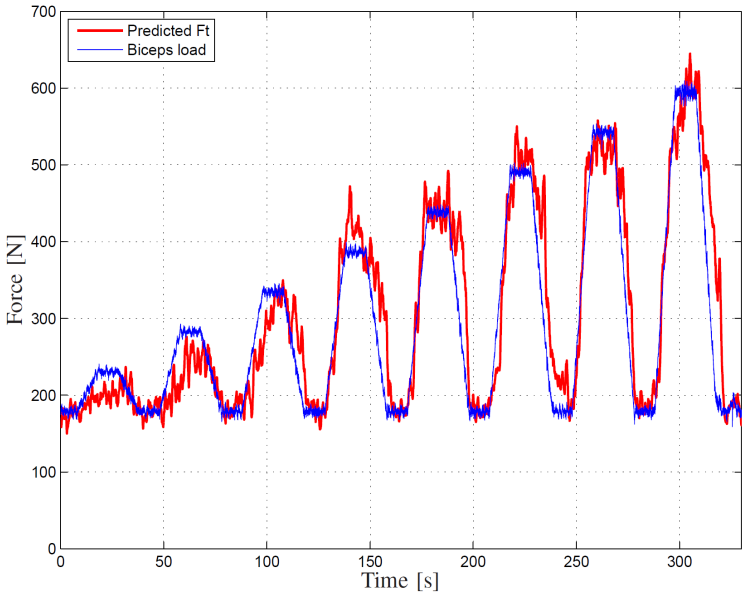

FIGURE 5.7: Biceps load force (blue) calculated from the profile of the force applied to the wrist and estimated biceps tendon force (red).

considering the temporal windows coinciding with the constant trend of the trapezoidal profile of Fig. 5.7 (with $N = 8$), and computing the mean value of the load and the model-predicted force of the biceps. As it can be seen in Fig. 5.7, the predicted muscle tendon force follows the load on the biceps with acceptable error. In particular, simplifications in the the assumptions and uncertainties in the measurement and in the choice of the musculoskeletal parameters are the principal cause of the the difference between measured and predicted signals.

5.2.2 Experimental Evaluation of an Assistive Application

The TSA module described in Subsec. 5.1.1 has been used as WAD for the support of the elbow joint, in an assistive application that exploits the muscle model proposed in this section. Specifically, the muscle model takes as input the measured sEMG activity in order to compute the force generated by the biceps muscle. Such output is then used to regulate the TSA module to produce the necessary support to the user. The target assistance consists limit the muscle force to a desired value, that is achieving a desired compensation of the muscle effort during isometric contractions. A subject is involved in an experimental validation of the sEMG-based

HRI system, wearing the WAD as shown in Fig. 5.8. The TSA module is fixed on a shoulder support that has been specifically designed and realized by 3D printing rapid prototyping, and it is fixed to the trunk of the user by means of two elastic bands. Furthermore, a spherical joint is implemented in the connection point between the TSA module and the shoulder support in order to let the overall structure properly fit the user posture without invalidating the WAD functionalities. On the user's forearm, an armband is firmly fixed, on which the twisted cable of TSA module is connected in order to support the user movements. The posture of the subject reflex that one already illustrate in Subsec. 5.2.1, that can be seen also in Fig. 5.5, as well as the placing of the differential sEMG electrodes pair in proximity of the biceps brachii muscle.

sEMG-Driven Control Loop

A particular control loop that exploits the sEMG signals and the proposed muscle model in order to properly regulate the WAD support action has been designed and implemented. The objective of the TSA module regulation is to automatically compensate an external load profile applied to the user forearm (see Fig. 5.5), in terms of letting the biceps muscle exerting only a residual specified force to keep constant the elbow joint configuration.

The sEMG-based control loop for regulation of the desired behaviour of the WAD is depicted in Fig. 5.9. During this experimental validation, the user is asked to hold the arm in a fixed position with the elbow flexed at 90 degrees compensating the load applied to his wrist with an isometric contraction of the biceps, resulting in an increase of the muscular activity detected by the sEMG signal. Such informational content is translated in a muscle force feedback thanks to the in-loop integration of the muscle model described in Subsec. 5.2.1. Specifically, within the control loop, the proposed muscle model is used to convert the sEMG signals into the force acting on biceps tendon, allowing to directly specify a reference tendon force reference as an input of the control scheme. In other words, a target limitation to the maximum force exerted by the tendon on the body segment can be defined, independently from the load applied to the user forearm (within the limits of the force that the WAD can provide). The mentioned control objective is therefore achieved by means of a PI controller that computes the reference force for the TSA module low-level controller (Fig. 5.9) in such a way the correct support can be automatically provide to the user's forearm.

The result of the experimental validation of the system can be seen by the graphs reported in Fig. 5.10. In particular, in Fig. 5.10(a) the biceps tendon force online estimated by the sEMG-driven muscle model is plotted together with a trapezoidal force profile F_L (see eq. (5.7)–(5.8)) applied as a load to the user's forearm; the TSA module WAD is not active, therefore the user is in charge of fully compensating the external load by his biceps effort, and the estimated tendon force actually follows the load force profile, confirming an acceptable accuracy of the proposed muscle

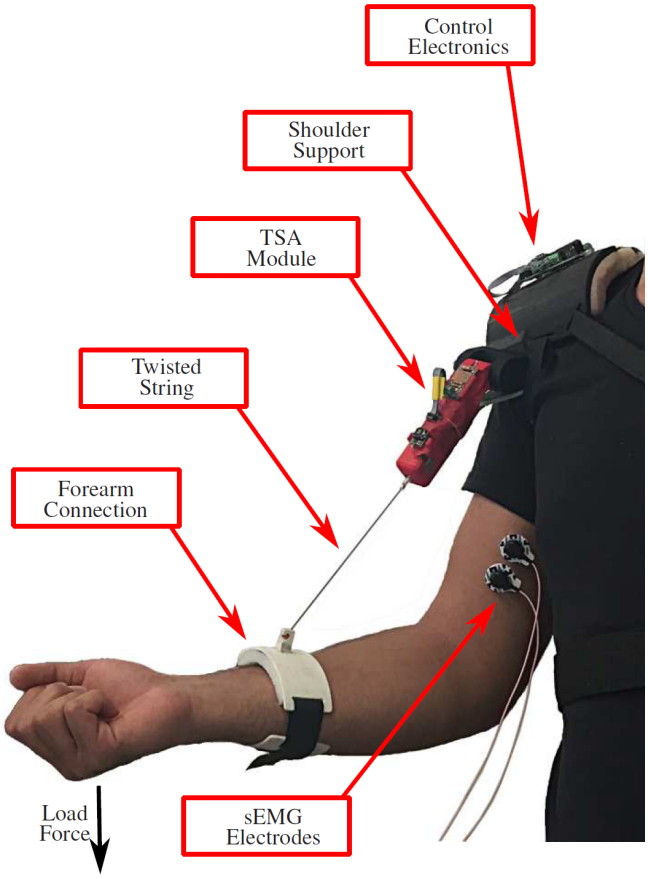

FIGURE 5.8: The TSA module worn by the subject for sEMG-model-driven assistive application.

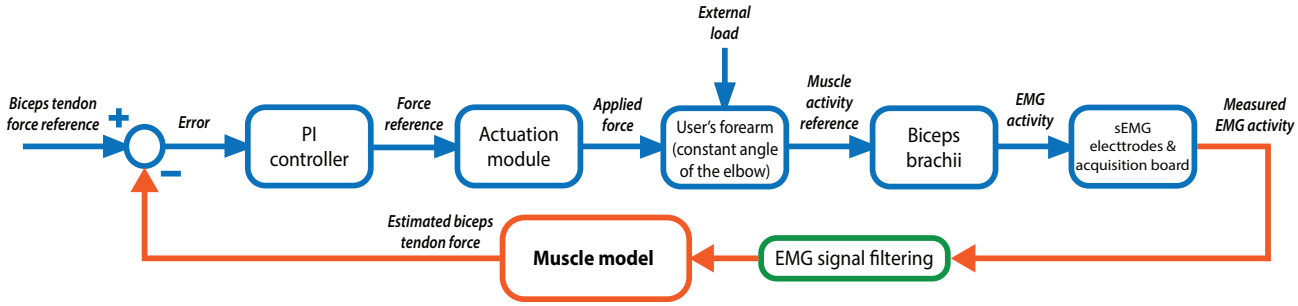

FIGURE 5.9: Muscle model in-loop control architecture for the automatic regulation of TSA module support.

model. On the other hand, in the behaviour reported in Fig. 5.10(b), the sEMG-based control loop of the TSA module is active for the same trapezoidal load profile, setting the reference muscle tendon force equal to 350 N (reference input in the scheme of Fig. 5.9). In particular, in this last figure, it is possible to observe that the support provided by the WAD is able to limit the force exerted by the biceps, making the tendon force F_t following with a reasonable oscillating trend the indicated reference value.

5.2.3 Conclusion

In the HRI for WADs reported in this section, the sEMG signal has been used as input to a muscle model for isometric contractions, with the goal of computing the force generated by the biceps to counteract an external load profile applied to the user's forearm. Although some errors in the load force reconstruction are shown after parameter identification (ascribable to parameter uncertainties), the result is considered reasonably acceptable (see Fig. 5.7), and the achieved performance allows to successfully use the proposed muscle model to regulate the support action of a TSA module assistive device. In particular, the compensation of the force generated on the tendon by the biceps brachii can be seen in Fig. 5.10(b). This result is intended as the positive outcome of a validation study to demonstrate the feasibility of the proposed sEMG-based human-in-the-loop approach for WADs. Specifically, TSA module can be successfully used to provide actual and effective support for assistive applications.

5.3 sEMG-Driven Assistive Application for Load Lifting Tasks

The interface presented in the following subsections has the goal to extend to a dynamic musculoskeletal situation the support action provided by sEMG-driven elbow WADs, with the aim of achieving an actual compensation of the the user's muscle efforts. Specifically, in the study that has been curried out within the research work reported of this thesis, it is considered the elbow assistance during lifting tasks of a load. In particular, the proposed myoelectric HRI – differently from the validation study of the previous section in isometric conditions – wants to bypass the use of physiological models for the estimation of muscular forces and joint torques, since they require complex subject-dependent training sessions for the identification/tuning of several parameters, causing a limitation in the use of sEMG-based WADs in real applications and with different users (see also Chap. 3).

5.3.1 The Load Lifting Tasks Protocol

Fig. 5.11 depicts a future conceptual view of the elbow WAD based on the fixation of the TSA module on the back of the user. Differently, for the experimental evaluation of the myoelectric control strategy that is presented in the next Subsec. 5.3.2,

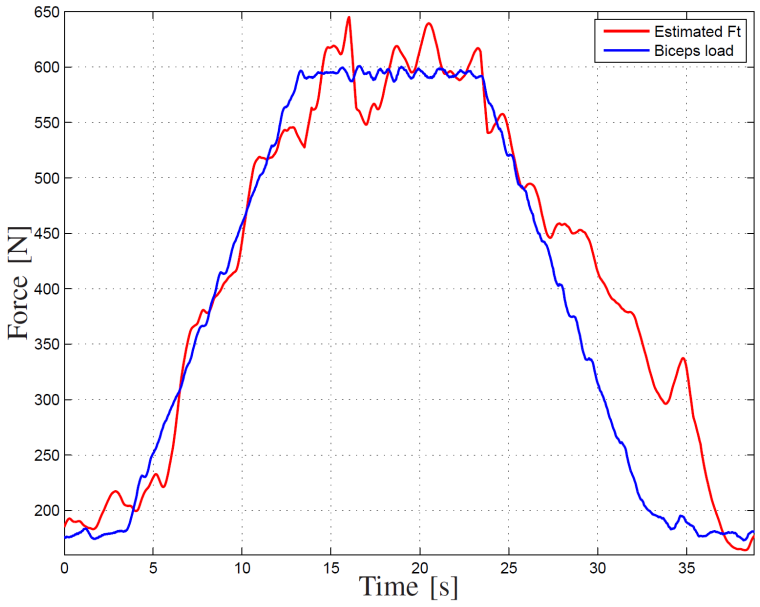

(a) The action of the TSA module WAD is not actived.

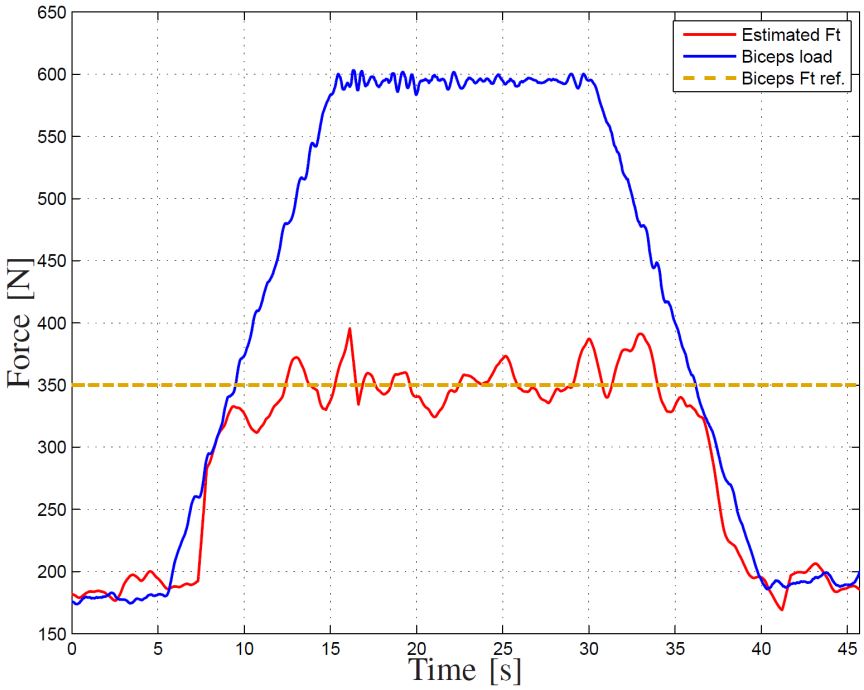

(b) The action of the TSA module WAD is actived.

FIGURE 5.10: The estimated biceps tendon force F_t and the value of the muscle load during the experimental validation. In the bottom graph, the WAD assistance is provided to the subject according to the biceps tendon force reference set in the control loop.

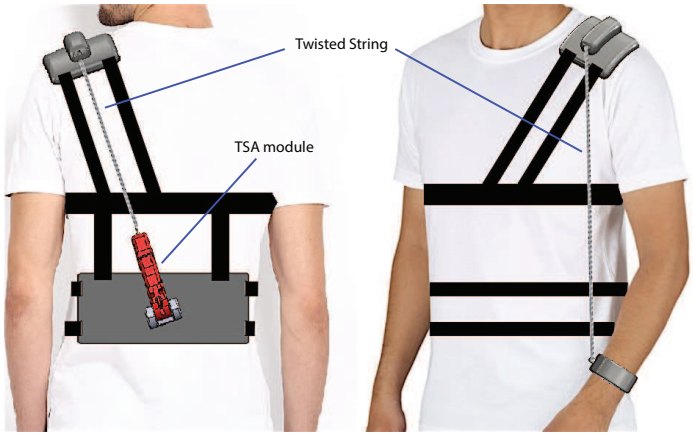

FIGURE 5.11: Future conceptual design of the TSA module-based WAD for elbow assistance during load lifting tasks.

the TSA module has been fixed to a rigid structure, realizing a preliminary setup configuration. In Fig. 5.12 it is possible to observe the setup layout used to support the biceps muscle activity during the lifting tasks, involving the elbow joint through forearm flexion/extension motions. Besides the sEMG-based control interface, future developments will see the mechanical design and evaluation of the configuration illustrated in Fig. 5.11.

The fixation of the TSA module to a rigid structure rely on the necessity to have available the necessary string length, since the string contraction has to stay within the 20% of the full string length (this also justify the design of Fig. 5.11). Therefore, within this study the friction and curvature related phenomena introduced by the twisted string path across the shoulder (Fig. 5.11) have been avoided, while dedicated investigation on the TSA transmission characteristics are under development (Palli, Hosseini, and Melchiorri, 2016).

The load lifting tasks protocol consists of flexions of the elbow when a load of 2 kg is applied on the wrist. The TSA module is fixed to the rigid structure by means of a spherical joint, and the string end is connected to and armband worn by the user on his/her forearm. The arm of the subject is parallel to the trunk while comfortably sitting on a chair. The task to be performed is composed by five consecutive forearm motions, each one consisting in a flexion followed by an extension. Furthermore the five flexions are executed with and without the load applied to the wrist for the purpose of comparison. Specifically, the user is required to perform smooth and reasonably slow movements covering the elbow angle range between approximatively 10^o and 90^o.

5.3.2 Myoelectric Control Strategy

The sEMG-based HRI rely on a control strategy that has the goal of computing automatically a force reference value F_{ref} for the TSA module-based WAD, the latter already presented in Subsec. 5.1.1. The myoelectric control is designed in order to

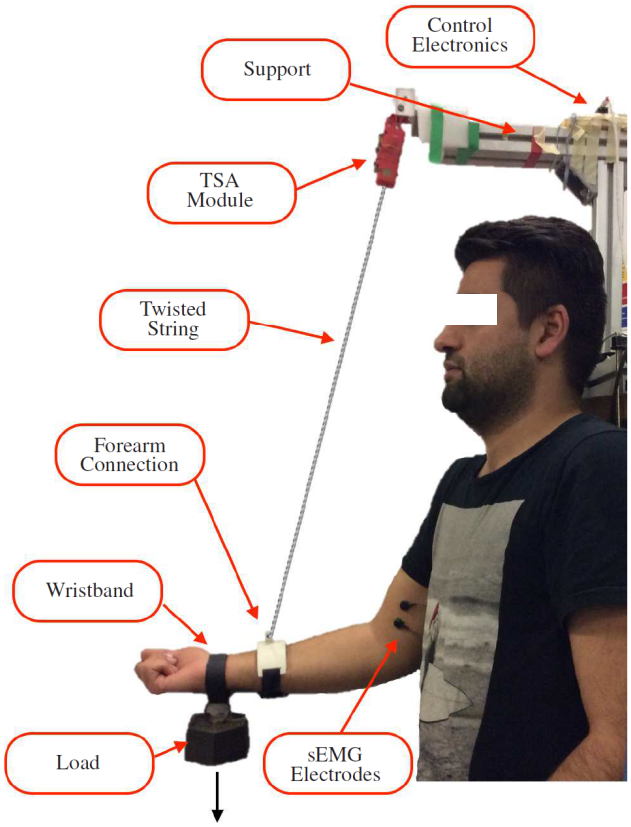

FIGURE 5.12: Setup configuration used for the lifting tasks.

apply to the user's forearm a suitable support during lifting tasks of a load applied on the wrist, such that an arbitrary level of compensation of the muscle effort can be obtained. That is, the muscle activity of the biceps can be limited under a certain threshold value during the lifting tasks.

The implemented control loop is explained with relation to the scheme observable in Fig. 5.13. According to the blocks and variables of this figure, the reference force for the F_{ref} is given by a sEMG-driven control loop that is characterized by a combined proportional and integral action (sEMG-driven PI controller), that however follows a particular switching logic, explained in the following. First, the controller is based on the sEMG-based signals error e_{EMG} computed as

$$e_{\text{EMG}} = T_L - EMG_{\text{meas}}\,, \tag{5.9}$$

where T_L is a lower threshold used as sEMG reference value and EMG_{meas} is the sEMG signal measured from the biceps. The PI controller based on this sEMG error implements a dynamic action in accordance with a specific Double Threshold Strategy (DTS): *(i)* the controller is activated in case EMG_{meas} continuously surpasses a higher threshold value T_H ($T_H > T_L$) for a period of 0.5 s, on the other hand *(ii)* the deactivation occur when the increasing of F_{ref} (and therefore of F_{applied}) makes EMG_{meas} decrease and touch the lower threshold value T_L. Note that the last output

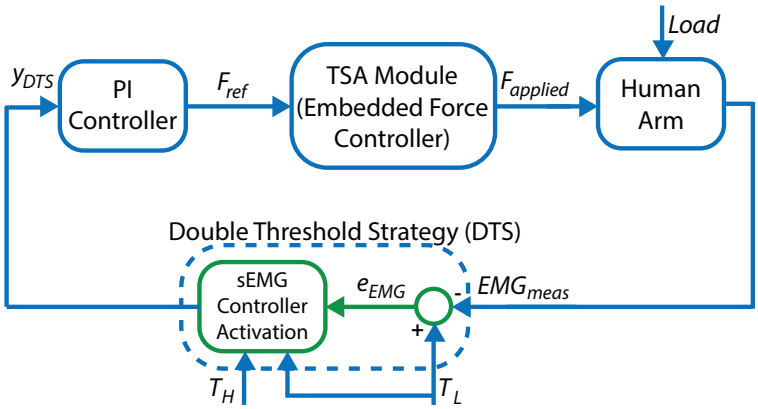

FIGURE 5.13: sEMG-based control loop for the TSA module automatic assistance to the user.

value of the controller is kept constant during the not active status. In this way, the input of the sEMG-driven PI controller y_{DTS} (Fig. 5.13) is given

$$y_{\text{DTS}} = \begin{cases} e_{\text{EMG}} & \text{, sEMG-driven controller active} \\ 0 & \text{, sEMG-driven controller not active.} \end{cases} \tag{5.10}$$

In practice, the behaviour resulting from the presented sEMG-based control interface is that during a lifting task that involves the elbow joint, the activation of the controller makes F_{ref} increase in such a way that the biceps sEMG activity decreases until it touches the lower threshold T_L, thanks to user's CNS adaptation to the support provided on the forearm by the TSA module action.

As reported in the following subsection, the control solution has been evaluated by means of load lifting tasks. Furthermore, an online adjustment procedure is also introduced, in order to let the sEMG-based HRI be easily used by different users in the face of thei musculoskeletal variability.

5.3.3 Experimental Session and Results

Experiments have been performed involving four healthy male subjects, namely S1, S2, S3, S4 (mean age 30, standard deviation 2.58). The goal of this validation test consists in assisting the user during a lifting task of a 2 kg load applied to the wrist, according to the protocol described in Subsec. 5.3.1. In this relation, in the first part of the experiment, the load is applied to the armband, and the subject executes the flexion/extension motions freely, with the TSA module only accompanying the user movements without providing any assistive force. In Fig. 5.14, as an example for the subject S2, the behaviour of the biceps activity during this support-free task is shown. Note that the elbow angle is computed based on the setup geometry and the module's DC motor encoder signal. Thereafter, in the second phase of the experiment, each subject repeat the lifting motions of the 2 kg load while assisted by the force provided by the TSA module.

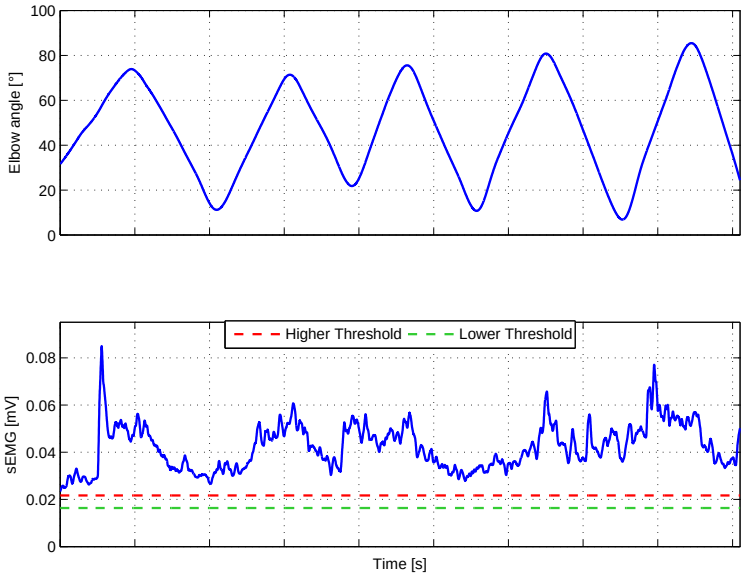

FIGURE 5.14: sEMG signal behaviour during the lifting task without the assistive support for the subject S2.

In Fig. 5.15 the behaviour and effects of the sEMG-based control strategy during the lifting task of the 2 kg load are shown for the subject S2. In relation to the graphs of the figure, it is possible to observe that the sEMG signal surpasses the higher threshold T_H (red) during the execution of the first lifting motion. The sEMG-driven controller is consequently activated, in accordance with the eq. (5.10), causing the increasing of F_{ref} in such a way that the biceps sEMG activity decreases until it reaches the lower threshold (green). This is possible since the user exploits the help provided by TSA module action on the forearm. Thereafter, the value of EMG_{meas} remains in the neighbourhood of the threshold T_L without surpassing T_H for the subsequent elbow flexions, except for peaks that are successfully filtered by the overall DTS, i.e. the sEMG controller action is not activated is these cases. Indeed, the implementation of such DTS presents two remarkable advantages: *(i)* a more reliable regulation of the sEMG signal (which presents a substantial inherent variability), with respect to a single threshold value approach and *(ii)* the capability of filtering sEMG peaks that surpass the higher threshold T_H for a short time (less than 0.5 s), which are usually present in case of slightly faster motions or unaware impulsive contractions, avoiding an increasing of the sEMG controller integral action not oriented to compensate the applied load.

Selection of the Threshold Values

In order to present comparable performance and results of the sEMG-based control among the users involved in the experiment, for this study the threshold values T_L and T_H are determined for each subject by means of a simple calibration phase. Specifically, the sEMG signal of the users with the elbow flexed at 90° and with the application of a load of 0.5 kg is recorded. Then the thresholds are computed as

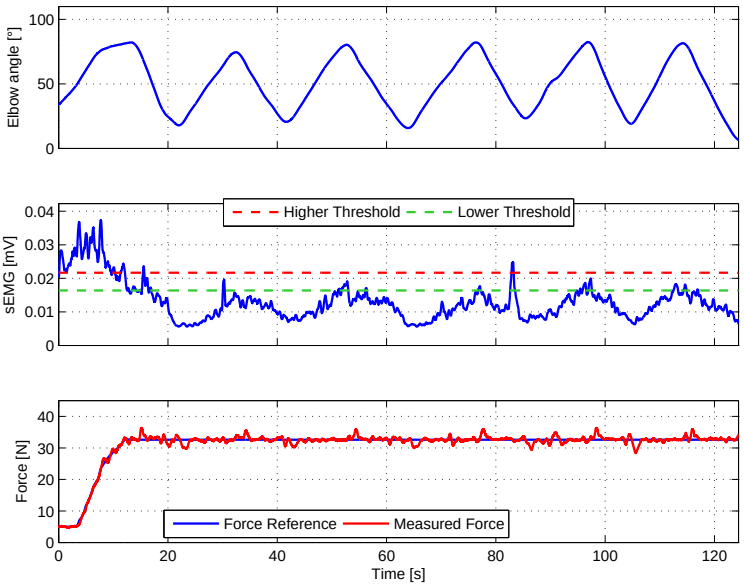

FIGURE 5.15: Resulting behaviour for the subject S2 during the lifting task with the presence of the assistive support.

TABLE 5.2: Threshold values over the four subjects.

	S1	S2	S3	S4	Mean value
T_L [mV]	0.014	0.016	0.011	0.013	0.014 ± 0.003
T_H [mV]	0.018	0.022	0.013	0.018	0.019 ± 0.004

$$T_L = m_{\text{EMG}} - \sigma_{\text{EMG}}\,, \quad T_H = m_{\text{EMG}} + \sigma_{\text{EMG}}, \tag{5.11}$$

where m_{EMG} is the mean value of the sEMG calibration recording and σ_{EMG} is the standard deviation computed over the same recording. Tab. 5.2 reports the threshold values for the four subjects.

Online Automatic Adjustment Procedure

It is important to highlight that, although the behaviour reported in In Fig. 5.15 is observable in all the four subjects, such common performance, however, are only achievable after a proper user-dependent selection and adjustment of the proportional and integral gains of the sEMG-based PI controller. As a consequence, this makes necessary a calibration phase in which the parameters have to empirically be adjusted in order to reach a suitable and fast behaviour (i.e. already from the first flexion of the lifting tasks). Such empirical phase can likely require a great amount of user's mental effort and concentration in order to finally trust and, therefore, benefit the assistive support, easily causing frustration and discouragement.

In order to avoid this empirical tuning of the parameters, a simple and online

TABLE 5.3: Quantitative outcomes of the lifting task experiments for the four subjects.

Subject	Max. TSA Force Ref. [N]	Mean Max. TSA Force Ref. [N]	Required no. of preparatory flexions	Mean sEMG peak during lifting tasks [mV]	Lower Thre. [mV]	Higher Thre. [mV]
S1	33.99	36.03	5	0.0235 ± 0.012	0.014	0.018
S2	41.61		4	0.0159 ± 0.001	0.016	0.022
S3	32.32		3	0.0116 ± 0.0004	0.011	0.013
S4	36.21		4	0.0222 ± 0.016	0.013	0.018

procedure for the adjustment of the control action to different users has been introduced in the experimental session. It consists in setting more relaxed parameters of the PI controller (i.e. the controller gains) and performing a few preparatory flexion/extension elbow motions in order to automatically obtain the right amount of support without any parameter calibration at the presence of the experimenter. Specifically, the user is asked to perform a sequence of flexion/extension movements with the 2 kg load applied, holding the elbow joint at the upper position of 90° for few seconds before executing the extension to complete the motion (approximatively 1—3 s). In this way the assiting force is gently increased against a compensation of the muscle activity at each iteration, since the sEMG-based controller is activated during the flexion phase (the biceps activity surpasses the threshold T_H) and deactivated for the extension phase (the sEMG signal touches the threshold T_L). Finally, the adjustment procedure is completed when the lifting movements do not make the controller increase the assistive force anymore, and the user starts the lifting tasks experiment in an online fashion. Fig. 5.16 shows the effect of the sEMG-based control together with the adjustment phase for the four involved subjects, plotting the graphs of the same quantities of Fig. 5.15. With regard to the Fig. 5.16, the vertical orange dashed line divides the adjustment phase from the lifting tasks experiment. As it is possible to observe, five iterations of the flexion/extension motions are sufficient to reach the right amount of force provided by the TSA module in order limit the biceps sEMG activity according to the DTS of the controller. Furthermore, after the adjustment procedure the controller is still able to increase the TSA module reference force in case the sEMG signal surpasses the higher threshold for more than $2s$ (i.e., the adjustment procedure presented small imprecisions), as can be observed for the subject S1 in Fig. 5.16 in proximity of the time $200s$. Thereafter, the users successfully exploit the external support provided by the TSA module, and the lifting task is properly accomplished limiting the biceps muscle activity according to a sEMG level necessary for 0.5 kg when the elbow is flexed at 90°.

Tab. 5.3 reports a quantitative description of the lifting task experiments for the four subjects, in relation to the maximum TSA reference force, number of necessary preparatory flexions and sEMG peak values after the adjustment procedure.

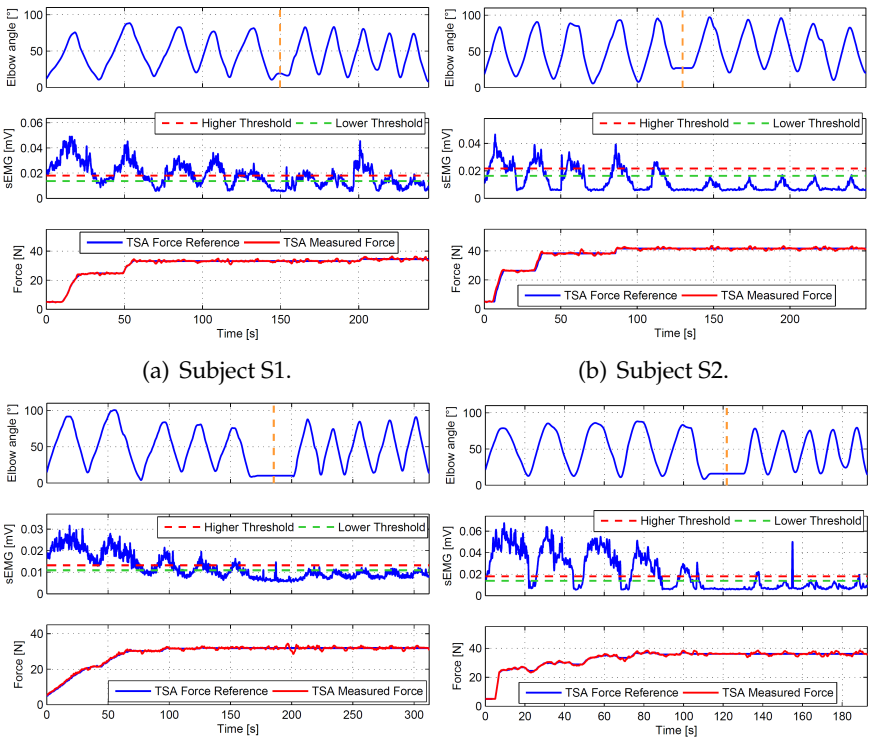

(a) Subject S1. (b) Subject S2.

(c) Subject S3. (d) Subject S4.

FIGURE 5.16: The online adjustment procedure and the lifting tasks with the assistive support.

5.3.4 Conclusion and Future Work

The control interface presented in this section rely on a sEMG-based error related PI action, together with a double-threshold-driven switching activation logic, for the regulation of the elbow assistance provided by a WADs. The support aims to automatically reduce the biceps muscle effort during lifting tasks. The TSA module has been used for the experimental session with four healthy subjects, performing lifting tasks of a 2 kg load, with the aim of limiting the biceps sEMG signal to a muscle activity level related to 0.5 kg (see Subsec. 5.3.3). A fast, automatic and online calibration procedure has been conducted for each subject during the experiments, demonstrating that the system is easily adjustable to different users, as shown in the results where for all subjects the muscle activity has been successfully limited under an arbitrary threshold value. In particular, the proposed HRI for WADs do not make use of sEMG-driven dynamic muscle models and/or joint torque estimation techniques, exploring a simplification in the use of the myoelectric signal, with the aim of avoiding approaches that generally require long and complex subject-dependent algorithm training sessions.

The outcomes of the research work on the sEMG-based HRI for WADs here reported provide positive outlooks for future developments in several directions: the implementation of the proper WAD configuration for the TSA module (see Fig. 5.11), the adaptation and test of the HR control interface with users with neuromuscular

diseases, the consideration within the sEMG-driven control loop for loads with an online variable weight and the use of the biceps and triceps antagonistic muscle couple within the assistive paradigm.

Chapter 6

Conclusions

Robotics is on a road towards control problems that are more and more related with a closer collaboration and interaction between artificial devices and mankind, nowadays more than ever.

In recent decades, the scientific community is exploring the design of robotic systems that take inspiration from humans as a way to replicate their great ability and flexibility in the accomplishment of motor control related tasks. To this end, the human-in-the-loop paradigm is one of the most investigated and used method to transfer human skills to robots.

In this context, the research for intuitive and natural control solutions is a fundamental aspect. This is particularly important from the user's point of view for the teleoperation of artificial hands and wearable assistive devices, on which the interest of the research work reported in this thesis has been focused. In this relation, the development of proper control interfaces (i.e., HRI) can benefit several applications from different fields: *(i)* for robotic hands, the telemanipulation in industrial or human hostile environments (e.g. spatial operations, underwater applications or in the case of dangerous situations or disasters) and in the field of prosthetics; *(ii)* for wearable assistive robots, the compensation of neuromuscular disorders, the improvement of rehabilitation techniques and the empowering and assistance of motor performance for weak people (e.g. in case of long term hospitalization or advanced age).

In Chap. 1 the concept of HRI has been introduce and contextualized, highlighting how the interaction between a user and a teleoperated device can be both physical and cognitive. Importantly, in this context, it has been explained the fundamental necessity to detect user's intentions within the idea of HRI system development, and at the same time to perceive a sensory awareness from the artificial device.

Both in the field of teleoperation of robotic hands and wearable devices (i.e., WADs), and particularly in the rehabilitation area of interest, the use of surface electromyography (i.e., sEMG) is one of the most promising technique investigated in the last decades for the human intentions detection in HRIs for control purposes. For these reason, in Chap. 2 the neuromuscular aspects of the motor control that underlie the sEMG signal generation have been reported, in order to provide the concepts on which the decoding of the related informational content is based. Together, also

the technological aspect of the recording and acquisition of the signal is outlined. Furthermore, the contents within Chap. 2 have also illustrated the hierarchical and synergistic organization of the human motor control system, introducing important elements that have been considered in the design of the HRIs within the present thesis work.

In Chap. 3 a review of the sEMG-based HRIs for control purposes of artificial hands and WADs has been outlined. It has been reported how the myocontrol of robotic hands is extensively studied and implemented in literature works, due to its great potentialities. However, the review has also shown the limits that nowadays are present in this kind of HRI approaches, principally due to instability and reliability issues of the myocontrollers. More intuitiveness and naturalness in the control, a useful and easily interpretable feedback, and incremental adaptation of the interfaces are the horizons for the near future. The review have regarded also the myoelectric HRIs for wearable assistive robots, emphasizing how the principal element for the design of control interfaces for this kind of applications is the reactivity in detecting human intentions. Indeed, the presence of a close and strict physical and cognitive interaction requires short times for providing a correct amount of assistive action to the user of the robot. In this relation, it has been also shown that various approaches adopt complex algorithms for the estimation of human joint torques from the sEMG, whereas a simplification in the use of myoelectric signals could bring to assistive applications employable in real-life scenarios, also in virtue of recent improvements in embedding sensors and actuators in novel WADs.

Chap. 4 presents the deign and implementation of a sEMG-based HRI for the control of an anthropomorphic hand and an industrial gripper. The interface has been developed to provide to the users an interface able to combine intuitiveness and naturalness in the control, together with a good level of stability and reliability. To this end, along the chapter it has been shown that the design of the HRI exploits sEMG signals together with neuromuscular information in order to allow the user regulate in a natural fashion the closure and the stiffness of the robotic hands during grasping tasks. This myoelectric control, named grasp proprtioanl myocontrol, has been combined with the possibility of selecting the grasp shape though gestures classification, thanks to ML-based pattern recognition of the sEMG signals and a FSM logic. The evaluation of the interface has been conducted by means of grasping experiments, in which four subjects controlled the dexterous anthropomorphic robotic hand and the industrial gripper, the latter mounted on a manipulator. The results report for a mean overall grasp success ratio of 96.3% and for an actual natural and intuitively goal-oriented modulation of the proportional degrees of control provided.

Continuing, the development and evaluation of control interfaces for a TSA module WAD are the contents presented in Chap. 5. In the considered assistive applications, the device is used to support the elbow joint, and the goal of the HRI design is to automatically compensate the biceps muscle effort when a load is applied to the

forearm. The first reported myocontrol approach is a preliminary study of an assistive application using the TSA module in isometric muscle conditions. In particular, the sEMG signal has been used to drive a muscle model for the computation of the biceps tendon force against an external load profile applied to the user's forearm. It has been shown through the results of an experimental validation that the model was successfully used to regulate the support action of the TSA module assistive device, limiting the force exerted on the biceps tendon in accordance to a reference value, by means of a sEMG-driven HR control loop. Moreover, in the chapter it is reported also the design of a control interface for dynamic elbow assistive applications with the TSA module WAD. It has been illustrated that this solution rely on a sEMG-based error related PI action, together with a switching activation logic based on a double threshold strategy (i.e., DTS), for the automatic regulation of the assistance provided by a WADs. It has been illustrated that the proposed HRI do not make use of sEMG-driven dynamic muscle models and/or joint torque estimation techniques, exploring a simplification in the use of the myoelectric signal, with the aim of avoiding approaches that generally require long and complex subject-dependent algorithm training sessions. The results reported for the experimental session carried out with four subjects show that the muscle activity of a user during the execution of lifting tasks of a 2 kg load can be limited under an arbitrary threshold value thanks to a sEMG-based controller. Furthermore, the experiments demonstrate also that the system is easily adaptable to different users, thanks to a fast, automatic and online adjustment procedure introduced to avoid empirical tuning of the controller gains at the presence of the experimenter.

6.1 Future Work

The outcomes of the research work presented in this thesis open the possibility to several future improvements, taking as starting point the aquired stock of knowledge and the results obtained. In particular, it is possible to think about future developments with respect to the specific design and implementation of the HRIs presented in Chap. 4 and Chap. 5.

With regard to the teleoperation system for robotic hands, the first improvement that can be thought is related to the feedback information. The implemented HRI is only equipped with a sound feedback. First, it is important to say that it does its work: the user is able to properly understand when a gesture has been recognized by the ML-based classifier (first type of sound of the feedback), and he/she is totally aware about the level of grasp stiffness currently modulated on the grasping device (second type of sound feedback). However, the user has to use headphones and to remain concentrated in listening the sound, and therefore this kind of feedback is not felt as natural and comfortable. A more effective feedback information could be given by the introduction of other modalities, for example based on a haptic

feedback. This kind of modality can be perceived as a proprioceptive sensory information, and therefore it can drastically improve the performance of the HRI from a user-centred point of view. In addition, the use of an haptic feedback can open further interesting future studies on how to provide the sensory information to the users, and therefore on how humans in general interpret external stimuli. Also, a different aspect that could be investigated on the sEMG-based control for artificial hands is the possibility of extracting more information about grasp executions from measurements of intrinsic hand muscles activity. Finally, it can be explored the possibility of sensor fusion approaches to improve both control and feedback signals (e.g. exploiting inertial sensors).

Future developments are possible also with respect to the work carried out for the design of sEMG-based HRIs for WADs. In relation to the assistance of the elbow joint during the lifting tasks of a load applied to the forearm, it is necessary to adapt the myoelectric control paradigm to the possibility of loads that can vary in time. To do this, it can be useful to consider, within the design of the HRI, the sEMG signals from the antagonistic muscle couple composed by biceps and triceps. Furthermore, an investigation about the exploitation of contractions and co-contractions of biceps and triceps can be also important for the future development of a WAD that includes two TSA modules in an antagonistic configuration. This would enable the realization of a proper wearable assistive robot for the fully support of the elbow joint, including the possibility of regulating its impedance by co-activation of the TSA-based devices.

Bibliography

Adams, Julie A and Marjorie Skubic (2005). "Introduction to the special issue on human–robot interaction". In: *IEEE Transactions on Systems, Man, and Cybernetics-Part A: Systems and Humans* 35.4, pp. 433–437.

Ajiboye, AB and RF Weir (2009). "Muscle synergies as a predictive framework for the EMG patterns of new hand postures". In: *Journal of neural engineering* 6.3, p. 036004.

Ajoudani, Arash (2016). *Transferring Human Impedance Regulation Skills to Robots*. Springer.

Ajoudani, Arash et al. (2014). "Exploring teleimpedance and tactile feedback for intuitive control of the pisa/iit softhand". In: *IEEE transactions on haptics* 7.2, pp. 203–215.

Artemiadis, Panagiotis K and Kostas J Kyriakopoulos (2006). "EMG-based teleoperation of a robot arm in planar catching movements using ARMAX model and trajectory monitoring techniques". In: *Robotics and Automation, 2006. ICRA 2006. Proceedings 2006 IEEE International Conference on*. IEEE, pp. 3244–3249.

— (2009). "EMG-based position and force estimates in coupled human-robot systems: Towards EMG-controlled exoskeletons". In: *Experimental Robotics*. Springer, pp. 241–250.

— (2011). "A switching regime model for the EMG-based control of a robot arm". In: *IEEE Transactions on Systems, Man, and Cybernetics, Part B (Cybernetics)* 41.1, pp. 53–63.

Asimov, Isaac (1942). "Runaround". In: *Astounding Science Fiction* 29.1, pp. 94–103.

Baklouti, Malek et al. (2008). "Intelligent assistive exoskeleton with vision based interface". In: *Smart Homes and Health Telematics*, pp. 123–135.

Battye, CK, A Nightingale, and J Whillis (1955). "The use of myo-electric currents in the operation of prostheses". In: *Bone & Joint Journal* 37.3, pp. 506–510.

Benatti, Simone et al. (2015). "Multiple Biopotentials Acquisition System for Wearable Applications." In: *BIODEVICES*, pp. 260–268.

Berger, Denise J and Andrea d'Avella (2014). "Effective force control by muscle synergies". In: *Frontiers in computational neuroscience* 8.

Berry, Michael W et al. (2007). "Algorithms and applications for approximate nonnegative matrix factorization". In: *Computational statistics & data analysis* 52.1, pp. 155–173.

Biddiss, Elaine and Tom Chau (2007). "Upper-limb prosthetics: critical factors in device abandonment". In: *American journal of physical medicine & rehabilitation* 86.12, pp. 977–987.

Bitzer, Sebastian and Patrick Van Der Smagt (2006). "Learning EMG control of a robotic hand: towards active prostheses". In: *Robotics and Automation, 2006. ICRA 2006. Proceedings 2006 IEEE International Conference on*. IEEE, pp. 2819–2823.

Bizzi, E et al. (2008). "Combining modules for movement". In: *Brain research reviews* 57.1, pp. 125–133.

Buchthal, Fritz and Henning Schmalbruch (1970). "Contraction times and fibre types in intact human muscle". In: *Acta Physiologica* 79.4, pp. 435–452.

Burdet, Etienne, David W Franklin, and Theodore E Milner (2013). *Human robotics: neuromechanics and motor control*. MIT press.

Burdet, Etienne et al. (2014). "Interaction force, impedance and trajectory adaptation: by humans, for robots". In: *Experimental Robotics*. Springer, pp. 331–345.

Burgar, Charles G et al. (2000). "Development of robots for rehabilitation therapy: The Palo Alto VA/Stanford experience". In: *Journal of rehabilitation research and development* 37.6, pp. 663–674.

Čapek, Karel (1925). *RUR (Rossum's universal robots): a fantastic melodrama*. Doubleday, Page.

Castellini, Claudio (2016a). "Incremental learning of muscle synergies: from calibration to interaction". In: *Human and Robot Hands*. Springer, pp. 171–193.

— (2016b). "Living with a prosthesis that learns: A case-study in translational medicine". In: *robohub.org*.

Castellini, Claudio and Patrick van der Smagt (2009). "Surface EMG in advanced hand prosthetics". In: *Biological cybernetics* 100.1, pp. 35–47.

— (2013). "Evidence of muscle synergies during human grasping". In: *Biological cybernetics* 107.2, pp. 233–245.

Cavallaro, Ettore E et al. (2006). "Real-time myoprocessors for a neural controlled powered exoskeleton arm". In: *IEEE Transactions on Biomedical Engineering* 53.11, pp. 2387–2396.

Chang, Chih-Chung and Chih-Jen Lin (2011). "LIBSVM: a library for support vector machines". In: *ACM Transactions on Intelligent Systems and Technology (TIST)* 2.3, p. 27.

Choi, Changmok and Jung Kim (2011). "Synergy matrices to estimate fluid wrist movements by surface electromyography". In: *Medical engineering & physics* 33.8, pp. 916–923.

Cortes, Corinna and Vladimir Vapnik (1995). "Support-vector networks". In: *Machine learning* 20.3, pp. 273–297.

d'Avella, Andrea et al. (2006). "Control of fast-reaching movements by muscle synergy combinations". In: *Journal of Neuroscience* 26.30, pp. 7791–7810.

De Luca, Carlo J et al. (2010). "Filtering the surface EMG signal: Movement artifact and baseline noise contamination". In: *Journal of biomechanics* 43.8, pp. 1573–1579.

De Rossi, Danilo et al. (2009). "Wearable kinesthetic systems and emerging technologies in actuation for upperlimb neurorehabilitation". In: *Engineering in Medicine*

and Biology Society, 2009. EMBC 2009. Annual International Conference of the IEEE. IEEE, pp. 6830–6833.

Despopoulos, Agamemnon and Stefan Silbernagl (2003). *Color Atlas of Physiology*.

Di Nuovo, Alessandro et al. (2016). "Experimental evaluation of a multi-modal user interface for a robotic service". In: *Conference Towards Autonomous Robotic Systems*. Springer, pp. 87–98.

Di Pino, Giovanni, E Guglielmelli, and Paolo Maria Rossini (2009). "Neuroplasticity in amputees: main implications on bidirectional interfacing of cybernetic hand prostheses". In: *Progress in neurobiology* 88.2, pp. 114–126.

Erik Scheme, Kevin Englehart (2011). "Electromyogram pattern recognition for control of powered upper-limb prostheses: State of the art and challenges for clinical use". In: *Journal of rehabilitation research and development* 48.6, p. 643.

Fan, Richard E et al. (2008). "A haptic feedback system for lower-limb prostheses". In: *IEEE Transactions on Neural Systems and Rehabilitation Engineering* 16.3, pp. 270–277.

Ferguson, Simon and G Reg Dunlop (2002). "Grasp recognition from myoelectric signals". In: *Proceedings of the Australasian Conference on Robotics and Automation, Auckland, New Zealand*. Vol. 1.

Ficuciello, Fanny et al. (2014). "Postural synergies of the UB Hand IV for human-like grasping". In: *Robotics and Autonomous Systems* 62.4, pp. 515–527.

Finley, F Ray and Roy W Wirta (1967). "Myocoder studies of multiple myopotential response." In: *Archives of physical medicine and rehabilitation* 48.11, p. 598.

Fleischer, Christian and Gunter Hommel (2007). "Calibration of an EMG-Based Body Model with six Muscles to control a Leg Exoskeleton". In: *Robotics and Automation, 2007 IEEE International Conference on*. IEEE, pp. 2514–2519.

Fougner, Anders et al. (2012). "Control of upper limb prostheses: terminology and proportional myoelectric control—a review". In: *IEEE Transactions on neural systems and rehabilitation engineering* 20.5, pp. 663–677.

Fuglevand, Andrew J et al. (1992). "Detection of motor unit action potentials with surface electrodes: influence of electrode size and spacing". In: *Biological cybernetics* 67.2, pp. 143–153.

Gijsberts, Arjan et al. (2014). "Stable myoelectric control of a hand prosthesis using non-linear incremental learning". In: *Frontiers in neurorobotics* 8.

Gomi, Hiroaki and Rieko Osu (1998). "Task-dependent viscoelasticity of human multijoint arm and its spatial characteristics for interaction with environments". In: *Journal of Neuroscience* 18.21, pp. 8965–8978.

Goodrich, Michael A and Alan C Schultz (2007). "Human-robot interaction: a survey". In: *Foundations and trends in human-computer interaction* 1.3, pp. 203–275.

Gopura, Ranathunga Arachchilage Ruwan Chandra, Kazuo Kiguchi, and Yang Li (2009). "SUEFUL-7: A 7DOF upper-limb exoskeleton robot with muscle-model-oriented EMG-based control". In: *Intelligent Robots and Systems, 2009. IROS 2009. IEEE/RSJ International Conference on*. IEEE, pp. 1126–1131.

Gopura, RARC and Kazuo Kiguchi (2009). "Electromyography (EMG)-signal based fuzzy-neuro control of a 3 degrees of freedom (3DOF) exoskeleton robot for human upper-limb motion assist". In: *Journal of the National Science Foundation of Sri Lanka* 37.4.

— (2012). "Application of surface electromyographic signals to control exoskeleton robots". In: *Applications of EMG in Clinical and Sports Medicine*. InTech.

Gopura, RARC, Kazuo Kiguchi, and DSV Bandara (2011). "A brief review on upper extremity robotic exoskeleton systems". In: *Industrial and Information Systems (ICIIS), 2011 6th IEEE International Conference on*. IEEE, pp. 346–351.

Gopura, RARC et al. (2013). "Recent trends in EMG-Based control methods for assistive robots". In: *Electrodiagnosis in new frontiers of clinical research*. InTech.

Hahne, Janne M et al. (2014). "Linear and nonlinear regression techniques for simultaneous and proportional myoelectric control". In: *IEEE Transactions on Neural Systems and Rehabilitation Engineering* 22.2, pp. 269–279.

Hannaford, Blake (1989). "A design framework for teleoperators with kinesthetic feedback". In: *IEEE transactions on Robotics and Automation* 5.4, pp. 426–434.

Hargrove, Levi et al. (2007). "A real-time pattern recognition based myoelectric control usability study implemented in a virtual environment". In: *Engineering in Medicine and Biology Society, 2007. EMBS 2007. 29th Annual International Conference of the IEEE*. IEEE, pp. 4842–4845.

Heckman, CJ and Roger M Enoka (2012). "Motor unit". In: *Comprehensive Physiology*.

Hocaoglu, Elif and Volkan Patoglu (2012). "Tele-impedance control of a variable stiffness prosthetic hand". In: *Robotics and Biomimetics (ROBIO), 2012 IEEE International Conference on*. IEEE, pp. 1576–1582.

Hogan, Neville (1984). "Adaptive control of mechanical impedance by coactivation of antagonist muscles". In: *IEEE Transactions on Automatic Control* 29.8, pp. 681–690.

Hogan, Neville et al. (1992). "MIT-MANUS: a workstation for manual therapy and training. I". In: *Robot and Human Communication, 1992. Proceedings., IEEE International Workshop on*. IEEE, pp. 161–165.

Homer (circa 800 BC). *Iliad*.

Hosseini, Mohssen et al. (2017). "A Wearable Robotic Device Based on Twisted String Actuation for Rehabilitation and Assistive Applications". In: *Journal of Robotics* 2017.

Huang, Vincent S and John W Krakauer (2009). "Robotic neurorehabilitation: a computational motor learning perspective". In: *Journal of neuroengineering and rehabilitation* 6.1, p. 5.

Hug, François (2011). "Can muscle coordination be precisely studied by surface electromyography?" In: *Journal of electromyography and kinesiology* 21.1, pp. 1–12.

Ison, Mark and Panagiotis Artemiadis (2014). "The role of muscle synergies in myoelectric control: trends and challenges for simultaneous multifunction control". In: *Journal of neural engineering* 11.5, p. 051001.

Jaquier, Noémie et al. (2017). "Combining Electromyography and Tactile Myography to Improve Hand and Wrist Activity Detection in Prostheses". In: *Technologies* 5.4, p. 64.

Jiang, Ning, Kevin B Englehart, and Philip A Parker (2009). "Extracting simultaneous and proportional neural control information for multiple-DOF prostheses from the surface electromyographic signal". In: *IEEE Transactions on Biomedical Engineering* 56.4, pp. 1070–1080.

Jiang, Ning et al. (2012). "Myoelectric control of artificial limbs—is there a need to change focus?[In the spotlight]". In: *IEEE Signal Processing Magazine* 29.5, pp. 152–150.

Jones, Lynette A and Susan J Lederman (2006). *Human hand function*. Oxford University Press.

Kadaba, MP et al. (1985). "Repeatability of phasic muscle activity: performance of surface and intramuscular wire electrodes in gait analysis". In: *Journal of Orthopaedic Research* 3.3, pp. 350–359.

Kandel, Eric R et al. (2000). *Principles of neural science*. Vol. 4. McGraw-hill New York.

Kapur, Pulkit et al. (2009). "Vibrotactile feedback system for intuitive upper-limb rehabilitation". In: *EuroHaptics conference, 2009 and Symposium on Haptic Interfaces for Virtual Environment and Teleoperator Systems. World Haptics 2009. Third Joint*. IEEE, pp. 621–622.

Kiguchi, Kazuo and Manoj Liyanage (2008). "A study of a 4DOF upper-limb power-assist intelligent exoskeleton with visual information for perception-assist". In: *Robotics and Automation, 2008. ICRA 2008. IEEE International Conference on*. IEEE, pp. 3666–3671.

Kiguchi, Kazuo et al. (2008). "Development of a 3DOF mobile exoskeleton robot for human upper-limb motion assist". In: *Robotics and Autonomous systems* 56.8, pp. 678–691.

Kobayashi, Hiroshi and Hirokazu Nozaki (2007). "Development of muscle suit for supporting manual worker". In: *Intelligent Robots and Systems, 2007. IROS 2007. IEEE/RSJ International Conference on*. IEEE, pp. 1769–1774.

Kong, Kyoungchul and Doyoung Jeon (2005). "Fuzzy control of a new tendon-driven exoskeletal power assistive device". In: *Proceedings of the IEEE/ASME International Conference on Advanced Intelligent Mechatronics (AIM 2005)*, pp. 146–151.

Kontarinis, Dimitrios A and Robert D Howe (1995). "Tactile display of vibratory information in teleoperation and virtual environments". In: *Presence: Teleoperators & Virtual Environments* 4.4, pp. 387–402.

Lagarias, Jeffrey C et al. (1998). "Convergence properties of the Nelder–Mead simplex method in low dimensions". In: *SIAM Journal on optimization* 9.1, pp. 112–147.

Lee, MH et al. (2010). "Development and assessment of an EMG-based exoskeleton system". In: *6th World Congress of Biomechanics (WCB 2010). August 1-6, 2010 Singapore*. Springer, pp. 648–650.

Lenzi, T et al. (2011). "Proportional EMG control for upper-limb powered exoskeletons". In: *Engineering in Medicine and Biology Society, EMBC, 2011 Annual International Conference of the IEEE*. IEEE, pp. 628–631.

Lenzi, Tommaso et al. (2012). "Intention-based EMG control for powered exoskeletons". In: *IEEE transactions on biomedical engineering* 59.8, pp. 2180–2190.

Lloyd, John E et al. (1999). "Programming contact tasks using a reality-based virtual environment integrated with vision". In: *IEEE Transactions on Robotics and Automation* 15.3, pp. 423–434.

Lo, Ho Shing and Sheng Quan Xie (2012). "Exoskeleton robots for upper-limb rehabilitation: State of the art and future prospects". In: *Medical engineering & physics* 34.3, pp. 261–268.

Loureiro, Rui et al. (2003). "Upper limb robot mediated stroke therapy—GENTLE/s approach". In: *Autonomous Robots* 15.1, pp. 35–51.

Melchiorri, Claudio et al. (2013). "Development of the ub hand iv: Overview of design solutions and enabling technologies". In: *IEEE Robotics & Automation Magazine* 20.3, pp. 72–81.

Miller, Levi Makaio and Jacob Rosen (2010). "Comparison of multi-sensor admittance control in joint space and task space for a seven degree of freedom upper limb exoskeleton". In: *Biomedical Robotics and Biomechatronics (BioRob), 2010 3rd IEEE RAS and EMBS International Conference on*. IEEE, pp. 70–75.

Milner, Theodore E (2009). "Impedance Control". In: *Encyclopedia of Neuroscience*. Springer, pp. 1929–1934.

Milner-Brown, HS, RB Stein, and R Yemm (1973). "The contractile properties of human motor units during voluntary isometric contractions". In: *The Journal of physiology* 228.2, pp. 285–306.

Muceli, Silvia and Dario Farina (2012). "Simultaneous and proportional estimation of hand kinematics from EMG during mirrored movements at multiple degrees-of-freedom". In: *IEEE Transactions on Neural Systems and Rehabilitation Engineering* 20.3, pp. 371–378.

Muceli, Silvia, Ning Jiang, and Dario Farina (2014). "Extracting signals robust to electrode number and shift for online simultaneous and proportional myoelectric control by factorization algorithms". In: *IEEE Transactions on Neural Systems and Rehabilitation Engineering* 22.3, pp. 623–633.

Nielsen, Johnny LG et al. (2009). "Enhanced EMG signal processing for simultaneous and proportional myoelectric control". In: *Engineering in Medicine and Biology Society, 2009. EMBC 2009. Annual International Conference of the IEEE*. IEEE, pp. 4335–4338.

Nowak, Markus, Thomas Eiband, and Claudio Castellini (2017). "Multi-modal myocontrol: Testing combined force-and electromyography". In: *Rehabilitation Robotics (ICORR), 2017 International Conference on*. IEEE, pp. 1364–1368.

Nowak, Markus, Sarah Engel, and Claudio Castellini (2017). "A PRELIMINARY STUDY TOWARDS AUTOMATIC DETECTION OF FAILURES IN MYOCONTROL". In: *MEC17 Proceedings*.

Öberg, Tommy (1995). "Muscle fatigue and calibration of EMG measurements". In: *Journal of Electromyography and Kinesiology* 5.4, pp. 239–243.

Oskoei, Mohammadreza Asghari and Huosheng Hu (2007). "Myoelectric control systems—A survey". In: *Biomedical Signal Processing and Control* 2.4, pp. 275–294.

— (2008). "Evaluation of support vector machines in upper limb motion classification using myoelectric signal". In: *14th International Conference on Biomedical Engineering: ICBME 2008*.

Osu, Rieko and Hiroaki Gomi (1999). "Multijoint muscle regulation mechanisms examined by measured human arm stiffness and EMG signals". In: *Journal of neurophysiology* 81.4, pp. 1458–1468.

Palli, G, M Hosseini, and C Melchiorri (2016). "Experimental Evaluation of Guided Twisted Actuation". In: *IFAC-PapersOnLine* 49.21, pp. 380–385.

Palli, G. and C. Melchiorri (2008). "Velocity and disturbance observer for non-model based load and friction compensation". In: *Proc. IEEE Int. Workshop on Advanced Motion Control*. Trento, Italy, pp. 194–199.

Palli, Gianluca et al. (2013). "Modeling and control of the twisted string actuation system". In: *IEEE/ASME Transactions on Mechatronics* 18.2, pp. 664–673.

Palli, Gianluca et al. (2014). "The DEXMART hand: Mechatronic design and experimental evaluation of synergy-based control for human-like grasping". In: *The International Journal of Robotics Research* 33.5, pp. 799–824.

Peerdeman, Bart et al. (2011). "Myoelectric forearm prostheses: State of the art from a user-centered perspective". In:

Perotto, Aldo O (2011). *Anatomical guide for the electromyographer: the limbs and trunk*. Charles C Thomas Publisher.

Pons, José L (2008). *Wearable robots: biomechatronic exoskeletons*. John Wiley & Sons.

Pratt, Jerry E et al. (2004). "The RoboKnee: an exoskeleton for enhancing strength and endurance during walking". In: *Robotics and Automation, 2004. Proceedings. ICRA'04. 2004 IEEE International Conference on*. Vol. 3. IEEE, pp. 2430–2435.

Processing Foundation (2016). URL: www.processing.org.

Rahman, Mohammad Habibur et al. (2006). "Robotic exoskeleton for rehabilitation and motion assist". In: *Industrial and Information Systems, First International Conference on*. IEEE, pp. 241–246.

Ratanaswasd, Palis et al. (2005). "Modular behavior control for a cognitive robot". In: *Advanced Robotics, 2005. ICAR'05. Proceedings., 12th International Conference on*. IEEE, pp. 713–718.

Robotis Corp. (2016). URL: www.en.robotis.com.

Rocon, Eduardo et al. (2007). "Design and validation of a rehabilitation robotic exoskeleton for tremor assessment and suppression". In: *IEEE Transactions on Neural Systems and Rehabilitation Engineering* 15.3, pp. 367–378.

Rosheim, Mark (2006). *Leonardo s Lost Robots*. Springer Science & Business Media.

Santello, Marco, Martha Flanders, and John F Soechting (1998). "Postural hand synergies for tool use". In: *Journal of Neuroscience* 18.23, pp. 10105–10115.

Santello, Marco et al. (2016). "Hand synergies: integration of robotics and neuroscience for understanding the control of biological and artificial hands". In: *Physics of life reviews* 17, pp. 1–23.

Scholtz, Jean C (2002). "Human-robot interactions: Creating synergistic cyber forces". In: *Multi-Robot Systems: From Swarms to Intelligent Automata*. Springer, pp. 177–184.

Schonle, Philipp et al. (2013). "A DC-connectable multi-channel biomedical data acquisition ASIC with mains frequency cancellation". In: *ESSCIRC (ESSCIRC), 2013 Proceedings of the*. IEEE, pp. 149–152.

Sharma, Rajeev, Vladimir I Pavlovic, and Thomas S Huang (1998). "Toward multimodal human-computer interface". In: *Proceedings of the IEEE* 86.5, pp. 853–869.

Sheridan, Thomas (1986). "Human supervisory control of robot systems". In: *Robotics and Automation. Proceedings. 1986 IEEE International Conference on*. Vol. 3. IEEE, pp. 808–812.

Sheridan, Thomas B (1992). *Telerobotics, automation, and human supervisory control*. MIT press.

Shoham, Moshe (2005). "Twisting wire actuator". In: *Journal of Mechanical Design* 127.3, pp. 441–445.

Skubic, Marjorie and Richard A Volz (2000). "Acquiring robust, force-based assembly skills from human demonstration". In: *IEEE Transactions on Robotics and Automation* 16.6, pp. 772–781.

Song, R and KY Tong (2005). "Using recurrent artificial neural network model to estimate voluntary elbow torque in dynamic situations". In: *Medical and Biological Engineering and Computing* 43.4, pp. 473–480.

Sugar, Thomas G et al. (2007). "Design and control of RUPERT: a device for robotic upper extremity repetitive therapy". In: *IEEE transactions on neural systems and rehabilitation engineering* 15.3, pp. 336–346.

Taylor, Russell H et al. (2000). "Medical robotics and computer-integrated surgery: information-driven systems for 21st century operating rooms". In: *Journal of Japan Society of Computer Aided Surgery* 2.2, pp. 47–53.

Topp, Robert et al. (2002). "The effect of bed rest and potential of prehabilitation on patients in the intensive care unit". In: *AACN Advanced Critical Care* 13.2, pp. 263–276.

Tsukahara, Atsushi, Yasuhisa Hasegawa, and Yoshiyuki Sankai (2009). "Standing-up motion support for paraplegic patient with Robot Suit HAL". In: *Rehabilitation Robotics, 2009. ICORR 2009. IEEE International Conference on*. IEEE, pp. 211–217.

Vallery, Heike et al. (2009). "Reference trajectory generation for rehabilitation robots: complementary limb motion estimation". In: *IEEE transactions on neural systems and rehabilitation engineering* 17.1, pp. 23–30.

Vredenbregt, J and G Rau (1973). "Surface electromyography in relation to force, muscle length and endurance". In: *New Concepts of the Motor Unit, Neuromuscular Disorders, Electromyographic Kinesiology*. Vol. 1. Karger Publishers, pp. 607–622.

Walsh, Conor James, Ken Endo, and Hugh Herr (2007). "A quasi-passive leg exoskeleton for load-carrying augmentation". In: *International Journal of Humanoid Robotics* 4.03, pp. 487–506.

Wiener, Norbert (1964). *God and Golem, inc: a comment on certain points where cybernetics impinges on religion*. Vol. 42. MIT press.

Winter, DA (1976). "Biomechanical model relating EMG to changing isometric tension". In: *Dig. 11th ICMBE, Ottawa*.

Winter, David A (2009). *Biomechanics and motor control of human movement*. John Wiley & Sons.

Wolf, Michael T et al. (2013). "Gesture-based robot control with variable autonomy from the JPL BioSleeve". In: *Robotics and Automation (ICRA), 2013 IEEE International Conference on*. IEEE, pp. 1160–1165.

Wolpaw, Jonathan R et al. (2002). "Brain–computer interfaces for communication and control". In: *Clinical neurophysiology* 113.6, pp. 767–791.

Young, Aaron J et al. (2013). "Classification of simultaneous movements using surface EMG pattern recognition". In: *IEEE Transactions on Biomedical Engineering* 60.5, pp. 1250–1258.